STUDY OF LOW MIGRATABLE PHOTOPOLYMER NETWORKS

Doctoral Thesis
By
Melahat Sahin

December 2017

Department Polymer Engineering and Science

Chair in Chemistry of Polymeric Materials

Thesis Advisor: Prof. Dr. Wolfgang Kern

FOREWORD

The research work was performed within the "Produktion der Zukunft" program of the Austrian Federal Ministry for Transport, Innovation and Technology and the Federal Ministry of Economy, Family and Youth and within the framework of the COMET-K1 project "*Solid state NMR techniques for characterization of network structures*" (project-no.: V-1.S2) at the Polymer Competence Center Leoben GmbH (PCCL, Austria) within the framework of the COMET-program of the Federal Ministry of Transport, Innovation and Technology and the Federal Ministry of Economy, Family and Youth with contributions by the Chair of Chemistry of Polymeric Materials (Montanuniversitaet Leoben), the Chair of Materials Science and Testing of Plastics (Montanuniversitaet Leoben) and Semperit Technische Produkte GmbH. The PCCL is funded by the Austrian Government and the State Governments of Styria, Lower Austria and Upper Austria.

I would like to thank my supervisor Professor Dr. Wolfgang Kern for providing me with the opportunity to perform my thesis at the Montanunversitaet Leoben and at the Polymer Competence Center Leoben GmbH.

My sincere appreciation and gratitude is devoted to Dr. Sandra Schlögl for her guidance, endless patience, help and encouragement to overcome the difficulties during the study. This work would not have been possible without her.

Special thanks go to Dr. Krzysztof Krawczyk and Dr. Santhosh Ayalur for their support and precious discussions during my PhD. It was a pleasure to work with them. I do not think I can ever repay the debt I owe to Krzysztof.

I want to thank Dr. Armin Holzner and Dr. Raimund Schaller from the company Semperit Technische Produkte GmbH for their cooperation.

I would like to dedicate this thesis to my parents and my fiancée Doruk Tayli for their understanding, patience and support in every stage of my life.

December, 2017 Melahat Sahin

AFFIDAVIT

I declare in lieu of oath, that I wrote this thesis and performed the associated research myself, using only literature cited in this volume.

EIDESSTATTLICHE ERKLÄRUNG

Ich erkläre an Eides statt, dass ich diese Arbeit selbstständig verfasst, andere als die angegebenen Quellen und Hilfsmittel nicht benutzt und mich auch sonst keiner unerlaubten Hilfsmittel bedient habe.

_____ _____

Date **Signature**

COOPERATIONS

This PhD thesis has been realized in cooperation with scientific organizations and institutions. They are listed below:

- 3-(trimethoxysilyl)propyl 3-[bis(2,4,6-trimethylbenzoyl)phosphinoyl]-2-methyl-propionate (TMESI^2-BAPO) was provided by **Jieping Wang and Hansjörg Grützmacher**

  Department of Chemistry and Applied Biosciences, ETH Zürich, CH-8093 Zürich, Switzerland

- 1-{4-[2-(3-triethoxysilanylpropylcarbamoyloxy)ethoxy]-phenyl}-2-hydroxy-2-methyl-1-propane-1-one (TESI-IC2959) was provided by **Piotr Roszkowski**

  Faculty of Chemistry, University of Warsaw, Pasteura 1, 02-093 Warsaw, Poland

- Prop-2-yn-1-yl phenyl(2,4,6-trimethylbenzoyl)phosphinate (Modified TPOL) was provided by **Meinhart Roth.**

  Christian Doppler Laboratory for Functional and Polymer Based Ink-Jet Inks, Montanuniversitaet Leoben, Otto-Glöckel-Strasse 2, 8700 Leoben, Austria

- Solid state NMR measurements were carried out by **Santhosh Ayalur-Karunakaran**

  Polymer Competence Center Leoben GmbH, Roseggerstraße 12, 8700 Leoben, Austria

- Transmission electron microscopy (TEM) images of silica particles were provided by **Christoph Gammer**

  Erich Schmid Institute of Materials Science, Austrian Academy of Sciences, Jahnstrasse 12, 8700 Leoben, Austria

- Gel Permeation Chromatography (GPC) measurements were done by **Simone Radl**

  Polymer Competence Center Leoben GmbH, Roseggerstraße 12, 8700 Leoben, Austria

- Tensile test measurements were done by **Evelyn Sattler**

  Polymer Competence Center Leoben GmbH, Roseggerstraße 12, 8700 Leoben, Austria

- X-ray photoelectron spectroscopy (XPS) were carried out by **Baris Kaynak and Denise Dörfler**

  Chair of Chemistry of Polymeric Materials, Montanuniversitaet Leoben, Otto-Glöckel-Strasse 2, 8700 Leoben, Austria

- Zeta potential measurements were conducted by **Inge Mühlbacher**

  Institut für Chemische Technologie von Materialien Stremayrgasse 9, 8010 Graz, Austria

- Single fiber pull-out measurements were conducted in cooperation with **Gerhard Kalinka and Martina Bistritz**

  BAM Bundesanstalt für Materialforschung und -prüfung 5.6, Unter den Eichen 87, D-12205 Berlin

The results of this thesis were published in different scientific publications and two patents.

(1) Sahin, M., Ayalur-Karunakaran, S., Manhart, J., Wolfahrt, M., Kern, W. and Schlögl, S. (2017), Thiol-Ene versus Binary Thiol–Acrylate Chemistry: Material Properties and Network Characteristics of Photopolymers. Adv. Eng. Mater., 19: n/a, 1600620. doi:10.1002/adem.201600620

(2) Sahin, M., Schlögl, S., Kaiser, S., Kern, W., Wang, J. and Grützmacher, H. (2017), Efficient initiation of radical-mediated thiol-ene chemistry with photoactive silica particles. J. Polym. Sci. Part A: Polym. Chem., 55: 894–902. doi:10.1002/pola.28442

(3) Roszkowski, P., Sahin, M., Ayalur-Karunakaran, S., Gammer, C., Schlögl, S., Kern, W., & Krawczyk, K. K. (2017). Synthesis and evaluation of new radical photoinitiators bearing trialkoxysilyl groups for surface immobilization. Polymer, 129: 207-220. doi: 10.1016/j.polymer.2017.09.054

(4) Sahin, M., Krawczyk, K. K, Roszkowski, P., Wang, J., Kaynak, B., Kern, W., Schlögl, S.*, Grützmacher, H. (2017), Photoactive Silica Nanoparticles: Influence of Surface Functionalization on Migration and Kinetics of Radical-induced Photopolymerization Reactions. European Polymer Journal, In press. doi:10.1016/j.eurpolymj.2017.11.046

(5) "Method for Producing a Prophylactic Article" Holzner, A.; Kern, W.; Manhart, J. C.; Sahin, M.; Schaller, R.; Schlögl, S. Patent Number: WO2017147638 A1

(6) Method for Producing a Prophylactic Article" Holzner, A.; Kern, W.; Manhart, J.

C.; Sahin, M.; Schaller, R.; Schlögl, S. Patent Number: WO2017147639 A1

Three bachelor theses were performed within this project. Results of these theses were partially used and cited within this doctoral thesis.

Lin Zequing: Preparation and characterization of thiol-ene and thiol-acrylate networks, bachelor thesis, 2016. Some of the results of this thesis are shown in Section 5.1.

Markus Ast: He performed his experimental studies on the topic of "Synthesis of siloxane based crosslinkers for production of natural rubber based surgical gloves". Some of the results of this thesis are shown in Section 5.2.2.

Johanna Klobasa: Study of network formation of low migratable photopolymers, bachelor thesis, 2017. Some of the results of this thesis are shown in Section 5.3.1.

STUDY OF LOW MIGRATABLE PHOTOPOLYMER NETWORKS

ABSTRACT

Photo-crosslinked materials have widespread applications ranging from medical devices to food packaging. However, migration of chemicals from polymeric networks is a critical issue which does not only limit the use of these materials in many potential application fields but also pose the risk of serious health problems. The aim of this thesis is the preparation of low migratable 3-D polymer networks by taking advantage of light-induced reactions as well as the analysis of the main parameters that influence the network formation and the related network properties (e.g. tensile strength).

In the first part of this thesis, the influence of selected thiol and alkene structures on the network properties of thiol-ene based photopolymers were investigated by photopolymerizing cycloaliphatic and linear thiols with an allyl monomer or its acrylic counterpart. FT-IR spectroscopy was used to evaluate the crosslink kinetics and allowed a comparison of the step growth and chain growth mechanism of the two different systems. Furthermore, mechanical and thermal measurements as well as solid state NMR measurements were conducted to correlate network properties with macroscopic behaviour.

In the second part of this thesis, thiol-ene networks were prepared using low migratable thiol components. Natural rubber (NR) latex was used as the alkene component due to its technological relevance in the production of medical gloves and other products used in medical and nonmedical application. Three different systems of low migratable thiol crosslinker were used. In the first approach, commercially available multifunctional thiols with a high molecular weight were used as crosslinker. The second concept aimed at the synthesis of oligomeric siloxane based thiols, which were then applied as crosslinkers in the UV induced crosslinking of NR. The third system involved the application of thiol functionalized silica and zeolite particles as crosslinkers. Covalent attachment of the thiol groups on the particle's surface was obtained by a convenient silanization method. The use of either functional inorganic nanoparticles or high molecular weight thiols was expected to decrease the extractability of crosslinker from UV-cured NR samples compared to conventionally applied low molecular weight crosslinkers. Thus, these strategies are promising ways to enhance the skin compatibility and biocompatibility of photopolymers (e.g. applied in medical products). Migration of crosslinkers was examined by using a Soxhlet extraction procedure, whilst the extracts were characterized by elemental analysis. Furthermore, tensile tests and swelling measurements were conducted to characterize the mechanical properties of photochemically crosslinked NR films.

The third part of this work focuses on low migratable photoinitiators. The first section describes the immobilization of trialkoxysilyl functionalized photoinitiators onto the surface of silica particles. Immobilized photoinitiators are expected not to migrate out of the polymer network, which is a desired property in the design of photocurable coatings and medical products. The photoactive silica particles obtained under various experimental conditions were characterized and used as initiators in a thiol-ene resin. Network evolution of the resins initiated by the photoactive silica particles and their commercially available counterparts was investigated by FTIR spectroscopy. Migration of photoinitiators was investigated using a Soxhlet extraction procedure. The amount of extractable photoinitiator and cleavage products was evaluated by elemental analysis. In a second approach, a low migratable photoinitiator with a

polymerizable group was used in the UV-curing of NR latex via thiol-ene reaction. Mechanical properties of the cured samples and migration behaviour of the photoinitiator were compared with the samples prepared with the parent initiator.

ENTWICKLUNG UND CHARAKTERISIERUNG VON PHOTOPOLYMEREN NETZWERKEN MIT VERRINGERTEM MIGRATIONSPOTENTIAL

KURZZUSAMMENFASSUNG

Photovernetzte Materialien werden in unterschiedlichsten Industriezweigen wie der Medizintechnik oder der Verpackungsindustrie eingesetzt. Hierbei stellt jedoch die Migration von Chemikalien aus den polymeren Netzwerken einen erheblichen Nachteil dar, der nicht nur den Einsatz dieser Materialien für zahlreiche Anwendungsbreiche einschränkt sondern auch eine Gefahr für die Gesundheit des Verbrauchers darstellt.

Das Ziel der vorliegenden Arbeit umfasst die Herstellung von 3D polymeren Netzwerken, die eine verringerte Migrationsneigung aufweisen. Neben der Migration steht auch die Evaluierung von Schlüsselparametern, die die Netzwerkbildung und die entsprechenden Netzwerkeigenschaften (z.B. Zugfestigekeit) beeinflussen, im Fokus der Dissertation.

Im ersten Abschnitt der Arbeit wird der Einfluss von ausgewählten Thiolen und Alkenen auf die Netzwerkeigenschaften von Thiol-En Photopolymeren untersucht. Die Vernetzungskinetik wird mittels FT-IR Spektroskopie bestimmt und der Stufenwachstums- bzw. der Kettenwachstumsmechanismus der untersuchten Systeme verglichen. Zusätzlich werden die thermischen und mechanischen Eigenschaften der entsprechenden Thiol-En Photopolymere untersucht und Festkörper NMR Studien durchgeführt, um Netzwerkeigenschaften mit makroskopischen Eigenschaften zu korrellieren.

Im zweiten Abschnitt werden Thiol-en Netzwerke mit Thiolen, die ein geringes Migrationspotential aufweisen, hergestellt. Im ersten Lösungsansatz werden kommerziell verfügbare mehrfach funktionelle Thiole als hochmolekulare Vernetzer eingesetzt. Das zweite Konzept fußt auf der Synthese von oligomeren Siloxanen mit funktionellen Thiolgruppen, die als Vernetzer in der Photovulkanisation von NK eingesetzt werden können. Das dritte System zielt auf den Einsatz von modifizierten Silikapartikeln als Vernetzer. Hierbei werden funktionelle Thiole via Silanisierung kovalent an die Oberfläche des anorganischen Füllstoffs gebunden. Durch den Einsatz von funktionellen anorganischen Partikeln und hochmolekularen Verbindungen wird eine verringerte Extraktionsfähigkeit des Vernetzers im Vergleich zu konventionellen Systemen (niedermolekulare Thiole) erwartet. Diese Strategien stellen daher einen vielversprechenden Weg dar, um die Haut- und Bioverträglichkeit von Photopolymeren (z.B. eingesetzt in medizinischen Produkten) zu verbessern. Die Migration der Vernetzer wird mittels Soxhletextraktion charakterisiert, wobei die Extrakte über Elementaranalyse untersucht werden. Zusätzlich werden die mechanischen Eigenschaft und die Vernetzungsdichte der photochemisch vernetzten NK Latexfilme bestimmt.

Der dritte Abschnitt der vorliegenden Arbeit beschäftigt sich mit der Entwicklung von Photoinitiatoren mit geringer Migrationsneigung. Im ersten Schritt werden trialkoxysilyl-funktionelle Photoinitiatoren an die Oberfläche von Silikapartikeln immobilisiert. Auf Grund der kovalenten Bindung an den Füllstoff, sind die immobilisierten Photoinitiatoren nicht mehr in der Lage aus dem Polymernetzwerk zu migrieren, was entscheidende Vorteile in der Herstellung von photohärtenden Beschichtungen und Medizinprodukten bringt. Die photoaktiven Silikapartikel werden bei ausgewählten experimentellen Bedingungen hergestellt, charakterisiert und als Photoinitiator in Thiol-en Harzformulierungen eingesetzt. Die Konzentration des extrahierbaren Photoinitiators sowie der Spaltprodukte wird durch Elementaranalyse ermittelt. In einem zweiten Ansatz wird ein Photoinitiator mit einer polymerisierbaren Funktionalität eingesetzt, der im Zuge der Photoreaktion kovalent an die Polymermatrix bindet. Diese Photoinitiatoren werden für die Photovulkanisation von NK Latex via Thiol-en Reaktion eingesetzt. Die mechanischen Eigenschaften der vernetzten Filme sowie die Extrahierbarkeit des funktionellen Photoinitiators werden untersucht und mit Filmen verglichen, die einen Photoinitiator mit vergleichbarer Grundstruktur aber ohne polymerisierbarer Funktion enthalten.

CONTENTS

1 INTRODUCTION

Over the last decades radiation curing has found broad application in numerous fields, including protective and decorative coatings [1,2], photoresists [3–6], inks [7,8], dentistry [9–13] and medical uses [14]. The continuous demand for radiation curing technology stems from its outstanding characteristics such as short reaction times, processing at room temperature, low energy consumption, low costs, applicability to solvent free formulations [15], and availability of many resin components and light sources, etc. Despite a significant variety of commercially available photoinitiators and crosslinkers, the demand for low-extractable or non-extractable polymeric materials in application areas such as food packaging [16–19], dentistry [20–23] and medical gloves [24–26] push scientists to develop alternative initiators and crosslinkers. Extraction of unreacted initiator or cleavage products is a notably important problem and remains a challenging issue in coating and printing technology [17,18,27].

The migration ability of unreacted components of a resin system is mainly related to their molecular weight. Researches showed that small mobile chemicals present in the materials can leak out if they are brought in contact with food (e.g. food packaging), thus can cause potential health problems [18,27].

Functionalization of low molecular weight photoinitiators with polymerizable groups (e.g. acrylate and alkyne), which are capable of covalent bonding between photoreactive species and the polymer network during the photopolymerization process, is proposed as one strategy towards low migratable photoinitiators [28,29]. In another approach, photoreactive groups were directly copolymerized with selected co-monomers or attached to a polymer backbone as pendant groups [30].

In recent years, many efforts have been put on the development of high molecular weight photoinitiators [18,31]. Although the high photoreactivity of initiators is sacrificed when the migration ability is reduced, the approach is promising to pursue for the synthesis of new polymeric photoinitiators and crosslinkers. In this thesis, siloxane based oligomeric thiol crosslinkers were synthesized and employed to cure natural

rubber (NR) latex by taking advantage of thiol-ene click reactions. In particular, the influence of the thiol structure (SH equivalence, molecular weight and introduction of co-monomers) and the concentration of the crosslinker on mechanical properties and crosslink density of photo-cured NR films was studied. Along with oligomeric thiols providing a tailored SH equivalence and a controlled molecular weight, selected commercially available multifunctional thiol compounds were used as crosslinkers in thiol-ene photoreaction of NR latex.

Another promising way to increase the molecular weight and to reduce migration, respectively, is the covalent attachment of low molecular weight chemicals such as initiators or crosslinkers on the surface of filler materials (e.g. silica). Surface-bound initiators are expected to have less ability to leak out of the polymeric matrix compared to their free counterparts. Surface initiated polymerization has been a widely-used and well described topic in literature [32], in particular for 'living' radical polymerization [33,34]. Covalent attachment of free radical initiators to surfaces has been studied also in a few research papers [35–37] and many patents [38–41] showing the significance of photoreactive particles for industrial applications. In this study, Norrish type I initiators were attached to silica surface and then used in thiol-ene photopolymerization reactions. To demonstrate the versatility of the concept, the influence of the surface modification on the matrix-filler interface was investigated in glass fibre reinforced polymer composites. For this, glass fibre surfaces were modified with trialkoxy silanes bearing either functional acrylate or photoreactive bisacylphosphine oxides moieties. The modified fibres were embedded in a photo-curable acrylate matrix and the interface properties were characterized by single fibre pull-out tests and compared with non-modified glass fibres.

Low migratable photoinitiators and crosslinkers must also fulfil the mechanical and thermal requirements for the related applications without compromising on the performance of the current ones. In this regard, a good balance between molecular weight and sufficient efficiency in the crosslinking reaction plays a key role.

The present thesis gives a comprehensive survey of structure-property relationships in low-migratable thiol-ene photopolymers. In particular, the structure of both photoinitiator as well as thiol crosslinker is correlated with network evolution, mechanical

properties and migration behaviour of the photopolymer networks. Moreover, radiation cured materials that demonstrate both low extractability and excellent mechanical properties have been successfully developed.

2 THEORETICAL BACKGROUND

2.1 Photo-induced Reactions

The history of radiation curing has already begun in Ancient Egypt when embalmers covered dead bodies with a highly aromatic resin and then cured it under sunlight during the mummification process. Although there have been many applied light-induced reactions since then (e.g. first photoengraved printing plate was prepared in ~1815 by Nicéphore Niépce, first synthetic photopolymer was developed by Louis Minks in 1948), the first commercialized product did not come out until the 1960s.

Since the 1960s, radiation curing technology has been notably growing and has found widespread applications in our daily lives such as banknotes, UV printed plastic bottles, UV coated kitchen furniture, radiation cured laser blades, protective and decorative coatings on television cabinets and on various furniture [42].

Radiation curing refers to the utilization of light or high-energy electrons from an electron-beam source for the formation of non-soluble 3-D polymer networks. Photo-induced reactions commonly utilize light with wavelengths at the UV (100-400 nm) and visible region (400-700 nm). X-rays (0.1-10 nm) and γ-rays (0.001 nm) are only used in special applications (e.g. curing of highly pigmented coatings) as high-priced radiation equipment is required. In addition, strong shields are required to ensure the operational safety when working in this region of electromagnetic radiation. In contrast, radio waves (1 billion nm) and microwaves (1 million nm) don`t supply enough energy to induce photoreactions. The wavelength range of the electromagnetic spectrum, shown in brackets, is cited from reference [43], and these wavelength ranges do not have absolute boundaries.

When substances are exposed to irradiation, light can be absorbed, reflected or refracted. Absorption of light leads to excitation of molecules if the absorption spectrum of the molecule overlaps with excitation spectrum of the light source. Principles of excitation and relaxation will be explained in the following sections in detail.

2.1.1 Light Absorption and Emission

When light impinges on a molecule, energy of the photons is absorbed by the electrons of the molecule. Subsequently, the electrons are excited from the ground state to higher energy levels (excited states). The energy difference between ground state and excited states should be equal to the energy of the absorbed photon. The probability of these transitions is different from each other and depends on the type and number of the chromophore groups on the molecule. Combination of all transitions forms the absorption spectrum and provides information about the structure of a molecule. The absorption of an electron takes approximately 10^{-15} seconds.

Excited molecules have very short lifetimes since they are energetically unstable. After the excitation process, three different processes can occur rapidly [44]: (1) Non-radiative relaxation, (2) radiative relaxation (fluorescence or phosphorescence) and (3) photochemical reaction.

In addition to electronic energy states with their vibrational levels, absorption, non-radiative and radiative transitions between these electronic states are represented in the Jablonski diagram (developed by the Polish physicist Aleksander Jabłoński) as shown in Scheme 2.1. Non-radiative transitions are shown by dashed lines and radiative transitions by solid wavy lines. The vibrational ground states of each electronic state are indicated with thick lines, the higher vibrational states with thinner dashed lines. Emission from triplet and singlet states to singlet ground state is referred to phosphorescence and fluorescence, respectively.

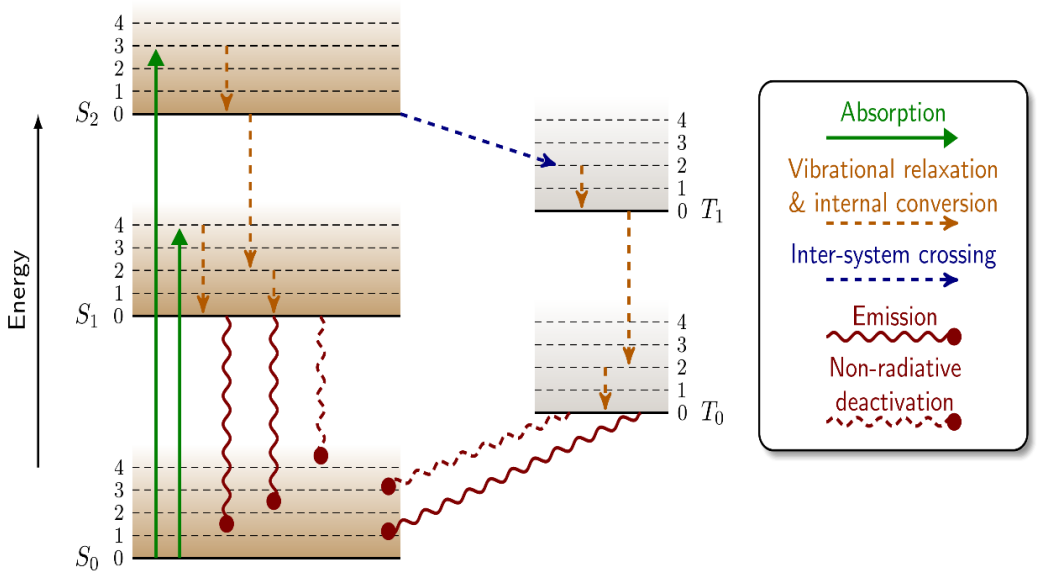

Scheme 2.1: A typical Jablonksi diagram of an organic molecule. Time scales of transitions are dependent on the type of molecule (excerpt from Ref [45]).

(1) Non-radiative transitions: Vibrational relaxations, intersystem crossing and internal conversions are non-radiative transitions. Internal conversion occurs between the two overlapping vibrational levels of different electronic states. Energy transfer between molecules is also responsible for non-radiative transitions. Transfer of energy between molecules can take place through molecular collisions, through quenching or through overlap in absorption and fluorescence spectra [44,46].

(2) Radiative transitions: Two types of radiative transitions are distinguished:

(a) Fluorescence: Based on Kasha`s rule, emission of the absorbed light only occurs from the lowest vibrational state of the lowest excited state (S_1) to the ground state (S_0). This phenomenon is known as fluorescence and occurs in a period of 10^{-9} - 10^{-7} seconds.

(b) Phosphorescence: For phosphorescence radiation, the excited electron undergoes intersystem crossing and changes its spin multiplicity from singlet to the triplet state. When an electron is in its triplet state, it can emit phosphorescence light and return to the ground state in a period of 10^{-4} - 10^{-1} seconds.

(3) Photochemical reactions: Photochemical reactions are defined as reactions induced by light. There are two fundamental laws in photochemistry:

1. Photochemical reactions occur if light is absorbed by molecules and this rule is also known as Grotthuss-Draper law [47].

2. Each absorbed photon causes activation of maximum one molecule, and this "photo equivalence law" is also known as Stark-Einstein law [48].

Photo-induced reactions have countless advantages compared to traditional thermal systems, including: high reaction rates at room temperature, spatial and temporal control of the reaction, and lower energy requirement than thermal polymerization, low costs, applicability to both solvent containing and solvent free formulations, and availability of many resin components and light sources.

There are several kinds of light induced reactions such as photoinduced polymerization and photo-modification [42].

Photo-modification is beyond the scope of this thesis. Thus, the theoretical background of photoinduced polymerization will be detailed in the following section.

A photopolymerizable mixture has two main components: a photoinitiator and a monomer, which has photo-reactive substituents. Depending on the application, a reactive diluent can be added to decrease the viscosity of the reaction mixture. A reactive diluent will participate in the polymerization. In addition to the reactive diluent, some fillers, stabilisers, dyes and other additives are typically added to the formulation to improve the processability and the final properties of the cured materials.

In photoinduced polymerization reactions, the formation of active initiating species is provided by a photoinitiator. Active initiating species can be a radical or a cation. The type of initiating species determines the type of photopolymerizations: “Free radical photopolymerization” and “Cationic photopolymerization”. It should be noted that these terms are also used for crosslinking reactions. Photoinitiators should be selected according to application, resin formulation and emission spectrum of the light source. Other important properties of a photoinitiator include shelf life, thermal stability, and efficiency in producing reactive species, quantum yield and its solubility.

In the following section, a detailed background on free radical photoinitiators is given.

2.1.2 Free Radical Photoinitiators

Free radical photoinitiators absorb light and generate radicals in the most cases from the excited triplet state.

These photoinitiators are classified into two main categories: Norrish type I photoinitiators (cleavage type) and Norrish type II photoinitiators (hydrogen abstraction type)

a) <u>Cleavage type photoinitiators (type I)</u>

Absorption of light by type I photoinitiators (PI) leads to a homolytic bond cleavage at the excited state. Subsequently, at least two different free radical species are produced [49]. These initiators are also called α-cleavage type photoinitiators since most cleavage reactions take place in α-position of the carbonyl group. Scheme 2.2 shows a typical bond cleavage mechanism for type I initiators.

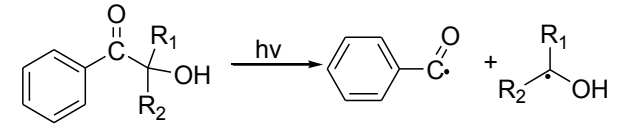

Type 1 photoinitiator-Hydroxyacetophenone

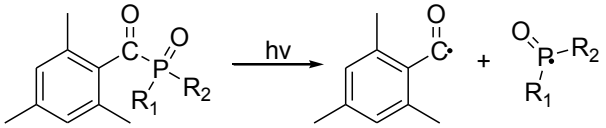

Type 1 photoinitiator-Acylphosphine oxide

Scheme 2.2: Two examples of homolytic cleavage of type 1 initiators upon irradiation (Excerpt from Ref. [50]).

In particular, the structure of the initiator is important in view of quantum yield, reactivity of radicals, absorbed wavelength range and its stability. For example, bis(acyl)phosphine oxide (BAPO) type photoinitiators have outstanding properties such as extended absorption up to 440 nm and rapid photobleaching (deeper light penetration due to transparent cleavage products) and high efficiency for formation of up to four radicals [51]. Thus, BAPO type initiators have found broad applications in outdoor coatings, highly TiO_2 loaded UV ink formulations [52] and applications using sunlight as a light source [53]. For stabilized clear varnish applications, BAPO is used in

combination with α-hydroxy ketone type initiators to increase curing speed on the surface of the coatings [54,55]. However, BAPO's low solubility and/or slow dissolution rate in formulations should be taken into consideration before application.

Oxime ester photoinitiators are soluble in many organic solvents and they have red-shifted maximum absorption [56].

2-Hydroxy-1-[4-(2-hydroxyethoxy) phenyl]-2-methyl-1-propanone) is a hydroxyl alkyl ketone type photoinitiator. It is a highly efficient, non-yellowing photoinitiator and is generally applied in water-borne acrylate based resins. Its absorption is up to 380 nm and it is commonly used in surface curing but is not efficient in thick films.

In addition, most α-amino ketone functional initiators are prone to yellowing.

Properties such as absorption profile, solubility and stability of photoinitiators can be changed by addition of different substituents to their structure. Structures of typical α-cleavage type photoinitiators are shown in Scheme 2.3 [57,58]

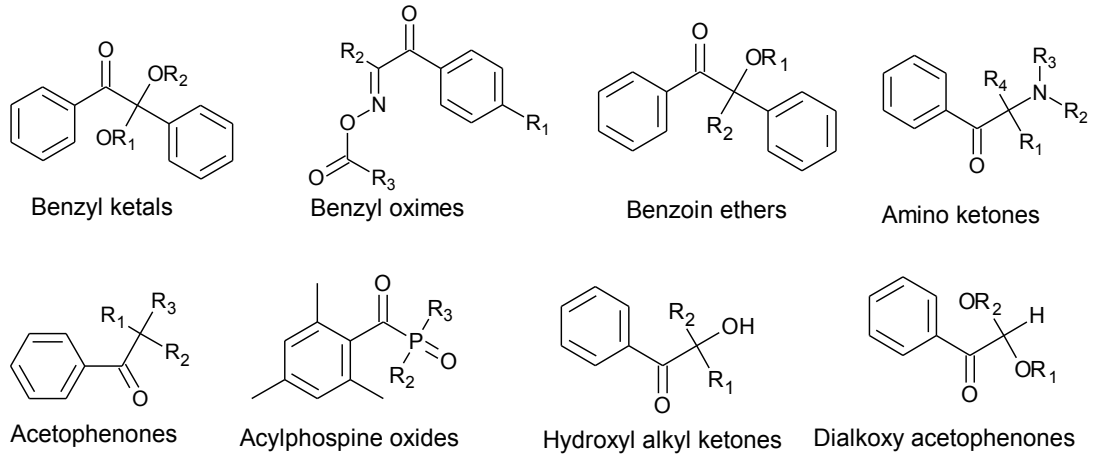

Scheme 2.3: Structures of commonly used type 1 photoinitiators (excerpt from Ref. [57,58])

b) Hydrogen abstraction type photoinitiators (type II)

Type II photoinitiators (sensitizer), unlike type 1 photoinitiators, do not undergo bond cleavage at the excited state since their excitation energy is lower than the cleavage energy of their bonds. Instead, they abstract one hydrogen atom from another molecule (a co-initiator). Since radicals produced by the sensitizer are ineffective to start the polymerization reaction, the co-initiator generates the initiating free radicals. Due to

this different mechanism, hydrogen abstraction type initiators are slower than type I photoinitiators.

Common type II photoinitiators are derivatives of thioxanthone, benzyl, coumarin, camphorquinone and benzophenone [59]. Structures of typical type II photoinitiators are shown in Scheme 2.5 [57]. Frequently used hydrogen donor compounds are ethers, amines, alcohols and thiols.

An exemplary initiation mechanism of type II photoinitiators is shown in Scheme 2.4.

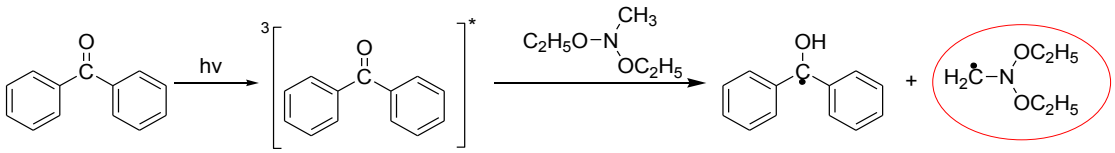

Scheme 2.4: Excitation of a type II initiator (benzophenone) and H abstraction from isopropanol as co-initiator upon irradiation (Excerpt from Ref. [60]).

Benzophenone has been one of the most used type II initiators. However, it does not absorb light in the UVA region. It has an absoption profile starting around ~290 nm and having a maximum of 254 nm. It is one of the shortest wavelength (highest frequency) absorbing photoinitiators for UV curable resins considering that oxygen absorbs light below 220 nm.

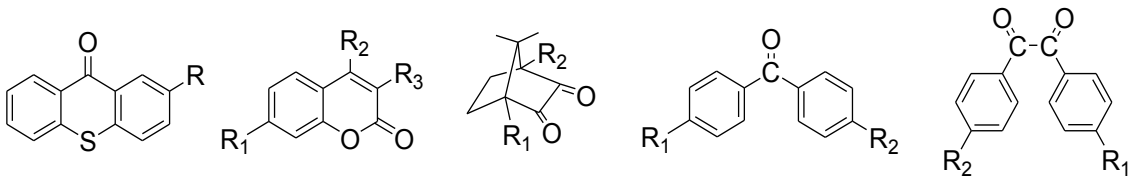

Scheme 2.5: Structures of typical H abstraction photoinitiators (excerpt from Ref. [57])

Important considerations about photoinitiators

There are some factors, which should be considered when using photoinitiators. Some crucial factors are listed below [42,55,61]:

(i) *Light absorption range:* Absorption wavelength of the photoinitiator should match with the emission spectrum of the lamp.

(ii) *Effect of pigments or coloured compounds:* Many pigments are not transparent in the UV region and do not transmit the UV light inside the resin mixture. Thus, only the surface of the resin is cured and deeper layers remain uncured. Acylphosphine oxides were developed to be used in white pigmented solutions. This kind of photoinitiators absorb UV light between 380 - 410 nm and white pigments are transparent in this UV region. Unfortunately, coloured pigments are not transparent in the UV region. Additionally, the pigment concentration is also an important factor in the curing profile of the resins and limits the applicability of photocuring techniques.

(iii) *Wavelengths:* The penetration depth of the light increases with rising wavelength of the light source. Thus, for thick coatings longer wavelength emitting lamps and long wavelength absorbing photoinitiators should be chosen.

(iv) *Molar absorption coefficients:* This parameter is related to the absorbed number of photons. If the molar absorption coefficient is higher, the probability of electronic transitions is also higher and as a result the amount of photoinitiator which is needed for curing is lower.

(v) *Aging*: During aging of the cured resin, some yellowing and discoloration can occur depending on the polymeric material and cleavage products of photoinitiator. This phenomenon should be considered before application of certain materials. UV absorbers and photo-oxidants may be used to decrease any weathering effects.

(vi) *Oxygen inhibition:* Atmospheric oxygen can quench the excited photoinitiator. Oxygen can also react with the cleavage products of photoinitiator and/or radical chains, and oxidize them into peroxides, hydroperoxides and carbonyl groups. To avoid the effect of oxygen, reactions are often carried out under inert gases or carbon dioxide. However, in this case, production cost may increase.

(vii) *Mixture of photoinitiators*: In numerous applications, a mixture of selected photoinitiators is employed to increase the initiation efficiency.

(viii) *Photobleaching of photoinitiators* [43]*:* Some photoinitiators (e.g. cleavage type phosphine oxide initiators) absorb light in visible region (>400 nm) so that their colour is yellow. After cleavage reactions, transparent free radicals form and colour of the photoinitiator disappears. This effect is called photobleaching. Photobleaching is important for production of clear coatings and deeper light penetration.

(ix) *Migration:* Low molecular weight substances can leak out and migrate to the material, which they are in contact with. Volatility and migration of photoinitiators often lead to foul smell and toxicity. Applications of high volatile and migratable photoinitiators should be avoided, especially in food and medical areas.

2.1.3 Low Migratable Free Radical Photoinitiators

Radiation curing is a widely used and well-established technology particularly in UV coatings due to the solvent-free formulations and fast curing speeds. The photoinitiator is one of the main components of a photoactive resin as it forms free radicals upon UV exposure[62,63]. However, diffusion of unreacted low molecular weight photoinitiators and their scission products as well as indirect transfer of the volatile photoinitiators to food and human body pose the risk of health problems especially in packageing industry [64–66]. While the extraction rate of photoinitiators` vapors is related to their boiling point and the chemical composition of the packaging material, the molecular weight of the chemicals is critical for direct migration to the food in contact with the packaging material [64,66]. Unreacted free molecules with a molecular weight around 250 g/mol are expected to migrate while their extractability decreases significantly when the molecular weight is around 500 g/mol [43]. Furthermore, the transfer of chemicals from the surface of the coating to a contact substance is affected by curing conditions of the coating (e.g. thickness of coating, radiation dose, degree of crosslinking) and storage environment of the final product[43]. If the curing process is performed under inert atmosphere (e.g. nitrogen, argon) the curing degree at a lower amount of photoinitiator might be improved, thus causing less amount of extractables and odour [67].

The most convenient strategy to prevent migration of photoinitiators is the use of high molecular weight compounds (>1000 g/mol) [30,43,68,69]. In this concept, many groundbreaking ideas have been proposed in literature. Self-initiating technology was introduced by Esselbrugge in which photo-labile chromophores are attached on the acrylate based oligomeric units [70]. Self-initiating resins do not require utilization of any separate initiators. The structure of an exemplary self-initiating resin is shown in Scheme 2.6.

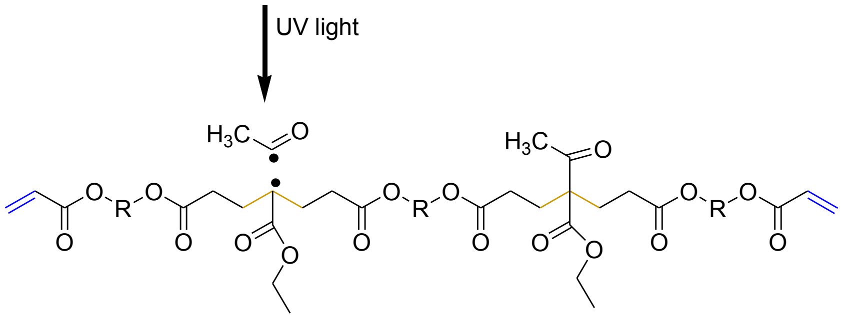

Scheme 2.6: An acrylate ester and beta ketoester functional oligomer structure and its photoreaction (excerpt from reference [70])

Another strategy towards high molecular weight photoinitiators involves the attachment of initiating moieties on polymer chains as end groups or pendant structures. Furthermore, photoinitiating species could be randomly distributed along the polymer chain. Some polymeric phototoinitiator structures are exemplified in Scheme 2.7.

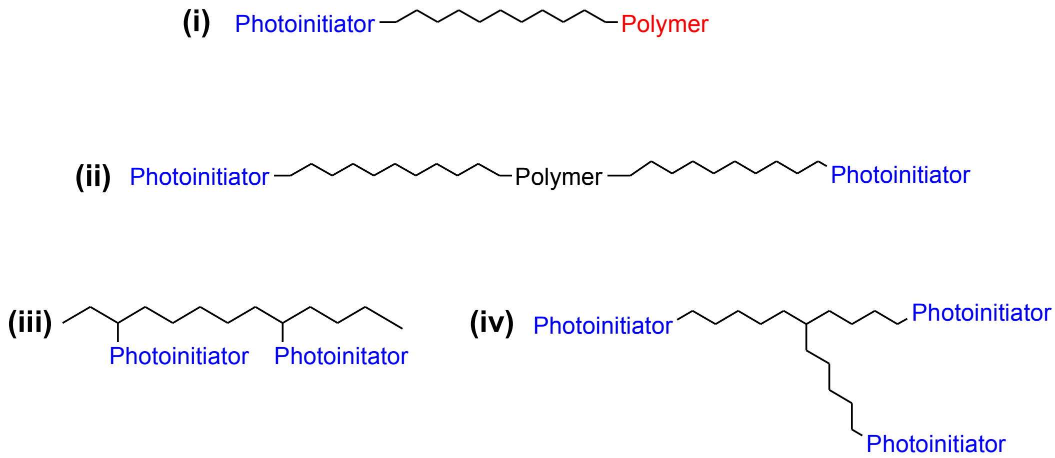

Scheme 2.7: Selected polymeric phototoinitiator structures (excerpt from [43])

Molecular organization of initiating species on the polymer chain affects the whole reactivity of polymeric photoinitiators. Pendant initiator moieties are expected to be sterically hindered while terminal ones are more convenient to react [71]. Moreover, the photoreactivity of a polymeric photoinitiator depends on both the type as well as the molar fraction of photoinitiating species.

Another approach towards low migratable photoinitiators is the utilization of monomeric initiators with polymerizable functions [62,72]. Polymerizable groups should be attached to less reactive part of the Type 1 photoinitiators. Although the extractable amount of photoinitiators is decreased due to the covalent bond formation between the

polymerizable group of photoinitiator and resins, such systems suffer from low reactivity [73].

Another strategy to increase the molecular weight of photoinitiators is the covalent attachment of low molecular weight initiators on the surface of filler materials (e.g. silica). Surface initiated polymerization is a well described topic in literature [32], in particular for 'living' radical polymerization [33,34]. Covalent attachment of free radical initiators to surfaces has been also studied in a few research papers [35–37] and many patents [38–41] showing the significance of photoreactive particles for industrial applications.

Some practical factors should be considered when using high molecular weight photoinitiators; (i), they increase the viscosity of the resin mixture, (ii) the solubility of polymeric photoinitators is different than their monomeric counterparts, and (iii) a higher weight percentage of polymeric initiator is required to reach the equal molar concentration of initiating species compared to monomeric photoinitiators.

2.1.4 Free Radical Photopolymerization

In photopolymerization reactions, a photoactive liquid resin mixture (containing monomers and initiator) is converted to a solid polymeric material due to a radiation induced chemical reaction [15,74]. Free radical photopolymerization reactions are initiated by free radical photoinitiators. In the scope of this study, the focus will be on the photopolymerization of (meth)acrylate and thiol-ene systems.

a) (Meth)Acrylate Photopolymerization

Photopolymerization of acrylate and methacrylate based functional monomers is widely used in industry such as dental fillings, coatings and it has also attracted increased attention in the growing field of additive manufacturing [75,76]. There are several advantages of commonly used (meth)acrylates such as fast curing rates and excellent storage behaviour. Depending on their structure, highly photo-crosslinked (meth)acrylates may comprise a high resistance to chemicals, temperature and light [77]. (Meth)acrylate polymers with aromatic units are hard materials while low-modulus (meth)acrylate based elastomers can be produced by introduction of linear aliphatic chains to the (meth)acrylate structure [77].

A general mechanism of acrylate photopolymerization is shown in Scheme 2.8.

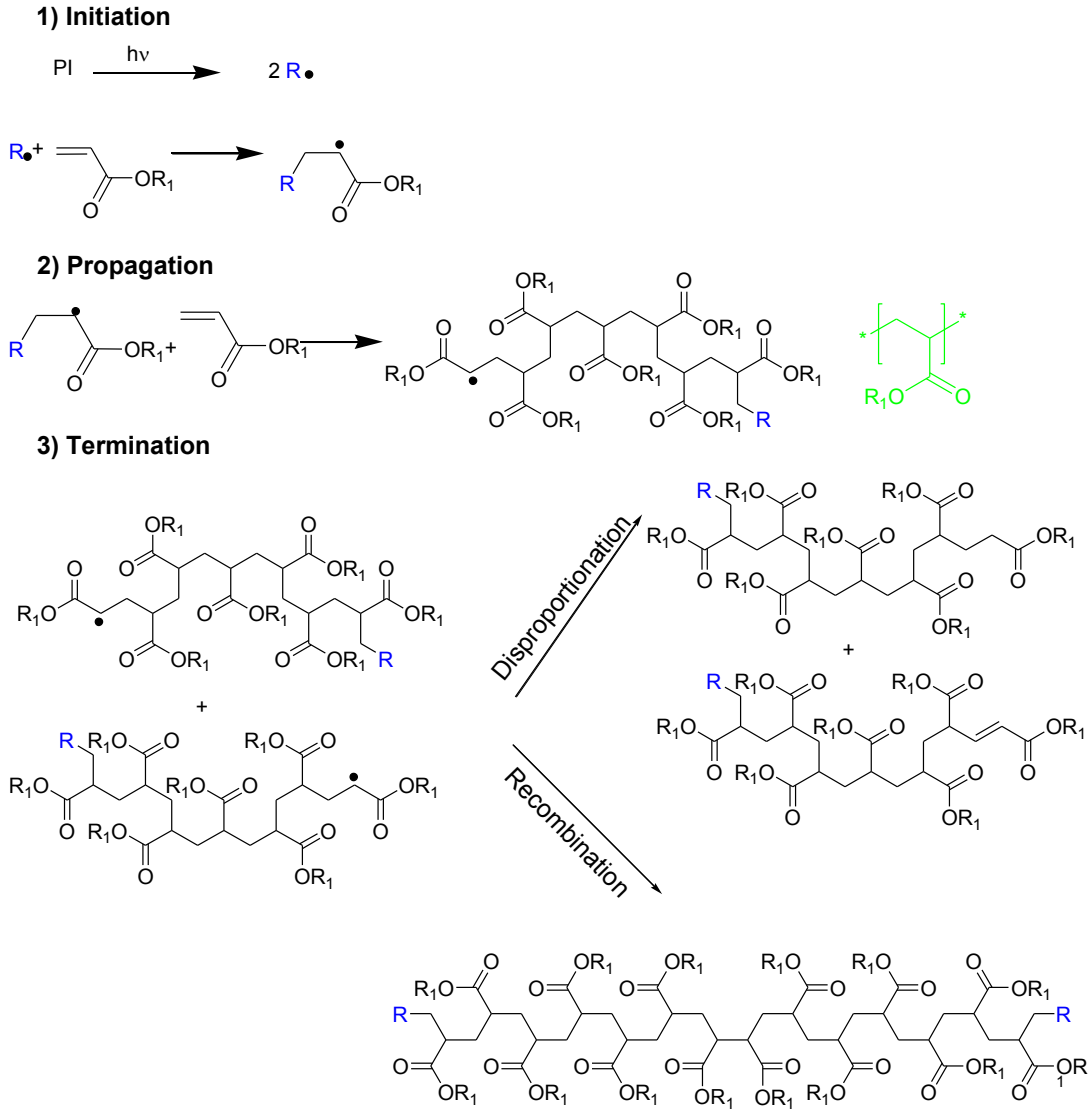

Scheme 2.8: A general mechanism of the photopolymerization of acrylates

(Meth)acrylate photopolymerization is based on chain-growth mechanism, in which polymers are obtained by addition of monomers to a growing chain. The chain-growth mechanism involves three main steps: initiation, propagation and termination. In the first step of free radical photopolymerization of (meth)acrylates, free initiating radicals are created upon the bond cleavage of an electronically excited photoinitiator. The free radicals attack the C=C bond of the (meth)acrylic monomer, and alkyl radicals are formed. In the propagation step the activated monomer radical reacts with the C=C bond of a second monomers. Finally, termination occurs through a radical combination

of growing chains or hydrogen abstraction of one chain from the other chain (disproportionation).

(Meth)acrylates are known for their inhomogeneous network formation, low monomer conversion and internal shrinkage stress [75,78,79]. Methacrylates show less toxicity compared to acrylates [79].

One drawback of (meth)acrylate photopolymerization is oxygen inhibition as shown below [58,80,81].

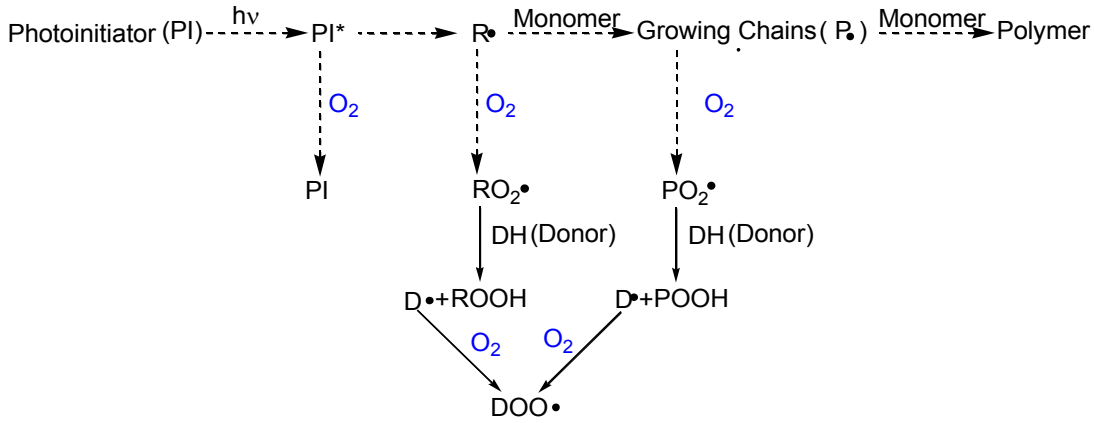

Scheme 2.9: Inhibition of (meth)acrylate photopolymerization by oxygen (Redrawn from reference[58,82])

Due to the high sensitivity to oxygen inhibition, the surface of (meth)acrylate based thin coatings remains uncured. The use of high lamp intensity and high concentration of initiator are strategies to decrease/eliminate oxygen inhibition [83,84]. Furthermore, reactions can be also carried out in inert atmosphere (nitrogen or carbon dioxide), at low temperatures to prevent oxygen inhibition. Other approaches rely on the employment of highly viscous resins and the application of the resins in thick layers [83].

b) Thiol-ene Photopolymerization

Thiol-ene photopolymerization describes an addition reaction between thiols and alkenes in the presence of initiating radicals formed by exposure to light. Addition of elemental sulphur to unsaturated polymers was first discovered by Goodyear in 1839 and known as vulcanization [85]. In 1905, Posner showed the addition of thiols to olefins [86]. Since then many scientists focused on the thiol-ene reaction's mechanism and its industrial applications. In 1993, a review on free radical thiol-ene photopolymeri-

zation was published [42]. In 2004, Hoyle et al. published a detailed review about reaction mechanism, kinetics, stability and applications of thiol-ene reactions. This reaction is a "click" reaction due to its outstanding advantages such as high efficiency, high speed, low shrinkage, availability of many starting compounds and low oxygen inhibition. Recent years have witnessed countless applications of thiol-ene click chemistry such as protective coatings [87–91], printing inks [92,93] and optical & electronic adhesives [94–96]. A general mechanism of thiol-ene photopolymerization is shown in Scheme 2.10.

In the first stage of the reaction, initiator radicals are formed after excitation of photoinitiator molecules. This process is typically induced by light. Subsequently, the free initiating radicals abstract a hydrogen atom from the thiol leading to the formation of thiyl radicals [14]. Previous studies showed that thiol-ene reactions also proceed in the absence of photoinitiator, due to a UV induced bond scission of the thiol moiety [74]. However, the reaction rate is much lower than in the presence of a photoinitiator.

The propagation step involves the addition of the thiyl radical to a C=C bond. Thus, a thioether link together with carbon-centered free radicals is formed. These free radicals abstract a hydrogen atom from another thiol groups and lead to formation of new thiyl radicals. This process is a repeated process, and is known as step-growth mechanism. An ideal thiol-ene reaction proceeds only by step-growth mechanism. However, reactivity of most alkenes is higher than thiols in most cases and carbon centered radicals can also attack other double bonds (homopolymerisation). Consequently, olefins are consumed faster than thiol components.

Termination of the reaction occurs by recombination of two radical species.

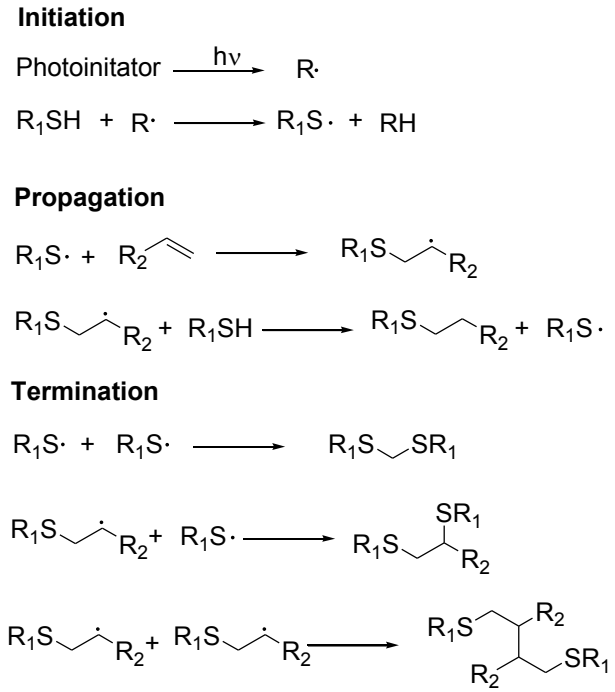

Scheme 2.10: General mechanism of thiol-ene photopolymerization [Redrawn from Reference [14]]

Monomer structures used in thiol-ene photopolymerization strongly affect the reaction kinetics and the properties of the cured photopolymers. Structures of common, commercially available "ene" and thiol functional monomers are shown in Scheme 2.11 and 2.12, respectively.

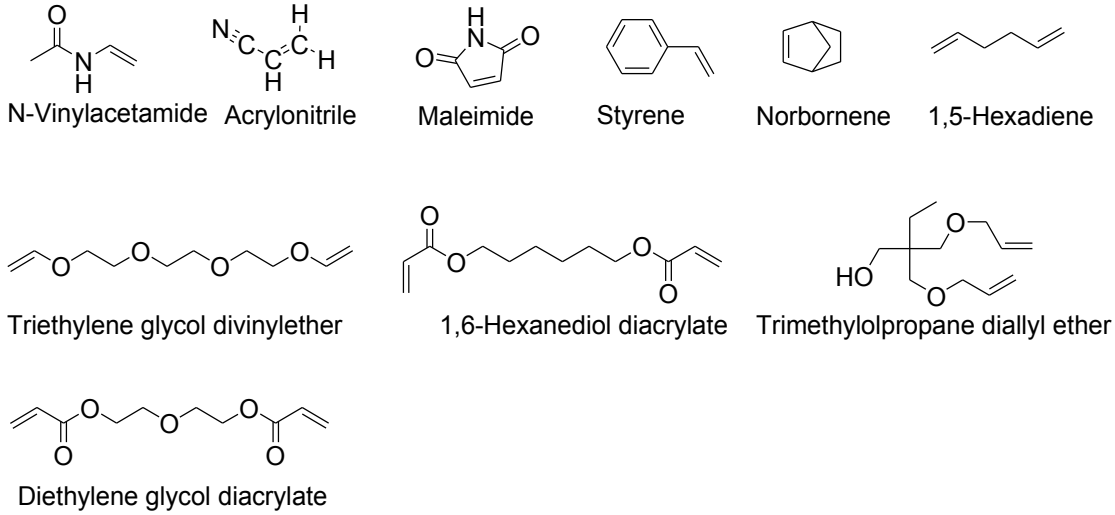

Scheme 2.11: Structures of selected alkenes used in thiol-ene photopolymerization [excerpt from reference [97]]

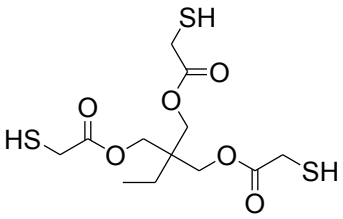

Trimethylolpropane tris(2-mercaptoacetate)

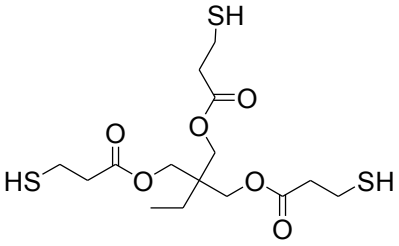

Trimethylolpropane tris(3-mercaptopropionate)

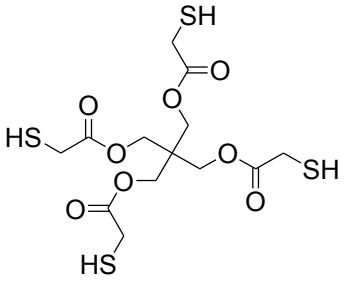

Pentaerythritol tetrakis(2-mercaptoacetate)

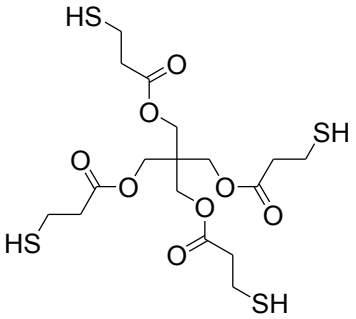

Pentaerythritol tetra(3-mercaptopropionate)

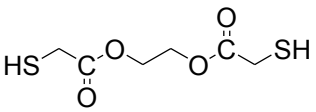

Glycol dimercaptoacetate

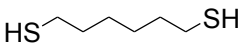

1,6-hexanedithiol

Scheme 2.12: Structures of selected thiols used in thiol-ene photopolymerization

Studies on the reaction kinetics of the thiol-ene photopolymerization revealed that the reaction rate strongly depends on the alkene structures [97,98]. Most alkenes with electron donating groups react faster than alkenes bearing electron withdrawing groups. In addition, non-conjugated dienes react faster than conjugated ones. The reactivity rate of alkenes can be ordered as follows [97]:

Norbornene > Vinyl ether > Propenyl > Alkene

Vinyl ester > *N*-Vinyl amides > Allyl ether

Allyl triazine > *N*-Vinyl amides > Allyl ether

Allyltriazine ~ Allyl isocyanurate > Acrylate > Unsaturated ester > *N*-substituted maleimide > Acrylonitrile ~ Methacrylate > Styrene > Conjugated dienes

Along with the alkene, the structure of the thiol component also affects the rate of thiol-ene reaction. There are some reports revealing that alkyl 3-mercaptopropionates

react faster than alkylthioglycolates which in turn are more reactive than alkylthiols [97] [42]. However, this order can also change depending on the alkene structures.

In addition to the type of functional groups (allylic, acrylic etc.), aromaticity, flexibility as well as multiplicity of functional groups have a strong influence on rate and conversion[99,100].

Despite many advantages, some thiol-ene base systems suffer from bad odour of the thiol component and yellowing of the cured polymer. However, several alternative low-odour monomers are commercially available which could be applied to decrease the problems to minimum.

In this thesis, high molecular weight thiol functional oligomeric siloxanes were synthesised. Owed to the high molecular weight, they are expected to comprise not only a reduced migration behaviour but also a reduced volatility and odour. The following section will be about general synthesis routes of polysiloxanes.

2.2 Synthesis of Functional Polysiloxanes

Silicone or siloxane polymers are referred to a group of polymers, which have alternated silicon-oxygen bonds (Si-O-Si) in their backbones. The general structure of a polysiloxane is illustrated in Scheme 2.13.

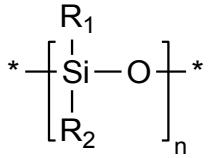

Scheme 2.13: General structure of siloxanes (R= methyl, phenyl, vinyl, etc.)

General properties of polysiloxanes are a low glass transition temperature (T_g) and a high flexibility. They also show outstanding properties such as biocompatibility, gas permeability, oxidative and thermal stability [101,102]. Siloxanes have partially ionic character due to the high electronegativity difference between silicon and oxygen atom. The electronegativity of silicon and oxygen is 1.7 and 3.5, respectively, based on Pauling electronegativity scale [101]. It should be noted that the 3-D structure of the polymers significantly influence the material properties of the polysiloxanes. Three

dimensional cubic, spherical or crosslinked siloxanes exhibit different properties compared to two- dimensional ladder and sheet like siloxanes [103].

On the flexible backbone of the siloxane polymers, various substituents (such as methyl, phenyl, hydrogen, acrylate, vinyl, thiol, epoxy etc.) can be introduced by side chain modification. Copolymeric and end-terminated siloxanes are also industrially available for various applications.

Organo-functionally terminated silicones are prepared via different strategies such as equilibration (redistribution) polymerization [101,104,105]. In this method, cyclic siloxanes are polymerized by ring opening mechanism in the presence of a strong acid (e.g. sulphuric acid) or a strong base as catalyst (e.g. tetraalkylammonium hydroxide and sodium hydroxide) [101]. This method also involves organofunctional end capping agents, which are used to terminate the chain ends. End capping agents have an important role in controlling the molecular weight of the resulting polymer and creation of telechelic polymers (telechelic polymers have organo-functionality at both chain ends). While equilibration polymerization is suitable for large-scale production, the polymers suffer from a high polydispersity. Nevertheless, equilibration polymerization is widely used in industry for production of high molecular weight siloxanes.

Polysiloxanes with narrow molecular weight distribution are typically synthesized via anionic or cationic ring opening polymerization. Starting compounds are again cyclic siloxanes -commonly D3 and D4 structures which are composed of three and four silane units, respectively (see Scheme 2.17 for D3 and D4 structures). Anionic ring opening polymerization (AROP) is typically initiated by organolithium bases [106,107]. Commonly used initiators are *n*-butyllithium and *sec*-butyllithium. Solvents with a low polarity such as tetrahydrofuran and toluene are often used.

Cationic ring opening polymerization of siloxanes is initiated by trifluoromethanesulfonic acid, lewis acids and cationic carbons as initiators [106]. It is characterized by lower polymerization rates than AROP.

Ionic (cationic & anionic) ring opening polymerization is a type of living polymerization technique, so it also has advantages and disadvantages of this technique. Along with narrow molecular weight distribution it benefits from the possibility to functionalize the living end of the polymers by modified termination agents [107]. It also allows

the preparation of block copolymers. Another advantage is the control of molecular weights by simply changing monomer to initiator ratio. However, the polymerization reaction suffers from high sensitivity against oxygen, water and carbon dioxide.

After a short introduction to ionic ring opening polymerization and equilibration polymerization methods, the following section will be focused on hydrolytic polycondensation of silanes, since this method was used for synthesis of thiol functional oligosiloxanes in this study.

Hydrolytic Polycondensation

In hydrolytic polycondensation, organosilane agents are used as starting monomers to obtain oligo- or polysiloxanes. General structure of an organosilane molecule is given in Scheme 2.14.

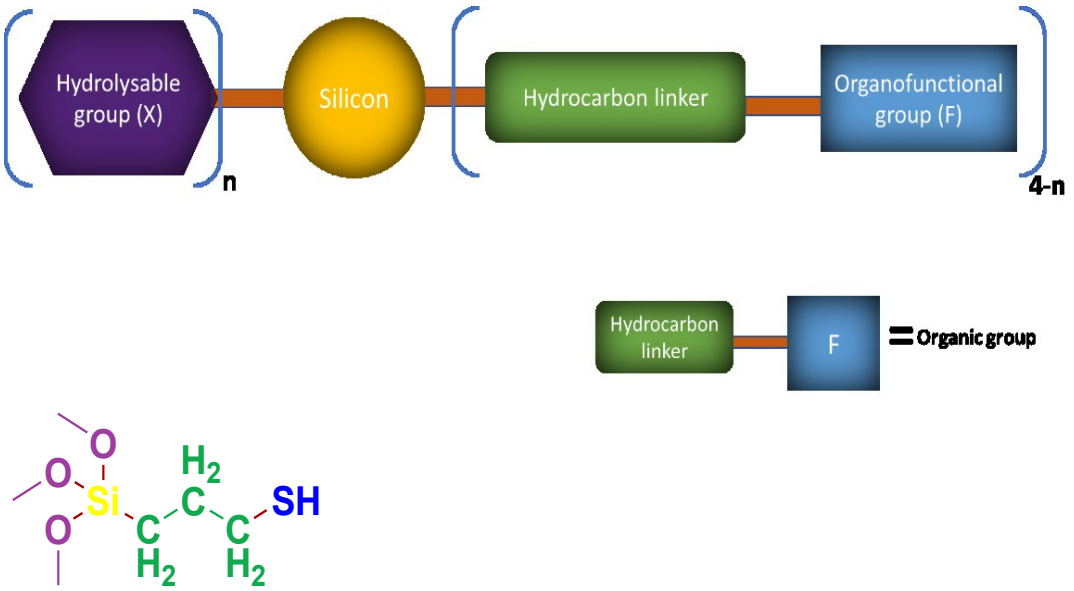

Scheme 2.14: General structure of silanes and the structure of (3-mercaptopropyl) trimethoxysilane as commercially available functional monomer

A typical organosilane agent has two different functional groups: non-hydrolyzable organic groups and hydrolysable groups. General hydrolysable groups (X) are alkoxy, acyloxy, halogen, isocyanate or amine. Methoxy, ethoxy and chloride groups are the most encountered hydrolysable groups. Hydrolysable groups are directly linked to the

silicon atom. The organic part of a silane molecule is linked to the silicon atom through a carbon-silicon bond. The organic part can bear reactive functional groups (F) such as epoxy, amino, thiol, methacrylate and vinyl moieties or it can contain non-reactive hydrocarbon chains. The type of organo-functional group and the spacer (linker) length is important for desired characteristics.

In silicone chemistry, polycondensation of silanes is an important route to produce polysiloxanes. In this method, silanols are firstly formed during hydrolysis of silanes, then silanol groups condense with each other to form oligomeric or polymeric molecules [108]. Rate of hydrolysis and condensation reactions are strongly dependent on the concentration of silane based monomers, pH value and temperature. Hydrolysis of alkoxy silanes has been intensively investigated in literature. Both acids and bases catalyse the hydrolysis. Researches showed that the hydrolysis rate of alkoxy silanes is slowest at neutral pH and increases in both acidic and basic pH values in excess available water [108,109].

Hydrolysis reactions proceed via nucleophilic substitution mechanism through a pentavalent state of the Si atom. Scheme 2.15 shows an (a) acid and (b) based catalysed mechanism of the silane hydrolysis [110].

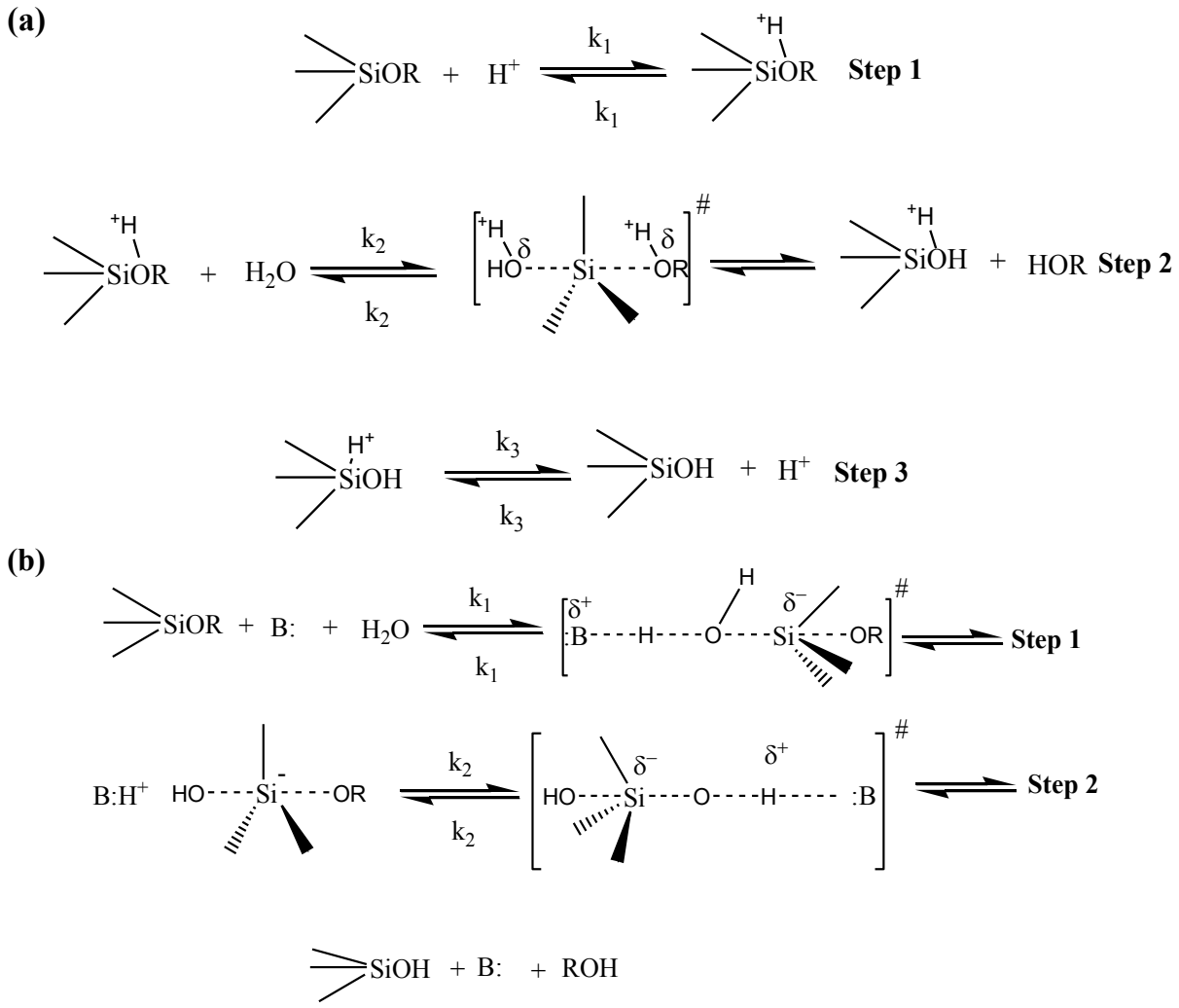

Scheme 2.15: (a) Acid and (b) base catalyzed hydrolysis mechanism of alkoxy silanes (proposed by F. D. OSTERHOLTZ and E. R. POHL)

The condensation rate of alkoxysilanes is also affected by changes in the pH value and undergoes a minimum around a pH of 4 (depending on the organic substituent this minimum can shift) [108].

Hydrolytic polycondensation of silanes with three hydrolysable groups results in the formation of gels, cubic-, ladder- or cage structures. Siloxanes with random branched structures, ladder like and cage structures are three main classes of silsesquioxanes. Silsesquioxanes have the empirical formula of $RSiO_{1.5}$. Example structures of silsesquioxanes are shown in Scheme 2.16.

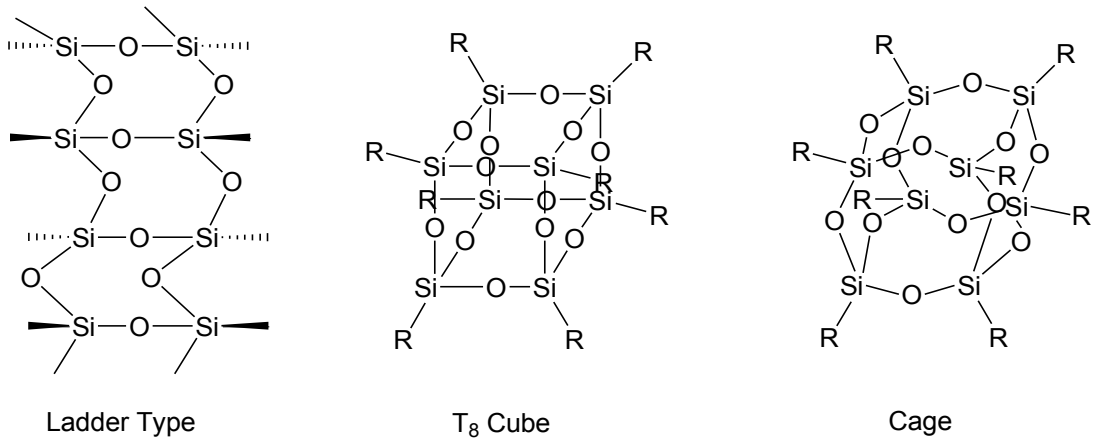

Scheme 2.16: Structure of silsesquioxanes

Basic conditions in general lead to the formation of insoluble gels. However, some base catalysed reaction conditions also result in the formation of silsesquioxanes [111].

Silsesquioxanes have distinguished properties such as outstanding mechanical properties, thermal stability and high optical clarity. Hence, they have applications in heterogeneous silica supported transition metal catalyst systems, hard coatings, electronics, cosmetics, production of ceramic materials and composites, etc. [111–115].

Polycondensation of silanes with two hydrolysable groups is applied to produce a mixture of linear and cyclic siloxanes (mostly D3, D4 structures, see Scheme 2.17). Higher concentration of the silane in the beginning of the reaction results in more D4 structure than D3 structure. These cyclic structures are used to produce high molecular weight polysiloxanes as already mentioned above.

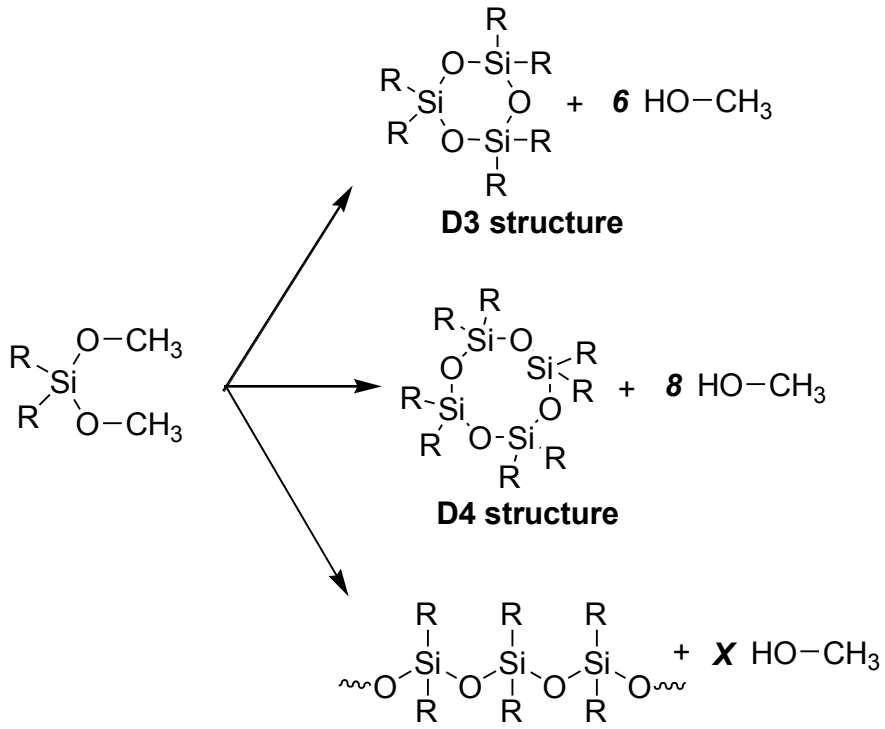

Scheme 2.17: Hydrolysis and condensation of silanes with two hydrolysable groups.

Polymers obtained via hydrolytic polycondensation method generally have a high polydispersity.

In this study, thiol and acrylate functional dialkoxy silanes were used as starting monomers to synthesize thiol functional homo-or co-oligomeric siloxanes. After characterization with GPC and ^{1}H-NMR techniques, their efficiency to crosslink NR latex was tested by taking advantage of thiol-ene click reactions.

In the following section, the modification of inorganic surfaces via convenient silanization will be detailed. In the present work, the surfaces of inorganic particles such as silica, and zeolite as well as glass fibers were modified by the condensation reaction of selected functional organosilanes across the surface hydroxyl groups of the inorganic substrate. Subsequently, the modified particles were used as crosslinker, initiator and adhesion promoters.

2.3 Modification of Inorganic Surfaces

Along with polymerization reactions, functional siloxanes are often used in the side chain modification of polymers. The modified polymers are then conveniently cross-linked across the hydrolysable pendant groups (e.g. alkoxy groups) [116].

Since the 1950s, organosilanes are also widely used in the modification of inorganic surfaces to control the interface properties in composite materials (e.g. increased adhesion between inorganic and organic materials and improved dispersibility of inorganic filler in a polymer matrix) [110,117]. Typically, the functional silanes are immobilized onto inorganic materials bearing hydroxyl groups on their surfaces such as silica, glass, alumina silicates and quartz. In contrast, alkali metal oxides and carbonates don`t form stable Si-O bonds.

The reactions mechanism of a silanization process is shown in Scheme 2.18 (see section 2.2 for a general organosilane structure). In the first step of the silanization, the alkoxy groups of the organosilane are hydrolysed in the presence of water to form silanol groups. Water is either present in the reaction medium as a solvent or is adsorbed on mineral surfaces such as silica and zeolite. Even moisture in the atmosphere can trigger the hydrolysis reaction. The silanol groups undergo a condensation reaction with each other and form hydrogen bonds with the hydroxyl groups on the inorganic surface. These hydrogen bonds are converted to covalent bonds after drying step at elevated temperature. In general, hydrolysis, condensation and hydrogen bond formation occur simultaneously (for details of hydrolysis and condensation, see Section 2.2). Both hydrolysis as well as condensation reactions are reversible.

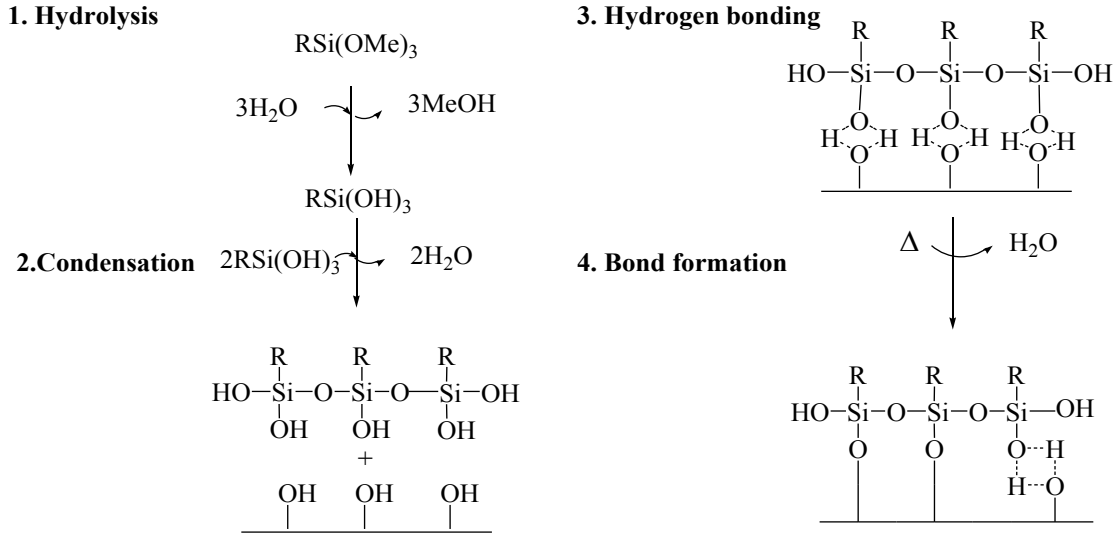

Scheme 2.18 Mechanism of the silanization of inorganic surfaces under hydrous conditions (redrawn from [118,119])

It should be noted that silanization reactions can also be conducted in anhydrous media. In this case, reaction conditions involve longer reaction times (e.g. 4-12 hours) and higher temperatures (e.g. 50-120°C).

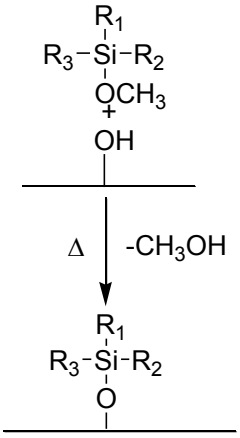

Scheme 2.19: Mechanism of the silanization of inorganic surfaces under anhydrous conditions

As already described in the silanization reaction mechanism, the density of silanol groups on the inorganic surfaces is an extremely important factor for the efficiency of surface modification [120,121]. In case of low silanol density on the particle surface, creation or activation of hydroxyl groups on the substrate's surface is beneficial prior to silanization as pointed out in literature. Dugas et al. demonstrated that rehydroxylation

of fumed silica is achieved by treating the filler for 4 h in boiling water [122]. Hydrogen fluoride etched silicon wafers were exposed to various acid mixtures (HNO_3, H_2SO_4–H_2O_2, HNO_3–HF, and H_2SO_4–H_2O_2–HF) for hydroxylation in another study [123]. Direct exposure of glass surfaces to wet cleaning agents such as methanol/HCl, H_2SO_4, NaOH, piranha and $K_2Cr_2O_7/H_2SO_4$ is also known to increase the amount of surface hydroxyl groups [124].

Furthermore, oxygen and air plasma is often applied not only to remove the organic contaminants but also hydroxylate the surfaces [121,125]. Elimination of organic impurities and activation of surface hydroxyl groups of stainless steel is also ensured by corona discharge technique as shown by Kaynak et al. [126]

Evolution of hydroxyl groups can be monitored by infrared spectroscopy. Silica surfaces exhibit characteristic Si-OH stretching vibrations at 3600 cm^{-1} (broad band) for hydrogen bonded silanols, while the peak at 3745 cm^{-1} (sharp) is attributed to isolated silanols [122,127]. The silanol density can be measured using thermal analysis as well as chemical grafting methods (e.g. silane grafting) whilst multiplicity of hydroxyl groups (single or geminal) can be measured by solid state NMR [122,128].

After elimination of impurities and activation of hydroxyl groups, oxide surfaces are treated with the selected organosilane.

Various methods can be applied for silanization of inorganic surfaces [129]: vapour phase deposition, anhydrous liquid phase deposition, spray-on method, deposition from aqueous alcohol solutions. In these methods, reaction conditions such as silane concentration, reaction temperature, drying (curing) temperature are important parameters as pointed out in various literature. However, general methods are summarized as following:

(i) Vapour phase deposition [130,131]: This method provides uniform silane monolayers on oxide surfaces. A chemical vapour deposition (CVD) system is used for this technique. In laboratory scale, this method can be applied using a desiccator. Silane vapours are deposited on the substrates inside the desiccator under vacuum at elevated temperature. It should be noted, that only a low amount of silane agent is required in this method.

(ii) Spray-on-method [132]: Filler and pigment materials can be silanized with this method. Silane solution in alcohol is pumped into the mixing powder in spray form. Then, the treated particles are dried. This process requires a high intensity mixer for solids. Water for hydrolysis of silane is assumed to be present on the surface of the particles.

(iii) Deposition from aqueous alcohol solution [133,134]*:* Alcohol-water solutions (generally 5% water and 95% alcohol) typically contain methanol, ethanol and isopropanol as alcohol component. Solution's pH value is adjusted to 4.5-5.5 with acetic acid. 1-2 wt.% silane is added to the solution under stirring. After hydrolysis of the silane (around 5 min), particles or large objects are put into the silane solution. In the case of particles, the solution is stirred. After the reaction time, the particles are filtered, dried and washed. In some applications, washing off the excess of silane is conducted prior to the drying step. In the case of chloro, epoxy and amino functional silanes, addition of acetic acid should be avoided since epoxy groups are sensitive to acidic and basic conditions (hydrolysis of the epoxy ring) and amino silanes form basic solutions. Chloro silanes readily form HCl in hydrous condition during hydrolysis.

(iv) Anhydrous liquid phase deposition [135–138]*:* The silane solution contains anhydrous solvents such as toluene, dichloromethane and tetrahydrofuran. After the addition of the particles, the solution is heated to reflux temperature under stirring. Long reaction times (e.g. 3 to 24 h) are applied. Then, filtration, washing and drying steps are carried out. A catalyst (2-3 wt.% of silane) such as *p*-toluene sulfonic acid, dibutyldiacetoxytin and titanium isopropoxide are often added to increase the efficiency of the silanization.

Drying of the treated particles or surfaces is generally carried out at 100-120 °C for a few hours.

Chemical modification of surfaces with silane agents has found broad applications in industry. Dipodal organosilanes with perfluorinated carbon units were used to produce anti-adhesive coatings by Kaynak et. al for injection molding tools [126]. Silanization reactions are also used for biological applications. In one study, (3-aminopropyl) triethoxysilane (APTES) was deposited on glass surfaces using different silanization methods to form an amine- reactive film [139]. In another study, the silicon surfaces were modified with APTES to provide uniform and stable surfaces for immobilization

of the biomolecules [140]. Preparation of an aqueous suspension of organosilanized colloidal silica particles was described in one patent[141] and possible applications were stated as density gradient separation media, anti-abrasion coatings and toner materials. In a different study, glass surfaces were modified with alkoxysilyl functional photoinitiator, and then acrylate based polymer chains were grafted from photoactive glass surfaces[35]. The silanization concept is also applied to improve the interfacial adhesion between glass fibers and matrix resins[142]. Furthermore, silica particles were modified with (3-triethoxysilylpropyl)-tetrasulfide (TESPT) before inclusion of them to styrene-butadiene rubber (SBR) and polybutadiene rubber (BR) blend to supply covalent bond between silica filler and rubber [143].

2.4 Characterization of Network Structures

2.4.1 Swelling

One of the characteristic property of polymeric networks is their ability to swell in good solvents. When a crosslinked polymer is placed in a good solvent, the outer surface of the polymer interacts with the solvent and the solvent molecules migrate inside the network. The swelling process stops when the network comes to a steady state. In the steady state, there is an equilibrium between the elastic forces caused by polymeric network and free energy of mixing. The swollen state is affected by temperature, solvents, pH, nature of the polymer, number of crosslinking points, etc.

Crosslinked polymers contain an insoluble network and unreacted starting compounds (monomers, initiators, crosslinkers, etc.) [144]. During the swelling process, unreacted chemicals and unattached polymer chains are dissolved in the solvent. Swelling experiments can be easily applied to characterize the fraction of soluble and insoluble parts. Insoluble network constitutes the gel fraction of the polymer whilst the soluble part is referred to the sol fraction [144]. Gel and sol fraction, crosslinking density, molecular weight between crosslinking points and swelling degree can be calculated by equilibrium swelling measurements.

The swelling degree of a network can be calculated using initial and swollen weights of the polymer as shown in Equation 2.1. In a typical experiment, the crosslinked polymer is weighed and placed in a good solvent. A good solvent is meant to be capable

to induce swelling of the network and to solubilize the unattached polymer and unreacted starting compounds. During swelling measurements, the polymer is removed from the solvent, wiped off and weighed. Swelling equilibrium of gels is determined by the weight of the swollen sample.

$$Swelling\ degree = \frac{Swollen\ weight}{Initial\ Weight} = \frac{m_{swollen}}{m_0} \qquad 2.1$$

Gel fraction is defined as the amount of insoluble polymer obtained from one gram of starting reactants (comonomers, crosslinker, initiator). It can be calculated by measuring the insoluable dried network as shown in Equation 2.2. In a typical experiment, a known amount of polymeric network (for gels solvent weight inside the network should be excluded) is immersed in a good solvent and then allowed to swell until the whole extractables are leached out by the solvent. Then, the insoluble part of the sample is taken out of the solvent and dried until constant weight. The gel fraction is then estimated according to Equation 2.2.

$$Gel\ Fraction = \frac{Dry\ weight}{Initial\ Weight} = \frac{m_{dry}}{m_0} \qquad 2.2$$

Crosslink density, molecular weight of crosslinks and number of crosslinks can be calculated only if Flory interaction parameters are known [145–148]. Since it is out of scope in this thesis, it won`t be further detailed.

2.4.2 Solid State NMR

Dipolar coupling (magnetic dipole-dipole coupling interaction) is defined as the interaction of two magnetic dipoles such as ^1H carrying nuclei. Under static conditions, it depends on the inverse cube of internuclear distance between the two magnetic dipoles and the angle between the internuclear vector and the magnetic vector (B_0)[149]. Under homogenous orientation conditions such as in single crystals, the orientation dependence can be exploited to get information about internuclear distances and geometry of a molecule.

However, molecular motion has a strong influence on the observed dipolar couplings. Time averaging due to fast segmental motions and structural averaging due to multiple orientations in an ensemble reduce the dipolar couplings to a so called “residual dipolar

couplings (D_{res})". For instance, molecular orientations of isotropic liquids changing rapidly in the NMR time scale (MHz) due to Brownian motions result in complete averaging of the observed coupling to zero [150]. In the opposite case, where the segments do not move in the NMR time scale such as in a solid below its melting/glass transition temperature, the observed dipolar coupling value is close to the theoretical value and is known as the "rigid-lattice" limit, where the terminology refers to the rigid lattice where the spins are static in the relevant time scale. In between these two extremes lies the whole system of solids which are of high technical importance known as soft matter such as polymers, elastomers, liquid crystals, large proteins and protein aggregates. In polymers, motional restrictions such as entanglements, crosslinks, hydrogen bonds, π-π stacking etc. induce local order and restrict complete averaging of dipolar couplings leading to a residual value. Measuring this averaged value by advanced methods leads to quantitative description and determination of such motional effects. In Table 2.1, typical residual dipolar coupling values for different systems are given. Accordingly, as the mobility of molecules decreases, anisotropy increases during which D_{res} also goes from small to larger values.

Table 2.1 Increase of D_{res} values from monomeric structures to rigid polymer networks

	Monomers	**Oligomers**	**Polymers**	**Entangled polymers**	**Elastomers**	**Rigid networks**
D_{res}	~mHz	mHz to Hz	~100's Hz	100's Hz to kHz	100's Hz to few kHz	1 MHz

Relevant to this work, are elastomers and other networks, where the crosslinking of polymer chains leads to a decrease in the amplitude of chain motion and a reduction in configurational space that chain segments can explore that result in motional anisotropy. Since D_{res} is proportionally affected by the changes in motional anisotropy, it is directly proportional to the crosslink density, realistically assuming that other interactions are absent or negligible. This is the principle behind determining crosslinking density with D_{res} in the systems used in this study. Among several existing methods to determine D_{res}, a method that has gained popularity recently for its application on a cost-effective equipment is so called low-field double quantum NMR

(LF-DQ NMR henceforth denoted as DQ-NMR). A pure DQ coherence excited NMR signal carries only structural information, however inadvertently, in practice is also affected by relaxation effects. If through clever manipulation, these relaxation effects can be delineated, the structural information, i.e. D_{res} can be obtained by the use of an appropriate model. Hence, in a practical solid state DQ NMR experiment, at a high enough temperature where complete segmental averaging has taken place and the chain motion is restricted only by motional restrictions, two signals are recorded as a function of the excitation time; (i) the double quantum signal S_{DQ} and (ii) the reference signal S_{ref} [151]. S_{DQ} signal arises from the motional-restricted network chains while S_{ref} results from all the other coherences (predominantly single quantum coherence from mobile chains such as loops, tails, etc.), that have not been previously excited by the first function. Since both signals decay during the time-period of the experiment due to the same transverse relaxation effects, determination of the non-DQ coherences, which in physical form correspond to non-load bearing chains($S_{defects}$) and subsequent pointwise division of S_{DQ} by ($S_{DQ}+S_{ref}-S_{Defects}$)**,** results in a normalized DQ signal which upon application of an appropriate model helps in extracting D_{res}. Important to note is that the highly mobile artifacts (compC) such as monomers, additives appear as the long-time tail of the sum signal ($S_{DQ}+S_{ref}$) and slightly less mobile non-network chains (compB) appear as the long time tail of the difference signal after accounting for component C, i.e. tail of ($S_{DQ}-S_{ref-}$ compC), after which the above mentioned normalization can be carried out.

Double quantum NMR measurements provide quantitative access to D_{res}, which in turn for elastomers provides insights into network density, modality, distribution and fraction of non-network-bound chains (e.g. loops, tails, residual monomers, photo-initiators or their cleavage products) [152–156].

2.4.3 Thermal and Mechanical Properties

Thermal and mechanical properties play an important role to determine the application field of polymeric materials. Understanding the relationship between structural characteristics and thermo-mechanical properties of polymers is necessary for further re-

search and developments. In this thesis, low migratable photoinitiators and crosslinkers were developed without compromising on the mechanical-thermal properties of the photopolymers obtained by commonly used low-molecular weight photoinitiators. Thus, in the first part of this thesis, structural and thermo-mechanical relationships in thiol-ene and thiol-acrylate networks were investigated. In the following chapter, the definition of some mechanical and thermal terms, measurement methods and requirements for the aimed applications will be detailed.

a) Thermal Properties

Thermogravimetric analysis (TGA) is a common and versatile method to determine properties of polymer based materials such as decomposition pattern [157,157–161], inorganic and organic content[162,163], temperature stability[164] and oxidation [165,166]. In TGA experiments, the weight change of a sample against temperature is measured [167,168]. In this method, a sample is exposed to either an increasing temperature programme with a defined heating rate or a constant isothermal temperature. Analysis can be carried out under different atmosphere such as air, carbon dioxide, oxygen or inert gas [167]. In this thesis, TGA was applied to determine the organic content of modified silica particles. In addition, the decomposition profile of the functionalized particles was determined by TGA. [36,169]

In thermal analysis, one of the frequently encountered terms is "glass transition temperature (T_g)". It is the temperature where amorphous polymers turn from a hard, glassy state to a soft, rubbery state [170]. Since crystalline polymers also have some amorphous parts, glass transition is also seen in this kind of materials. Rigidity of chain backbone and pendant groups, flexibility, tacticity, symmetry, polarity, molecular weight and crosslinking are the influencing parameters on T_g. Urethane, amide, imide and aromatic groups contribute to rigidity while oxyethylene and siloxane linkages contribute to the flexibility of polymer structures. As the rigidity increases, T_g shifts to higher values[170]. Higher polarity, higher molecular weight and crosslinking leads to an increase in T_g whilst the increased symmetry, branching, flexibility of backbones and side chains result in a decrease in T_g. Flexible silicon based polymers which have low T_g values (sometimes below 0°C)[171] can be used as sealants at room temperature

(above their T_g). On the other hand, polystyrene is in glassy state at room temperature[172] and has many applications below its T_g such as protective packaging, lids, bottles, etc.

There are various approaches to measure the T_g such as differential scanning calorimetry (DSC), dynamic mechanical analysis (DMA) and thermal mechanical analysis (TMA). In a typical DSC measurement, a sample with a known mass is heated or cooled in a pan (e.g. aluminium pan). Heat capacity changes according to the reference pan (empty pan) are determined as heat flow versus time or temperature.

The following equations describe the physical properties and thermal properties of polymers, which can be derived from DSC experiments:

$$Heat\ flow = \frac{Heat}{Time} = \frac{q}{t} \qquad 2.3$$

$$Heating\ Rate = \frac{Temperature\ Increase}{Time} = \frac{\Delta T}{t} \qquad 2.4$$

$$Heat\ Capacity = \frac{Heat\ flow}{Heating\ rate} = \frac{q}{\Delta T} = C_p \qquad 2.5$$

A typical DSC thermogram is shown in Scheme 2.20.

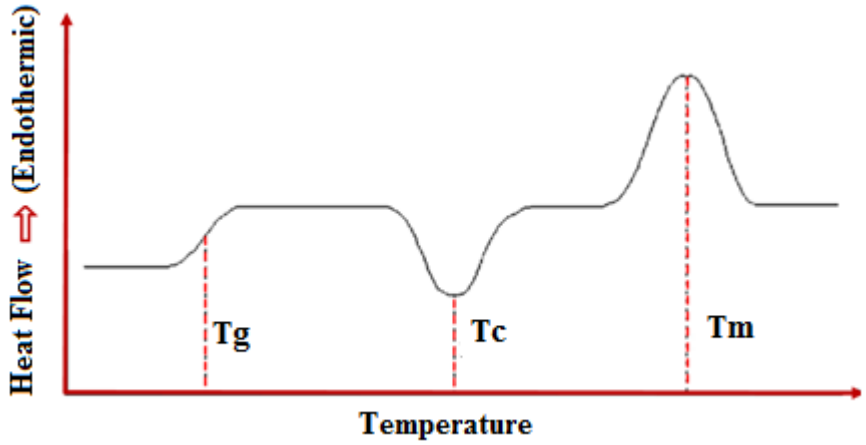

Scheme 2.20: Typical DSC transitions (T_m = melting temperature, T_c = crystallization temperature, T_g = glass transition temperature)

As can be seen in Scheme 2.20, glass transition, phase changes, curing, melting can be easily detected by DSC.

A DSC device can be also used for the analysis of a photo-curing reaction when it is equipped with a UV-lamp. Photo-DSC measurements are performed to determine curing kinetics and conversion of monomers in a light-sensitive resin [78,173]. Reaction time (t_{max}) along with peak shape provides information about reaction kinetics. t_{max} can be described as the time to reach maximum polymerization enthalpy. Furthermore, monomer conversion is proportional to total reaction enthalpy.Thus, it is possible to determine initiator efficiency, effect of different gas atmospheres (e.g. oxygen, carbondioxide, nitrogen etc.), influence of color, molecular weight and many other parameters on conversion and conversion rate of a light curing system.

b) Mechanical Properties

Mechanical properties are referred to a response of materials to stress and strain. General terms to describe the mechanical properties are defined as following:

(i) Stress (σ): Amount of force applied per unit area. The unit of stress is N/m^2 or Pa.

$$\sigma = \frac{F}{A} \qquad 2.6$$

There are three types of stress: Tensile, compressive and shear stress. Tensile and compressive stress is perpendicular to the sample surface whilst shear stress is applied parallel to the surface.

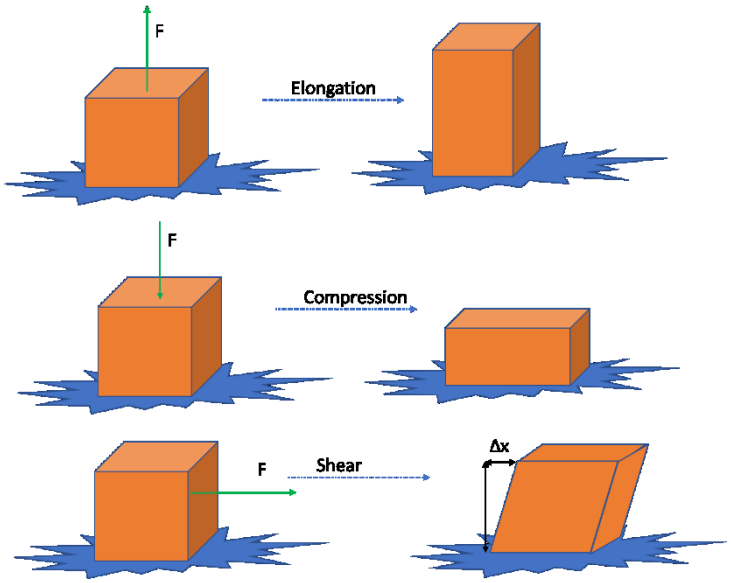

Scheme 2.21: A material`s response to tensile, compressive and shear stress

If the applied load acts to elongate a sample, then this type of stress is referred to tensile stress. Compressive stress tends to reduce the length of the sample.

(ii) Strength: Strength refers to the maximum stress that a material resists at the time of failure [174]. The unit of strength is N/m^2 or Pa. Yield strength refers to the lowest stress that induces a permanent deformation of the material. Tensile, compressional and flexural strength is the stress at which the material breaks down during elongation, compression and bending, respectively.

(iii) Strain (ε): Strain can be defined as dimensional change of a material normalized to its original dimension [175]. Tensile, compressive, volumetric and shear strain are the four main types of strain. Tensile strain is a result of an elongation of the sample. Compressive strain is related to a decrease of the length.

$$\varepsilon = \frac{l - l_0}{l_0} = \frac{\Delta l}{l_0} \qquad 2.7$$

(iv) Elongation [176]*:* After elastic elongation, materials go back to their original dimension. However, in plastic elongation materials are permanently deformed and can`t recover their original shape. Ultimate elongation is the maximum elongation percentage before a material breaks down under tensile stress.

$$Elongation\% = \frac{l}{l_0} * 100 \qquad 2.8$$

(v) Modulus (E): Modulus is described as the ratio between stress and elastic strain. Depending on the applied stress type, various terms are used for modulus such as shear modulus, tensile modulus (Young's modulus), and compressive modulus. The elastic modulus is defined as the slope in linear region of the stress-strain curve [176]. The unit of modulus is MPa or N/mm^2.

$$E = \frac{\sigma}{\varepsilon} \qquad 2.9$$

(vi) Toughness: Toughness is defined as the energy that a material absorbs before it breaks. In other words, toughness is the resistance of a material to fracture[176]. Scheme 2.22 shows material properties based on their stress-strain curve. The unit of toughness is MPa.

$$Energy = Stress * Strain \quad (2.10)$$

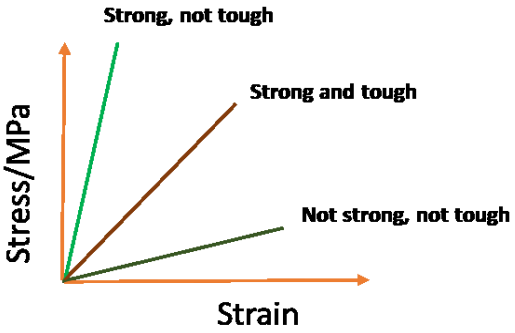

Scheme 2.22: Stress-strain response of a material according to its toughness.

Materials should meet certain mechanical requirements for their application. Glove materials are subjected to tensile tests for quality controls. The requirements for surgical gloves is given in Table 2.2 based on ASTM D3577-01a.

Table 2.2: Physical standards for surgical gloves according to ASTM D3577-01a [119]. The physical properties are measured using ASTM D412 [120]

Type	Before Aging			After Accelareted Aging	
	Minimum tensile strength	Minimum ultimate elongation	Maximum stress at 500% elongation	Minimum tensile strength	Minimum ultimate elongation
	MPa	%	MPa	MPa	%
Natural Rubber	24	750	5.5	18	560
Synthetic Rubber	17	650	7.0	12	490

3 EXPERIMENTAL

3.1 Materials

All materials applied in this thesis were used as received and they are described as following:

3-mercaptopropionic acid: It was used in the synthesis of thiols based on mercapto-propionate esters and supplied by Sigma-Aldrich. Its molecular weight was 106.14 g/mol.

4,4-isopropylidenedicyclohexanol: It was used as alcohol component in the synthesis of 4,4-isopropylidenedicyclohexanebis(3-mercaptopropionate). It was supplied by Sigma-Aldrich. Its molecular weight was 240.38 g/mol.

1,6-hexanediol: It was used in the synthesis of 1,6-hexane bis(3-mercaptopropionate). It was supplied by TCI. Its molecular weight was 118.18 g/mol.

Di(trimethylolpropane): It was used in the synthesis of di(trimethylolpropane tri(3-mercaptopropionate). It was supplied by Sigma-Aldrich. Its molecular weight was 250.33 g/mol.

Toluene (anhydrous): It was used as solvent in the synthesis of thiol based on mer-captopropionate esters. It was supplied by Sigma-Aldrich.

Toluene: It was used as a solvent in the swelling measurements of NR latex. It was purchased from Sigma-Aldrich. It was technical grade (95 %).

Diethyl ether (anhydrous): It was used as extraction solvent in the purification of thiol crosslinker based on mercaptopropionate esters. It was supplied by Sigma-Aldrich.

p-toluene sulfonic acid monohydrate: It was used as a catalyst in the synthesis of thiol crosslinker based on mercaptopropionate esters. It was supplied by Sigma-Aldrich. Its molecular weight was 190.22 g/mol.

Sodium bicarbonate: It was used as a base in the purification of thiol crosslinker based on mercaptopropionate esters. It was supplied by Sigma-Aldrich.

Magnesium sulfate ($MgSO_4$): It was used as a drying agent in the purification of thiol crosslinker based on mercaptopropionate esters. It was supplied by Sigma-Aldrich.

4,4-isopropylidenedicyclohexanebis(3-mercaptopropionate) (HBPA-SH): It was synthesized in our laboratory and used as the thiol component in thiol-ene reactions. Its molecular weight was 416 g/mol.

1,6-Hexane bis(3-mercaptopropionate) (HD-SH): It was synthesized in our laboratory and used as the thiol component in thiol-ene reactions. Its molecular weight was 294 g/mol.

Di[trimethylolpropane tri(3-mercaptopropionate)] (Di-TMPMP): It was synthesized in our laboratory and used as the thiol component in thiol-ene reactions. Its molecular weight was 602 g/mol.

Triallyl-1,3,5-triazine-2,4,6-trione (TATATO): It was used as an allyl monomer in thiol-ene reactions and supplied by Sigma-Aldrich. Its molecular weight was 249.27 g/mol.

Tris[2-(acryloyloxy)ethyl] isocyanurate (TAIC): It was used as an acrylate monomer in thiol-acrylate reactions and supplied by Sigma-Aldrich. Its molecular weight was 423.37 g/mol.

Ethyl-2,4,6-trimethylbenzoylphenyl-phosphinate (Irgacure TPOL): It was used as a photoinitiator. It was kindly received by BASF.

2-hydroxy-4'-(2-hydroxyethoxy)-2-methylpropiophenone (Irgacure 2959): It was used as a photoinitiator. It was supplied by TCI. Its molecular weight was 224.25 g/mol.

Bis(2,4,6-trimethylbenzoyl)-phenylphosphineoxide (Irgacure 819): It was used as a photoinitiator. It was supplied by BASF. Its molecular weight was 418.46 g/mol.

Natural Rubber (NR) Latex: NR latex was obtained by a Malaysian supplier.

Polyisoprene: Polyisoprene was supplied by Sigma Aldrich. Its molecular weight was 40,000 g/mol.

Ralox LC: It was used as an antioxidant in the preparation and curing of NR latex films. It was supplied by Solvadis. It was applied as an aqueous dispersion (53.2 wt.%).

Tween 20: It was used as a surfactant in the preparation and curing of NR latex films. It was supplied by Sigma-Aldrich.

(3-mercaptopropyl) trimethoxysilane: It was used in the modification of silica particles. It was supplied by Sigma-Aldrich. Its molecular weight was 196.34 g/mol.

(3-mercaptopropyl) methyldimethoxysilane: It was used in the synthesis of thiol functional oligomers. It was supplied by Sigma-Aldrich. Its molecular weight was 180.34 g/mol.

(Mercaptomethyl) methyldiethoxysilane: It was used in the synthesis of thiol functional oligomers. It was supplied by ABCR. Its molecular weight was 180.34 g/mol.

(3-acryloxypropyl) dimethoxymethylsilane: It was used as a co-monomer in the synthesis of thiol functional oligomers. It was supplied by ABCR. Its molecular weight was 218.32 g/mol.

Trimethylmethoxysilane: It was used as an end-capping agent in the synthesis of thiol functional oligomers. It was supplied by Sigma Aldrich. Its molecular weight was 104.22 g/mol.

Dipentaerythritol hexa(3-mercaptopropionate) (Di-PETMP): It was used as a hexafunctional thiol crosslinker in the photo-curing of NR latex. It was provided by Bruno Bock Thiochemicals. Its molecular weight was 783.1 g/mol.

***Trimethylolpropane tri(3-mercaptopropionate) (TMPMP)*:** It was used as a thiol crosslinker in the photo-curing of NR latex. It was provided by Bruno Bock Thiochemicals. Its molecular weight was 398.56 g/mol.

Ethoxylated-trimethylolpropane tri(3-mercaptopropionate) (ETTMP 700): It was used as a thiol crosslinker in the photo-curing of NR latex. It was provided by Bruno Bock Thiochemicals. Its molecular weight was ~700 g/mol.

Ethoxylated-trimethylolpropane tri(3-mercaptopropionate) (ETTMP 1300): It was used as a thiol crosslinker in the photo-curing of NR latex. It was provided by Bruno Bock Thiochemicals. Its molecular weight was ~1300 g/mol.

Chloroform ($CHCl_3$): It was used as a development solvent in the preparation of negative toned photoresists. It was purchased from VWR. It was technical grade.

Ethanol (CH_3OH): It was used as a solvent in the preparation of oligomeric siloxanes. It was purchased from VWR. It was technical grade (96%).

Hydrochloric acid (HCl): It was used as an acidic catalyst in the preparation of oligomeric siloxanes. It was purchased from Sigma-Aldrich.

Tetrahydrofurfuryl acrylate (THFA): It was used as an acrylate monomer. It was purchased from TCI. Its molecular weight was 156.18 g/mol.

1-{4-[2-(3-triethoxysilanylpropylcarbamoyloxy)ethoxy]-phenyl}-2-hydroxy-2-methyl-1-propane-1-one (TESI-IC2959): It was synthetized by Dr. Piotr Roszkowski and used for the modification of silica particles..

3-(trimethoxysilyl)propyl 3-[bis(2,4,6-trimethylbenzoyl)phosphinoyl]-2-methyl-propionate (TMESI^2-BAPO): It was synthetized by Dr. Jieping Wang and used for the modification of silica particles and glass fibres.

Prop-2-yn-1-yl phenyl(2,4,6-trimethylbenzoyl)phosphinate (Modified TPOL): It was provided by Dr. Meinhart Roth and used to initiate curing reaction of natural ruber latex.

Silica: Silica nanopowder with a specific surface area (BET) of 175-225 m^2/g were supplied by Sigma-Aldrich.

Trifluoroacetic acid: It is used as an acid catalyst in silanization reactions. It was supplied by Sigma-Aldrich.

Glass fibres: Glass fibres with a functional silane sizing were provided by Exel Composites GmbH

3-Methacryloxypropyltrimethoxysilane: It was purchased from Sigma-Aldrich. It was used in the surface modification of glass fibers.

Di(trimethylolpropane)tetraacrylate: It was purchased from Sigma-Aldrich. It was used as a photoactive resin in single fibre pull-out tests.

Concentrated sulfuric acid (H_2SO_4, 95w/v %): It was supplied by Sigma-Aldrich. It was used for the preparation of acidic piranha solution.

Ammonium hydroxide solution (NH_4OH): Ammonium hydroxide (30w/v %) was supplied by Roth. It was used for the preparation of basic piranha solution.

Hydrogen peroxide (H_2O_2): Hydrogen peroxide (30 w/v %) was obtained from VWR chemicals. It was used for the preparation of piranha solutions.

3.2 Synthesis of Low Molecular Weight Mercaptopropionate Esters

Network evolution of photoreactive thiol-ene resins depends on the structure of the starting monomers. In this concept, three different thiol structures based on mercaptopropionate esters were selected and synthesized. Synthesis of mercaptopropionate esters was accomplished according to previous literature [100]. Synthetic procedures for each thiol compound was carried out as described in the following sections.

3.2.1 1, 6-hexanebis(3-mercaptopropionate) (HD-SH)

10.78 g 1,6-hexanediol, 22.32 g 3-mercaptopropionic acid, 0.2 g *p*-toluene sulfonic acid and 150 mL anhydrous toluene were placed into a 500-mL round-bottom three-necked flask equipped with mechanical bar, Dean-Stark apparatus and reflux condenser. The reaction mixture was purged with nitrogen at least for half an hour and then heated to 110 °C. Reaction time was determined based on water evolution during reaction. After 3 hours, no water evolution observed and the reaction was stopped. The solvent was removed under reduced pressure. A malodour liquid was obtained, which was dissolved in 150 mL anhydrous diethyl ether. The organic phase was washed three times with 200 mL 5 wt.% sodium bicarbonate solution to neutralize the excess acid. Subsequently, the organic phase was washed with deionized water (3 x 200 mL) and dried over 50 g magnesium sulphate. After filtration of the drying agent, diethyl ether was removed under reduced pressure. HD-SH was obtained as a slightly yellow oil. Yield, 23 g (85% of theoretical yield).

^{1}H NMR (δ, 400 MHz, 20°C, $CDCl_3$)**:** 1.38 ppm (m, 4H), 1.64 ppm (m, 6H), 2.63 ppm (t, 4H), 2.73 ppm (q, 4H), 4.09 ppm (t, 4H),

FTIR (cm^{-1}): 2571 (SH stretching), 1728 (ester carbonyl group), 2938, 2863 (sp^3 C-H), 1463 (CH_2 bending)

3.2.2 4,4-isopropylidenedicyclohexanebis(3-mercaptopropionate) (HBPA-SH)

25 g 4,4-isopropylidenedicyclohexanol, 26.05 g 3-mercaptopropionic acid, 0.2 g *p*-toluene sulfonic acid and 150 mL anhydrous toluene were placed into a 500-ml round-bottom three-necked flask equipped with mechanical bar, Dean-Stark apparatus and reflux condenser. The mixture was purged with nitrogen at least for half an hour and then heated to 110 °C. Reaction time was determined based on water evolution during

reaction. After 10 hours, no water evolution was observed and the reaction was stopped. The solvent was removed under reduced pressure. A malodour liquid was obtained, which was dissolved in 150 mL of anhydrous diethyl ether. The organic phase was washed three times with 200 mL 5 wt.% sodium bicarbonate solution to neutralize the excess acid. Subsequently, the organic phase was washed with deionized water (3 x 200 mL) and dried over 50 g magnesium sulphate. After filtration of the drying agent, diethyl ether was removed under reduced pressure. HBPA-SH was obtained as a slightly yellow oil. Yield, 32 g (75 % of theoretical yield).

^{1}H NMR (δ, 400 MHz, 20°C, $CDCl_3$): 0.72 ppm (m, 6H), 1.06–1.14 ppm (m, 4H), 1.22–1.30 ppm (m, 4H), 1.45–1.48 ppm (m, 2H), 1.59 ppm (m, 2H), 1.68–1.72 ppm (m, 4H), 2.56–2.65 ppm (m, 4H), 2.69–2.77 ppm (m, 4H), 4.59–4.69 ppm (m, 2H)

FTIR (cm^{-1}): 2571 (SH stretching), 1728 (ester carbonyl group), 2943, 2867 (sp3 C-H), 1463 (CH_2 bending)

3.2.3 Di [trimethylolpropane tri (3-mercaptopropionate)] (Di-TMPMP)

11.38 g di(trimethylolpropane), 22.29 g 3-mercaptopropionic acid, 0.2 g *p*-toluene sulfonic acid and 150 mL anhydrous toluene were placed into a 500-mL round-bottom three-necked flask equipped with mechanical bar, Dean-Stark apparatus and reflux condenser. The reaction mixture was purged with nitrogen at least for half an hour and then heated to 115 °C. The reaction time was determined based on water evolution during reaction. After 6 hours, no water evolution was observed and the reaction was stopped. The solvent was removed under reduced pressure. A malodour liquid was obtained, which was dissolved in 150 mL of anhydrous diethyl ether. The organic phase was washed three times with 200 mL 5 wt.% sodium bicarbonate solution to neutralize the excess acid. Subsequently, the organic phase was washed with deionized water (3 x 200 mL) and dried over 50 g magnesium sulphate. After filtration of the drying agent, diethyl ether was evaporated under reduced pressure. Di-TMPMP was obtained as a slightly yellow oil. Yield, 20 g (74 % of theoretical yield).

^{1}H NMR (δ, 400 MHz, 20°C, $CDCl_3$): 4.02 ppm (s, 8H), 3.27 ppm (s, 4H), 2.76 ppm (t, 8H), 2.64 (t, 8H), 1.61 ppm (m, 4H), 1.44 ppm (q, 4H), 0.85 ppm (t, 6H)

FTIR (cm^{-1}): 2567 (SH stretching), 1728 (ester carbonyl group), 2968, 2941, 2881, 2811 (sp^3 C-H), 1463 (CH_2 bending), 1385 (CH_3 bending).

3.3 Synthesis of Siloxane Based Oligomeric Thiols

Synthesis of oligomeric thiols was accomplished by hydrolytic polycondensation method and adapted from Reference [177]. Different reaction conditions (e.g. initial monomer concentration, type of silanes and reaction time) were evaluated for obtaining high molecular weight thiols.

In a typical synthetic procedure 40.8 mL 0.1 molar $HCl_{(aq)}$, 2.75 g water and 11.73 g ethanol were placed into a 250 mL 3-necked round bottom flask and stirred at 50 °C for 20 minutes under nitrogen flow. Afterwards, a defined amount of silane (see Table 3.1) was added to the reaction mixture. After the end of reaction time, the mixture was poured into deionized water and extracted with 150 mL chloroform. The organic phase was further washed with 50 mL deionized water until the pH value of the aqueous phase was 7. Finally, chloroform was removed under reduced pressure and the product was obtained as a clear oily fluid. The yield exceeded 80 % of the theoretical yield for each reaction. All reaction conditions are summarized in Table 3.1.

Table 3.1: Reaction conditions for the synthesis of oligomeric siloxane

Name of Product	Starting Compound(s)	Amount (g)	Reaction Time (h)
Siloxane-1	(Mercaptomethyl)methyldiethoxysilane	5.0	3
Siloxane-2	(3-Mercaptopropyl)methyldimethoxysilane	5.0	3
Siloxane-3	(3-Mercaptopropyl)methyldimethoxysilane	5.0	6
Siloxane-4	(3-Mercaptopropyl)methyldimethoxysilane	5.0	9
Siloxane-5	(3-Mercaptopropyl)methyldimethoxysilane	10.0	3
Siloxane-6	(3-Mercaptopropyl)methyldimethoxysilane /***(3-Acryloxypropyl)-dimethoxymethylsilane***	4.5 /***0.5***	3
Siloxane-7	(3-Mercaptopropyl)methyldimethoxysilane /***(3-Acryloxypropyl)-dimethoxymethylsilane***	4.0 /***1***	3

Siloxane-8	(3-Mercaptopropyl)methyldimethoxysilane *Trimethylmethoxysilane*[*]	5.0/*0.327*[*]	3
Siloxane-9	(3-Mercaptopropyl)methyldimethoxysilane *Trimethylmethoxysilane*[*]	10.0/*0.654*[*]	3
Siloxane-10	(3-Mercaptopropyl)methyldimethoxysilane /***(3-Acryloxypropyl)-dimethoxymethylsilane*** *Trimethylmethoxysilane*[*]	4.5/***0.5***/*0.32*[*]	3

[*] (Trimethylmethoxysilane was used as an end-capping reagent)

The influence of the reaction parameters on the molecular weight of the synthesized siloxanes was evaluated by GPC measurements and is described in the results and discussion section (see section 5.2.2).

3.4 Surface Modification of Inorganic Particles

In this study, one of the approaches towards low migratable initiators and crosslinkers was the covalent attachment of functional chemicals on mineral surfaces. Silanization reactions were utilized for attaching potential photoinitiators and crosslinkers on particle surfaces.

In the first part of this chapter the preparation of thiol functional particles is described. In the following parts of the thesis, these particles were employed to crosslink natural rubber (NR) latex via thiol-ene reactions. In the second part, the covalent attachment of alkoxysilyl functional initiators on silica surfaces is described. These photoactive particles are utilized in the crosslinking of a thiol-ene resin.

3.4.1 Preparation of Thiol-Functional Particles

Commercially available thiol functional silanes were used to modify silica and zeolite surfaces. Prior to modification, these surfaces were characterized by X-ray photoelectron spectroscopy (XPS) to detect the metal impurities. Alkali metal impurities such as sodium, potassium and calcium do not form hydrolytically stable bonds with silicon and catalyse the cleavage of silicon-oxygen bonds. Thus, prior to silanization reactions zeolite was exposed to hydrochloric acid and nitric acid treatment to remove the surface impurities and to oxidize the surface. Silica surface does not contain metal impurities so surface activation (increase in hydroxyl groups) was carried out by corona treatment.

Pre-treatment of zeolite: 20 g zeolite was added to a stirred solution of 200 mL, 5 wt.% $HCl_{(aq)}$ solution. After mixing for 4 h, the dispersion was filtered and washed repeatedly with deionized water. Then, particles were added to 200 mL, 5 % (w/w) nitric acid solution. After 1 hour mixing, zeolite was filtered and washed with distilled water until pH is neutral.

Pre-treatment of silica: Silica particles were pre-treated by exposure to corona discharge (corona dosage amounted to 833 W min m^{-2}) using a Corona Treatment System TG3001 from Ahlbrandt (Lauterbach, Germany).

General silanization procedure: 10 g pre-treated particles were dispersed in 200 mL anhydrous toluene by ultrasonication for 10 min. 1 g MPTMS was then added to the reaction mixture. Silanization reactions were carried out under nitrogen atmosphere and under reflux for 8 h. The modified particles were filtered and washed with toluene repeatedly. Drying was carried out at 120 °C for 2 h. Acid pretreated zeolite particles were interestingly shows hydrophobic characters probably due to the acid catalysed formation of oligomeric thiol functional siloxanes.

3.4.2 Preparation of Photoactive Silica Particles

Photoactive silica particles were prepared by employing two different silanization method. Two different alkoxysilyl functional initiators,

a) 3-(trimethoxysilyl)propyl3-[bis(2,4,6-trimethylbenzoyl)phosphinoyl]-2-methyl-propionate (TMESI^2-BAPO)

b) 1-{4-[2-(3-triethoxysilanylpropylcarbamoyloxy)ethoxy]-phenyl}-2-hydroxy-2-methyl-1-propane-1-one (TESI-IC2959)

were grafted onto the silica nanopowder by method 1 and method 2, which are described in the following section.

Method 1

First, the silica particles were exposed to a corona dosage of 833 W min m^{-2}. Then, 5.0 g corona treated particles were dispersed in 180 mL of anhydrous dichloromethane by sonication. One of the silanes described above (250 mg; 5 wt.% of silica particles) was separately dissolved in 20 mL of anhydrous dichloromethane and added to the reaction

mixture, which was then heated to reflux temperature (55 °C) and stirred for additional 3 h. The reaction mixture was divided into several centrifugation tubes and centrifuged for 100 min at 4,000 rpm. The supernatant was discarded and the particles were dried overnight at 60 °C. To remove the physically attached reactants, the particles were dispersed in acetone by sonication and then centrifuged at 4,000 rpm for 99 min. The washing was repeated three times and the particles were dried overnight at 60 ˚C.

Method 2

A suspension of silica nanopowder (12.0 g) in toluene (275 mL) was stirred at room temperature until a homogenous gel suspension is obtained. A solution of one of the silane described above (3.6 mmol; 0.3 mmol for 1 gram silica) in toluene (45 mL) was added and the resulting suspension was vigorously stirred for 24 h. After this time trifluoroacetic acid (0.5 mL) and ethanol (96 %, 50 mL) were added and the reaction mixture was stirred for further 1 h, after which it was evaporated to dryness on a rotary evaporator (bath temperature set to 50 °C). The dry residue was re-suspended in ethanol (96 %, 200 mL) by sonication for 20 min to obtain a homogenous suspension. 13.5 mL distilled water and trifluoroacetic acid (0.5 mL) was added and the mixture was stirred at room temperature overnight. The solvent was evaporated under vacuum at 50 ºC to complete dryness. After evaporation of the solvent, the residue was suspended in toluene (200 mL) by sonication, and the solvent was removed on a rotary evaporator. Additional drying under high vacuum (0.1 mbar) at room temperature over 48 h gave the product in the form of a white, slightly aggregated powder. A fine powder could be obtained by gentle grinding of the solid residue in a mortar.

3.5 Preparation of Glass Fibre Reinforced Composite Materials

Sizing of glass fibres consists of several components such as film formers and silane coupling agents both of which increase the adhesion between the glass fibres and matrix. Since content of the sizing is confidential, it was removed in three steps in the content of this thesis. The desized glass fibres were treated with either a methacryloxy functional silane (GF 31) or a photoactive group bearing silane (TMESI^2-BAPO). The functional groups of both GF31 as well as TMESI^2-BAPO are able to react with an acrylate based resin. Details of desizing steps as well as modification with GF31 and TMESI^2-BAPO are given as following:

a) Desizing of Glass Fibers

In the first step, most of the sizing was removed during a Soxhlet extraction, which was carried out with acetone at 77 °C for 24 h. For this purpose, around 10 g glass fibres were packed into a cellulose extraction thimble (Mn: 645, inner diameter: 33 mm and height: 94 mm) and extracted with 250 mL acetone. The fibres were then removed and dried at 120 °C for 1 h. 0.67 wt.% of the total weight of the fibres was removed during the extraction procedure.

In the second step, the residual sizing was removed by treatment with 1:1 acidic piranha solution (30%H_2O_2:95%H_2SO_4) for 2 h at room temperature. Subsequently, the glass fibres were removed and washed repeatedly with deionized water.

Finally, the glass fibres were exposed to 1:1 basic piranha solution (30%H_2O_2:30%NH_4OH) for at least 20 min. Temperature was kept between 50 and 60 °C during the cleaning. Subsequently, glass fibres were washed repeatedly with deionized water.

In addition to removal of sizing, surface silanol formation was ensured by exposure to piranha solutions. Glass fibres were analysed in each desizing step. Before each analysis, they were dried at 130 °C for 1 h. In a general desizing procedure, no drying was applied between the second and third cleaning step.

To determine the moisture and residual sizing after the acetone extraction step, the glass fibres were thermally treated at 565 °C for 2 h. 0.20 wt.% of initial weight (weight of the glass fibres prior to Soxhlet extraction) was removed.

b) Surface modification of desized glass fibres

Surface modification was achieved by dipping the desized glass fibres into a 1 % (w/v) silane solution in anhydrous toluene for 24 hours at 60 °C. The fibres were then removed from the solution and dried at 120 °C for 2 hours. Physically attached silanes were removed by rinsing glass fibres a few times with acetone.

c) Preparation of photopolymer matrix for fibre pull-out tests

A di(trimethylolpropane) tetra acrylate resin containing 1 wt.% Irgacure 819 as a long wavelength absorbing initiator was prepared by mixing these two components overnight in a light-protected vial.

d) Single fibre pull-out tests

A single glass fibre was embedded in the acrylate matrix droplet by using a special embedding machine developed in Bundesanstalt für Materialforschung und -prüfung (BAM). Embedding length of a clamped single fibre was controlled by a light microscope mounted in this embedding machine. Firstly, a clamped single fibre was perpendicularly oriented and partly embedded within the matrix droplet, which was placed on an aluminium sample carrier. The acrylic matrix was cured for 4 min with a LED lamp having a light intensity of 1.18 J/cm^2 between 380 and 460 nm (distance between light source and sample surface was 1 cm).

Secondly, the fibre diameters were measured using an optical microscope.

In the third step, a single fibre placed on the aluminium sample carrier was fixed to a screw platform using a cyan-acrylate super glue for pull-out measurements. Free length of the fibre between the surface of the matrix and fibre-clamping mechanism was adjusted between 10 and 30 µm. In this measurement set-up, the screw platform was attached to a piezo motor, which was placed on a highly stiff frame. The pull-out test rate was fixed at 1 µm/s. During tests, force versus displacement signals were recorded.

3.6 Preparation and Curing of Natural Rubber Latex Films

3.6.1 Coagulant Dipping Process

A conventional coagulant dipping process was employed to prepare thin latex films. In this method, a former made of ceramics is immersed into a coagulant dispersion, withdrawn and dried. Then it is dipped into a latex formulation. After a certain dwell time, the former is withdrawn and dried.

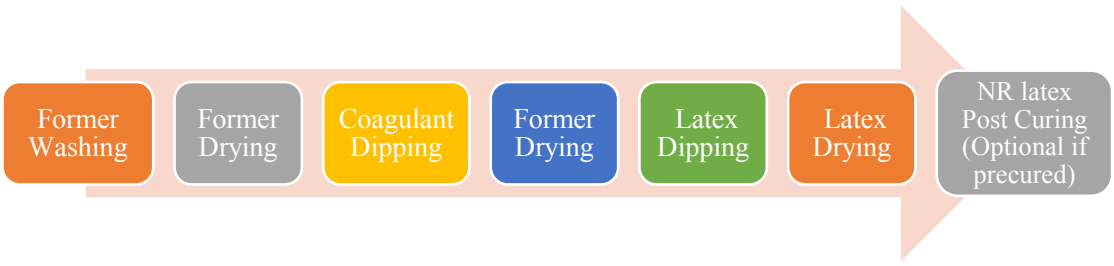

Scheme 3.1: Steps of coagulant dipping process used for the production of NR latex gloves

Details of the coagulant dipping process applied in this study was performed as following.

a) Preparation of NR latex dispersion

A typical natural rubber (NR) latex dispersion was prepared according to the following procedure:

1. 100 g of a commercially available NR latex with a dry rubber content (drc) of 60 % was diluted with 50 g deionized water to obtain 40 % drc. Then, 0.57 g (0.5 phr) Ralox was added to the stirred formulation. After ~1 min, 3 mL, 10 wt.% $KOH_{(aq)}$ was added to increase the stability of latex formulation. It should be noted that in the case of the photo-precuring process of NR latex, the anti-oxidant Ralox is added after the precuring is completed.
2. Thiol functional crosslinker, initiator, minimum required amount of Tween 20 as a surfactant and water were mixed in a small vial and sonicated until a homogenous emulsion was formed. The optimum amount of initiator and crosslinker was determined by tensile test measurements of the cured latex. In general, 1 to 4 phr of the crosslinker and 1 or 2 phr of the photoinitiator were applied. In a typical formulation, 0.6 g initiator (1 phr), 0.6 g crosslinker (1 phr), 1.2 g deionized H_2O and 0.12 g Tween 20 was mixed and sonicated.
3. Finally, the emulsion prepared in the second step was added to NR latex dispersion described in the first step. To obtain homogenous latex dispersions, it is further mixed for 40 min at room temperature.

Note: If functional particles were used as crosslinkers or photoinitiators, they were dispersed in the calculated amount of deionized water, which was used to dilute the NR latex from 60% drc to 40% drc. This dispersion was then directly added to NR latex.

Preparation of NR latex formulation was done under a UV light protected room.

b) Preparation of coagulation dispersion

Coagulant dispersion containing $CaCl_2$ as coagulant and $CaCO_3$ as release agent was kindly provided by Semperit Technische Produkte GmbH.

*c) **Dipping process***

In this study, finger-shaped porcelain formers were used for the dipping process. Prior to the dipping, formers were cleaned with deionized water and acetone, respectively. Prior to the dipping process, formers were dried in an oven at 100 °C for approximately 10 min.

For the dipping process, the temperature of the coagulant solution was adjusted to 70 °C. Then, one of the formers was dipped into the hot coagulant solution for 30 s. After this, the former was removed and dried in an oven at 120 °C at least for 1 min. In the next step, the former was dipped into the NR latex formulation for 20 s and slowly withdrawn. After removal, excess latex on the tip of the formed latex film was taken away by gently touching the tip on a tissue paper. Films with a thickness in the range of 300 µm were obtained, which were dried for 15 min at 120 °C. The dried latex films, which were characterized by swelling measurements, were directly cut off the formers. Other films were firstly powdered with corn starch and then stripped from the formers.

3.6.2 Photochemical Crosslinking of NR Latex

Photochemical crosslinking of NR latex was performed with a UV curing system provided by Fusion UV Systems Inc. A Gallium arc lamp was assembled to the system and energy was adjusted to 1.3 J/cm² (200 and 600 nm) per irradiation cycle. Illumination intensity was determined by a radiometer (Powerpuck II, EIT Instrument Markets, US).

UV light irradiation was carried on dried NR latex films (preparation was described in section 3.6.1), which is termed "post-curing." For post-curing 2 to 6 irradiation cycles were applied corresponding to an exposure dose of 2.6 and 7.8 J/cm^2, respectively.

Curing of liquid latex dispersions (prior to the dipping process) is termed "pre-curing". Influence of pre-curing on the mechanical properties was also tested for selected NR latex formulations. In this case, the preparation of latex dispersion was carried out as described in section 3.6.1 except the addition of Ralox. Then, a defined amount of the latex dispersion was placed into glass petri dishes yielding thin liquid films with a thickness of 1 mm. The exposure dose ranged from 3.9 to 6.5 J/cm^2 (3 to 5 cycles). The required amount of Ralox (usually 0.5 phr) was then added to the dispersion,

which was stirred for 30 min by means of a magnetic stirrer. Latex films were dipped from this pre-cured latex (see section 3.6.1) and part of the samples were additionally crosslinked via a post-curing step.

3.6.3 Ageing and Sterilization

Cured NR samples were stored at 70 °C for 7 days to evaluate their aging resistance. This accelerated aging procedure simulates the behaviour of the samples when they are stored longer times at lower temperature. Sterilization of both aged and non-aged samples were also carried out using gamma rays from a ^{60}Co-source with a dose of 25 kGy. The sterilization was done at Mediscan GmbH & Co KG in Seibersdorf. The aging and the sterilization of samples were conducted in accordance with ISO 10282 [178].

3.7 Preparation of Negative Photoresists

a) Patterning with the mask aligner device

Polyisoprene solutions 2 wt.% in chloroform were prepared by dissolving 0.2 g *cis*-1,4 polyisoprene (Mw = 40,000 g/mol) in 9.8 g chloroform. A defined amount of cross-linker and initiator was added to the solution, which was then spin cast on silicon wafers using EMS Spin Coater Model 4000 instrument with a speed of 1000 rpm for 30 s (ramp rate was 1000 rpm/s). Photo-patterning was achieved through a quartz-chromium mask using a mask aligner (SUSS Microtec, MJB4) equipped with an HgXe-lamp (500 W) in soft contact mode. The sample was illuminated for 80 s with a 20 mW/cm^2 light intensity. Irradiated films were subsequently developed with chloroform for around 5 s. Patterns were visualized by using an optical microscope (Olympus/Japan & BX51 Color View IIIu Soft Imaging System/ Germany).

b) Manual patterning

Resin mixtures were prepared by mixing equal molar ratio of thiol groups of thiol monomer with double bond groups of triallyl-1,3,5-triazine-2,4,6-trione (TATATO) or tris[2-(acryloyloxy)ethyl] isocyanurate (TAIC) monomer for the thiol-ene and thiol-acrylate reactions, respectively. Then a defined amount of initiator was added. Homogenization of the mixture was ensured by sonication for 1 min. The resin mixtures

were drop-cast on glass microscope slides. A quartz mask with 25 μm lines and spaces was aligned on the resin surface with a ~200 μm spacer between them. Irradiation was performed in non-contact mode using a high-pressure Hg lamp (Omnicure S1000, Lumen Dynamics, Canada) with an exposure dose of 162 mJ/cm^2. Development of negative toned photoresists was done by dipping the microscope slides in acetone for a few seconds. Patterns were displayed using an optical microscope (Olympus/Japan & BX51 Color View IIIu Soft Imaging System/ Germany).

4 CHARACTERIZATION METHODS

4.1 Fourier-Transform Infrared Spectroscopy (FTIR) Measurements

FTIR spectroscopy was carried out with a Vertex 70 spectrometer (Bruker, US). Typically, 16 scans were taken with 4 cm^{-1} resolution, in the range of 4000-800 cm^{-1}.

For the characterization of the silica nanopowders, approx. 15 mg of the dry product was pressed using a hydraulic press (Perkin Elmer). The obtained pellets were subjected to FTIR measurements using the ATR mode.

Other substances were directly characterized by FTIR in ATR mode without any pretreatment.

Crosslink kinetics were characterized by real-time FTIR measurements. The resin formulations were spin-cast on CaF_2 discs. The thin films were irradiated with an Omnicure S1000 high pressure Hg lamp (λ=250-470 nm; Lumen Dynamics; Canada) under nitrogen atmosphere for the thiol-ene and thiol-acrylate systems. The intensity of the light in the sample plane was measured with an integrating radiometer (Powerpuck II, EIT Instrument Markets, US). The reaction kinetics was followed by FTIR in transmittance mode, until full conversion was reached. The conversions of the thiol, allyl and acrylate functional groups were calculated using OPUS 7.0 Spectrum software.

Functional group conversion was calculated based on equation (1), where A_0 and A_t are normalized peak areas of the characteristic IR stretching vibrations prior to and after a selected time of UV exposure.

$$\%\ \text{Func. Group Conversion} = \left[\frac{A_0 - A_t}{A_0}\right] * 100 \qquad 4.1$$

4.2 Thermogravimetric Measurements (TGA)

TGA was carried on a ~15 mg sample in a ceramic pan with a Mettler Toledo instrument equipped with star-e system software. Analysis conditions are summarized in Table 4.1.

Table 4.1: Conditions used in thermogravimetric analysis.

Sample	Atmosphere (gas)	Flow Rate (mL/min)	Heating Rate (°C/min)	Temperature (°C)
Photoactive Particles	Oxygen	30	4	30-900
Thiol functionalized Particles	Nitrogen	30	10	30-900

4.3 Swelling Measurements

a) Photo-cured Natural Latex (NR)

Swelling degree and gel content of crosslinked NR latex films were determined by equilibrium swelling measurements. Five samples were averaged for each data point. In the first step, 50 to 90 mg sample was cut out of the cured latex film and weighted (m_0). Then, each sample was put into separate glass vials and filled with 20 mL toluene. Swelling measurement was done for 48 h at room temperature. After 48 h, the sample was taken out of the glass vials and excess solvent on the sample surface was wiped off with a tissue paper. Subsequently, the swollen samples were weighted for determination of their swelling degree ($m_{swollen}$). For calculation of gel content, swollen samples were dried at least for 48 h under a ventilating fume hood until constant weight was reached (m_{dry}). Swelling degree and gel fractions were calculated according to Equation 2.1 and 2.2, respectively as described in Section 2.4.1.

b) Photopolymer Networks

Gel contents of the photopolymer networks were calculated through swelling measurements. Rectangular samples with a mass of 50 ± 10 mg were cut and submerged into chloroform (20 mL) in small glass vials. After 24 h the samples were taken out and dried with a tissue. After 48 h of drying at 50 °C, gel fractions were calculated from dried weights according to Equation 2.2 as described in Section 2.4.1.).

4.4 UV-Vis Spectroscopy

UV-Vis measurements were carried out with a Varian (United States) Cary 50 UV-Vis spectrophotometer in absorbance mode. For sample preparation, defined amounts of samples were dispersed in 10 mL acetonitrile by sonication. In general sample concentrations are changing between 0.25 to 20 mg/mL. Higher concentrations were used for the absorbance measurements of photoactive particles while lower concentrated solutions were used for the absorbance measurements of free (unattached) initiator. UV-Vis spectra of samples were taken in a quartz cell with 0.1 cm path length.

4.5 Differential Scanning Calorimetry (DSC)

a) Photo-DSC

The photo-DSC experiments were performed on a NETZSCH photo-DSC 204 F1 Phoenix. Measurements were conducted at either 35 °C or 50 °C in aluminum crucibles under nitrogen atmosphere. The sample quantity was 8.00 (± 0.05) mg of resin. The Omnicure s2000 was used as the light source at 1 W/cm^2 resulting in an intensity of 80 mW/cm^2 at the surface of the sample (range of wavelength was 250 – 445 nm). For the determination of the reaction enthalpy and t_{max}, the samples were illuminated twice for 10 min each with an idle time of 2 min in between. For the analysis, the second run was subtracted from the first one to obtain the reaction enthalpy curve.

b) DSC

Differential scanning calorimetry measurements were carried out with NETZSCH DSC 204 F1 Phoenix using a nitrogen flow of 20 mL min^{-1}. The cured resins were heated from -80 to 80°C with a heating rate of 20°C min^{-1}. The glass transition temperature (T_g) was obtained from the second heating run and was read as the midpoint in heat capacity.

4.6 Tensile Testing

a) Tensile Testing of NR latex

Tensile tests were carried out with Zwick Z010 according to ASTM D412-98a standard [179]. Accordingly, shouldered test bars were stamped out of the photo-crosslinked NR latex films. The thickness of the samples was measured from three different areas

and values were averaged (film thickness typically ranged from 200 to 400 µm). In the next step, samples were amounted to the Zwick tensile tester. The total clamping length amounted to 75 mm. Tensile tests were conducted by using a 500 N load cell and manual foil grips. A pre-load of 0.02 MPa and a testing speed of 500 mm/min was applied for all measurements. Tensile strength, modulus (stress at 50% elongation) and the ultimate elongation at break were recorded. For reproducibility, at least four samples were tested for each data point and results were averaged.

Dimension of the prepared shouldered test bars for tensile test measurements is shown in Scheme 4.1.

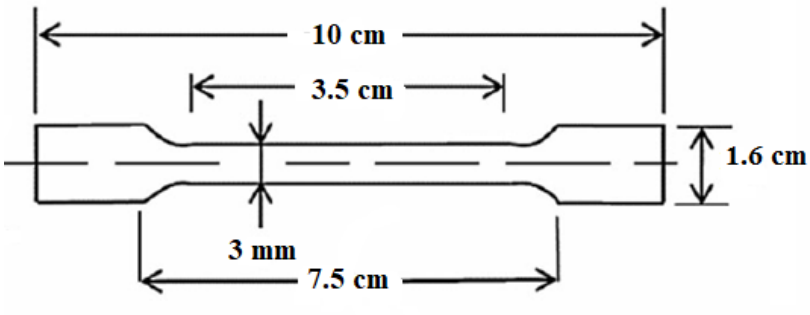

Scheme 4.1: Dimension of samples prepared for tensile test measurements.

b) Tensile Testing of Crosslinked Thiol-Allyl and Thiol-Acrylate Photopolymers

Free standing films with a film thickness of around 1 mm were produced by pouring the resin formulations (n_{thiol}/n_{alkene}:1, Lucirin TPO-L: 0.2 wt.%) in PTFE moulds with the shape of a shouldered test bar in compliance with ASTM Standard D412-98a. The photo-induced crosslinking was carried out under air using an Hg UV lamp (light hammer 6 UV curing system, Fusion UV Systems, United States). The exposure dose into the sample plane was 1.58 J/cm² (determined with a radiometer) per irradiation cycle with a wavelength range between 250 and 470 nm. Six irradiation cycles were applied for each sample.

Tensile testing of the free standing films was performed with a 10 kN universal tensile/compression testing machine (Z010, Zwick/Roell, Ulm) equipped with a 500 N load cell. A high-accuracy extensometer from Zwick Company was used for direct extension measurement on the specimens. The marks of the extensometer were placed

in the middle of the test specimen with a distance of 20 mm to each other. At lower strains (ε = 0.05-0.25 %) the test speed was 1 mm min^{-1} and at higher strains (ε > 0.25%) the test speed amounted to 20 mm min^{-1}. The elastic modulus was determined at 1 mm min^{-1} while further tensile properties such as strength and ultimate elongation were measured at 20 mm min^{-1}.

4.7 Transmission Electron Microscopy (TEM)

TEM was carried out using a Phillips CM12, operated at 120 kV. Bright-field TEM images at different magnifications were acquired to analyse the size distribution and morphology of the nanoparticles. To investigate the differently treated silica nanopowders, they were dissolved in methanol and drop cast on carbon grids. To avoid agglomeration, the solutions were sonicated for 1 min prior to drop casting.

4.8 Zeta Potential Measurements

Zeta potential measurements were carried out with an Electrokinetic Analyser (EKA, Anton Paar KG, Graz, Austria) to determine the isoelectric point. Streaming potential method was used to determine the zeta potential of the desized and modified glass fibres in 1 mM KCl. Zeta potential was measured starting from natural pH to lower acidic values by adding 50 mmol/L HCl using an autotitrating unit (RTU, Anton Paar KG, Graz, Austria).

4.9 NMR Measurements

4.9.1 Low Field NMR Measurements

NMR measurements were carried out on a Bruker Minispec mq20 desktop low field NMR spectrometer operating at a ^{1}H-NMR frequency of 19.5 MHz and a permanent magnet with a field strength of 0.47 T. The 90°/180° pulses were optimized for each sample and the values ranged between 2.6-2.7 μs and 5.1-5.2 μs respectively. The dwell time was kept short in order to have a spectral width of at least 1.25 MHz and the signal was acquired up to 0.5 ms. The samples were punched in the form of disc and stacked in a 8 mm tube up to a height of 5 mm and placed in the middle of the homogeneous part of the magnetic field for measurements. The samples were then

heated with dry air. A BVT3000 temperature controller was used for temperature regulation. The measurements were carried out at 100 ±0.1 ˚C after equilibrating the samples at this temperature for about 20 min.

For the recording of DQ build-up curves as a function of excitation (and reconversion) times, $\tau_{exc/rec}$, Baum-pines pulse sequence in a slightly modified form as well as the 3-pulse (also known as 5-pulse) DQ sequence was used [180–182]. The integral of the real part of the complex in-phase on-resonance signal for each excitation time was used to get the intensity of each point. This intensity data was subject to normalization as per the now common procedure which helps determining the non-elastic fraction as well as producing a dynamics-free multiple-quantum build-up curve. Complete details of the experiment and the procedure for normalization can be found in several manuscripts [151,181,183,184] After the above mentioned normalization procedure, in order to get a distribution curve (average D_{avg} and the distribution σ of the dipolar couplings), the normalized double quantum curves (nDQ) were inverse Laplace-transformed using a numerical inversion procedure based on Gaussian function as kernel and fast Tikhonov regularization (see eq 4 in [185]).

4.9.2 High Field NMR Measurements

^{1}H NMR measurements were conducted with a Varian 400 -NMR spectrometer operating at 399.6 MHz. Samples were dissolved in $CDCl_3$ with a concentration of 10 mg/mL. All spectra were referenced to $Si(CH_3)_4$.

4.10 Gel Permeation Chromatography (GPC)

Merck-Hiachi L6200 Intelligent Pump equipped with chromatography columns supplied from Polymer Standard Service was used for GPC measurements. Samples were dissolved in spectroscopic grade tetrahydrofuran and filtered through 0.2 μm filters. The conveyed volume of the pump was amounted to 1 mL/min and detection was carried out with the interferometric Differential-Refractometer Optilab DSP (Wyatt Technologie).

4.11 Elemental Analysis

Determination of C, H, N and S was done on a Eurovector EA 3000 CHNS-O Elemental Analyser. Digestion/mineralisation of the sample material was achieved by "flash combustion ®", applying 25 kPa oxygen at 1000 °C. Determination of P was performed by colorimetric determination as "molybdene blue [186]". Mag. Johannes Theiner from the Microanalytical Laboratory, University of Vienna performed the Elemental analysis.

4.12 X-ray Photoelectron Spectroscopy

XPS analysis was carried out with a K-Alpha photoelectron spectrometer (Thermo Scientific, United States) equipped with an Al-Kα X-ray source (hν = 1486.6 eV) and a hemispherical analyzer. The survey scan was carried out with a pass energy of 200 eV and an energy resolution of 1.0 eV. The narrow resolution spectra were typically recorded with a pass energy of 50 eV with 0.1 eV steps. The spot size was adjusted to 400 µm. The peaks were fitted using a Gaussian/Lorentzian mixed function employing Shirley background correction (Software Thermo Avantage v5.906). All analyses were performed at room temperature and hydrogen was omitted in these measurements.

4.13 Measurement of OH Number

The following procedure was adapted from reference [187]. Accordingly, 2 g zeolite particles were loaded into an Erlenmeyer flask in a stirred solution of 0.05 M $NaOH_{(aq)}$ solution (80 mL). After sealing of the flask, the particle dispersion was stirred at room temperature for 12 hours. The particles were then separated by centrifugation and 10 mL of the solution was titrated with 0.05 M $HCl_{(aq)}$ until neutralization. Titrant volume was recorded as (A). 0.05 M $NaOH_{(aq)}$ was also directly titrated with 0.05 M $HCl_{(aq)}$ until neutralization and titrant volume was recorded as (B). Number of OH groups per 1 g zeolite (X) was calculated based on the equation: X=[(B-A) x 0.05 x 8]/2

5 RESULTS AND DISCUSSION

5.1 Network Properties of Thiol-Ene and Thiol-acrylate Polymers

This study is published in Advanced Engineering Materials under the title "*Thiol-Ene versus Binary Thiol–Acrylate Chemistry: Material Properties and Network Characteristics of Photopolymers*", Volume 19, Issue 4, April 2017 (see Ref. [99]).

Lin Zequing performed his bachelor within this project. Selected results of his thesis are discussed within this chapter.

The versatile nature of photo-induced thiol-ene chemistry has made it one of the most popular reactions in design of polymer networks. In this part of the thesis, the properties of uniform thiol-ene networks were studied in detail and compared to binary thiol-acrylate networks. Regarding the thiol component, selected linear and cycloaliphatic alkyl thiol propionate esters were synthetized that bear two and four functional thiol groups (see Scheme 5.1). In terms of the "ene" component, 1,3,5-triallyl-1,3,5-triazine-2,4,6(1H,3H,5H)-trione and its acrylic counterpart tris[2-(acryloyloxy)ethyl] isocyanurate was applied to enable a direct correlation between thiol-ene and thiol-acrylate networks. In the presence of a unimolecular photoinitiator (Irgacure TPOL), photopolymerization was carried out upon UV exposure with high pressure mercury lamp at wavelengths between 250 and 470 nm. The crosslink kinetics of the different formulations was determined by FT-IR spectroscopy giving also insights into the yield of homopolymerization in thiol-allyl and thiol-acrylate formulations. Subsequently, low field NMR experiments were carried out to get information on the network structure whilst the thermo-mechanical properties were characterized by tensile tests and DSC measurements. In addition, gel fractions were calculated from swelling measurements and correlated with NMR experiments. By going from the molecular structure of the monomers over the dynamics of the polymer networks to the final mechanical properties, a correlation of process parameters and related thermo-mechanical performance of thiol-ene and thiol-acrylate networks was obtained. In addition, the applicability of

the systems for photolithographic processes was highlighted by fabrication of patterned polymer films.

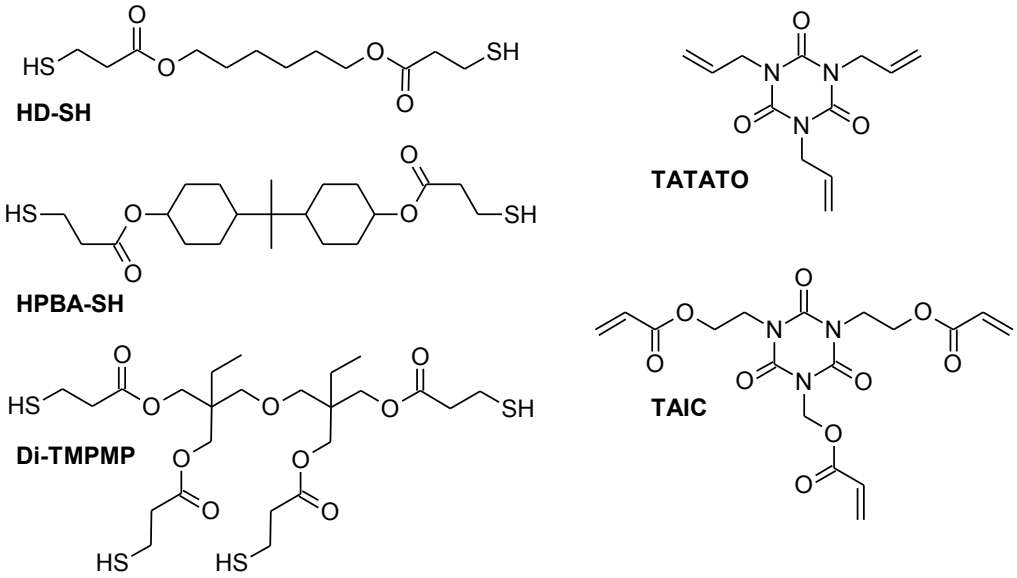

Scheme 5.1 Molecular structure of the monomers used for the preparation of thiol-allyl and thiol-acrylate networks

5.1.1 Influence of Thiol and Alkene Structure on Conversion

All formulations were prepared by mixing the thiol-ene resins in a 1:1 molar stoichiometric ratio of thiol-allyl and thiol-acrylate functional groups with 0.2 wt.% Irgacure TPOL. TAIC was melted at 60 °C prior to mixing. Irradiation dose was determined with a radiometer (UV Power Puck® II) and adjusted to 107 mW/cm^2. Quantitative conversion of functional groups was investigated by FTIR measurements in dependence on monomer functionality and chemical structure of substituents.

a) Influence of thiol structure

Three different mercapto propionate ester derivatives were synthetized and used as the thiol component of thiol-ene resins. Figure 5.1 shows the reaction kinetics of TATATO with (a) HD-SH, (b) Di-TMPMP and (c) HPBA-SH.

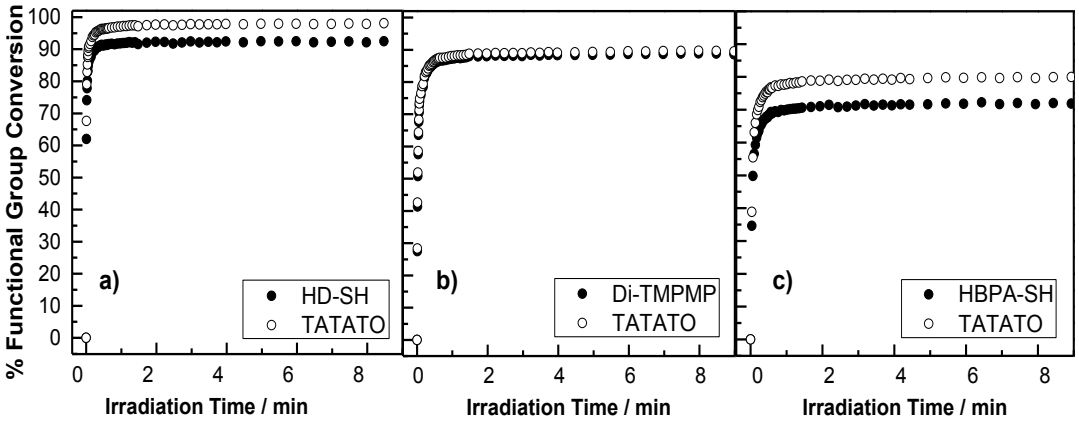

Figure 5.1: Reaction of TATATO with (a) HD-SH, (b) Di-TMPMP and (c) HPBA-SH by means of real time FT-IR spectroscopy:(❍) Conversion of the C=CH band at 3085 cm^{-1} and (●) conversion of the S-H band at 2570 cm^{-1} (Irradiation dose: 107 mW/cm^2, Irgacure TPOL: 0.2 wt.%), $Mol_{thiol}/Mol_{alkene}=1$)

In all three systems, fast polymerization rates and high conversions are observed. Curing of all photoactive resins is completed within 1 min. In addition, polymerization rate and conversion ratios of the resins are influenced by the structure of the thiol component. HD-SH yields the highest conversion whilst curing with HBPA-SH results in the lowest conversion and slowest polymerization rate. Between the three applied thiol structures, HD-SH is the most flexible one, while cycloaliphatic HBPA-SH is the most rigid structure. In contrast to HD-SH and HBPA-SH, Di-TMPMP comprises four thiol groups and is able to form four crosslinking points. It shows a lower conversion compared to bifunctional HD-SH which indicates that the photopolymerization reaction is also governed by diffusion limitations of the reactive monomers. Furthermore, Figure 5.1 also reveals that thiol and –ene groups are consumed at similar rates owning to step-growth mechanism of the thiol-ene reaction. Homopolymerization of allyl groups reaches a maximum around 10 % for the HBPA-SH/TATATO system. In particular, photopolymerization of TATATO with the tetra-functional Di-TMPMP leads to comparable SH and C=C double conversions (see Figure 5.1b). By comparing the thiol and allyl conversions it is interesting to note that the curing with HD-SH results in significantly higher C=C double bond conversion (98 %) suggesting that additional homopolymerization of the allyl monomers takes place (6 %) under these irradiation conditions. The results indicate that the amount of homopolymerization of the allyl monomer is influenced by the reactivity of the thiol monomers as well as by the diffusion

limitation of the reactive species. In the TATATO/HPBA-SH system the lowest SH and C=C double bond conversion is observed which can be mainly associated with the low reactivity of the cycloaliphatic thiol.

b) Influence of alkene structure

Along with the thiol, the influence of the alkene structure on the conversion of the thiol-ene resin mixtures was investigated. Copolymerization of the allyl functional monomer TATATO has already been discussed in the previous chapter. In this section, its acrylic counterpart TAIC was copolymerized with HD-SH, HBPA-SH and Di-TMPMP.

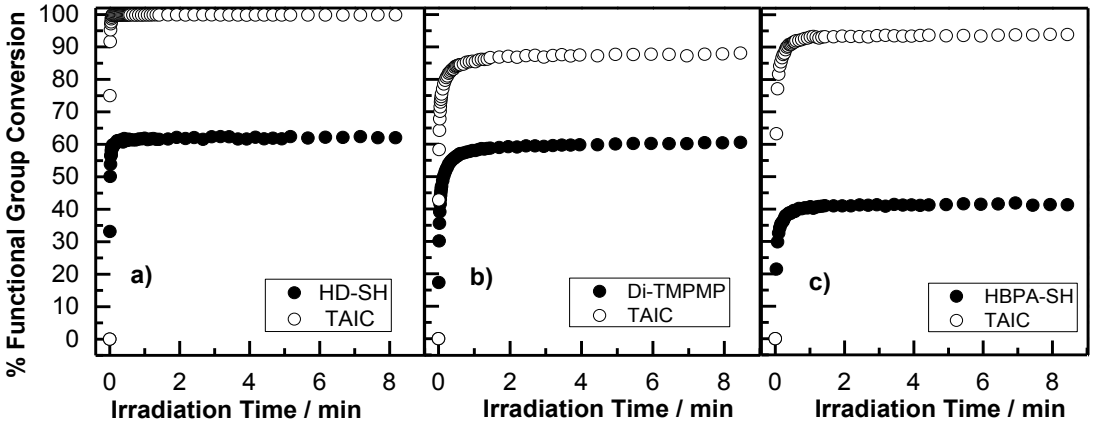

Figure 5.2: Monitoring the reaction of TAIC with (a) HD-SH, (b) Di-TMPMP and (c) HPBA-SH by means of real time FT-IR spectroscopy: (❍) Conversion of the C=CH wagging band at 1625 cm^{-1} and (●) conversion of the S-H band at 2570 cm^{-1}. (Irradiation dose: 107 mW/cm^2, Irgacure TPOL: 0.2 wt.% , Mol_{thiol}/Mol_{alkene}=1)

Irradiation of thiol-acrylate resin mixture does not only lead to thiol-acrylate copolymerization by step growth mechanism but also to acrylate homopolymerization via a chain growth reaction, thus, leaving a considerable amount of thiol groups unreacted. The C=C double bond conversion of TAIC is higher compared to the previously discussed thiol-ene systems using TATATO as ene monomer. Previous studies revealed that the rate of homopolymerization of typical acrylate monomers is around 1.5 times higher than the hydrogen abstraction from the thiol [188]. Due to the higher reactivity of the acrylate, the yield of homopolymerization is higher in thiol-acrylate networks than in thiol-allyl networks.

However, by studying the influence of the thiol on the amount of homopolymerization the same order is found in thiol-allyl and thiol-acrylate systems: Di-TMPMP < HD-SH < HPBA-SH. In addition, the results indicate that both di-functional thiols promote higher C=C double bond conversions in thiol-acrylate photopolymerizations compared to the tetra-functional thiol. A complete conversion of the C=C double bonds is observed in TAIC/HD-SH networks upon 10 s UV exposure whilst it reaches 93 % in TAIC/HPBA-SH systems. In contrast, the C=C double bond conversion does not exceed 87 % when the tetra-functional thiol Di-TMPMP is applied. This behaviour probably results from the higher crosslinking density of the polymer in TAIC/Di-TMPMP reaction system which limits the movement of the free monomers, thus prevents further reaction. It is evident that not only the choice of the ene monomer but also the selection of the thiol component is crucial for the network evolution in thiol-ene and thiol-acrylate photopolymerizations.

5.1.2 Thermal and Mechanical Properties of Thiol-ene Networks

DSC and tensile tests were performed to investigate the influence of the network structure on the thermo-mechanical properties.

Tensile test measurements were carried out according to procedure described in Section 4.6.b. For DSC analysis, resin mixtures were firstly cured in aluminum crucibles upon 1.43 min UV exposure (exposure dose: 107.3 mW/cm^2) and measurements were conducted as described in Section 4.5. In Table 5.1, the glass transition range and tensile properties of the different resin formulations are summarized.

Table 5.1: Glass transition regions and tensile properties of thiol-allyl and thiol-acrylate photopolymers

Photopolymer network	Tg[a] °C	Tg onset °C	Tg end point °C	Tensile strength MPa	Tensile strain at break %	Young's modulus MPa
TATATO/HD-SH	-13.4	-18.4	-11.0	1.2 ± 0.1	20.3 ± 1.3	6.5 ± 0.4
TATATO/Di-TMPMP	24.0	17.0	30.3	12.9 ± 3.1	36.1 ± 11.7	276 ± 25
TATATO/HPBA-SH	21.0	9.1	25.2	15.6 ± 2.9	3.5 ± 0.3	484 ± 156
TAIC/HD-SH	-3.2	-22.1	5.4	2.7 ± 0.3	29.1 ± 2.4	10.8 ± 3.1
TAIC/Di-TMPMP	2.6	-6.8	20.4	7.2 ± 1.7	33.4 ± 5.9	46.5 ± 22.7
TAIC/HPBA-SH	9.2	-8.8	34.9	7.3 ± 2.0	48.8 ± 17.5	66.2 ± 16.5

[a] (obtained from the turning point of the DSC curve.)

A Tg below 0°C is obtained for both thiol-allyl and thiol-acrylate networks if the curing is carried out with the bi-functional HD-SH. On the one side, this can be related to the low thiol functionality corresponding to a lower crosslink density and on the other side is attributed to the flexibility of the linear alkyl chains of the thiol structure. Thus, the corresponding tensile strength and Young's modulus for TATATO/HD-SH based networks are rather low and do not exceed 1.2 MPa and 6.5 MPa, respectively.

With respect to the TAIC/HD-SH network, it should be considered that the distinctive contributions from the acrylate homopolymerization as well as the higher monomer conversion promote a Tg that is around 10°C higher compared to the TATATO/HD-SH system. The acrylate homopolymerization and the related heterogeneity of the binary TAIC/HD-SH network is also reflected by the temperature ranges of the glass transition regions. Whilst TATATO/HD-SH networks are characterized by a rather narrow temperature range of the glass transition, it broadens substantially for TAIC/HD-SH systems. From the tensile measurements, it can be obtained that TAIC/HD-SH networks display higher tensile strength and Young's modulus compared to TATATO/HD-SH networks.

In contrast, curing of TATATO and TAIC with the bi-functional HPBA-SH results in networks with a higher Tg which can be related to the cycloaliphatic nature of the thiol. It is interesting to note that the Tg of the TAIC/HPBA-SH network is significantly

lower (9°C) compared to the corresponding thiol-allyl network (21°C). This trend can be explained by the combined effect of low SH-conversions and high amount of acrylate homopolymerization observed in TAIC/HPBA-SH systems which lead to a very broad glass transition region. Along with the Tg, the lower number of cycloaliphatic thiols incorporated in the polymer networks also govern the tensile properties. The photochemical crosslinking of TATATO with HPBA-SH yields rigid networks with a low ultimate elongation, high Young`s modulus and tensile strengths in the range of 15.6 MPa. However, in TAIC/HPBA-SH systems the low SH-conversion facilitates a distinctly lower Young's modulus together with a lower tensile strength and higher ultimate elongation.

By increasing the thiol-functionality from two to four, polymer networks with an even higher crosslink density are obtained since a higher number of crosslink sites is formed. Thus, the photopolymerization of TATATO with the tetra-functional thiol Di-TMPMP yields networks with a higher Tg. The tensile strength amounts to 12.9 MPa whilst the Young's modulus reaches 275.8 MPa. In terms of TAIC/Di-TMPMP networks the increase in Tg is less pronounced due to the simultaneous acrylate homopolymerization and lower SH-conversion which also governs the related tensile properties. Both a lower tensile strength and a lower Young's modulus are observed for TAIC/Di-TMPMP compared to the TATATO/Di-TMPMP counterpart.

5.1.3 Characterization of the Network Structure

Different degree of functional groups conversion (obtained from FTIR measurements) as well as the broad glass transition ranges (observed in DSC experiments) clearly indicate heterogeneity in all networks, but more specifically in the case of acrylic-thiol based systems. To further investigate network heterogeneity, DQ NMR was applied on these networks which has been mainly used in the past to investigate heterogeneous elastomers [181]. In this method, an NMR parameter called residual dipolar coupling (D_{res}) which is directly related to the order and mobility in the system which are in turn related to the network density in the studied system, is measured. However, an important point to note is that in contrast to elastomers where the measured residual dipolar coupling (D_{res}) and its distribution corresponds to the varying network chain length, here in these systems where the network chain length is uniform and constant,

the observed D_{res} and the heterogeneity corresponds to chain dynamics and modality respectively.

Figure 5.3 shows the normalized DQ build up curves for TATATO/HD-SH and TAIC/HD-SH networks, respectively. Clearly, the TATATO/HD-SH network shows a smooth mono-modal build-up while the curve for TAIC/HD-SH does not.

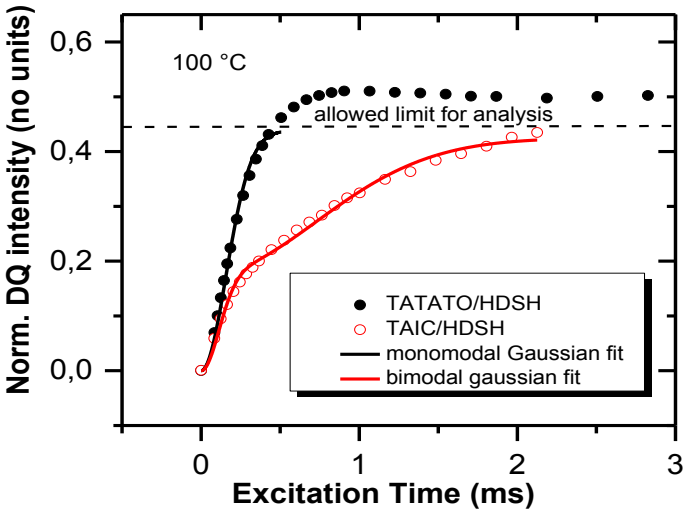

Figure 5.3: Normalized DQ curves for TATATO/HD-SH and TAIC/HD-SH networks. The modality of the curves can be clearly seen, as well as the best fit with Equation 2.

To extract D_{res}, given the near uniformity of network chain length in the HD-SH/TATATO, the curves were fitted assuming homogeneous networks with a model based on an inverse Gaussian function (see Equation 5.1). The results of the best fit are given in Table 5.2.

$$S_{nDQ}(D_{res,i}, f_i) = \sum_i f_i \left(0.5 * \left\{1 - \exp\left(-\frac{2}{5} D_{res1}^2 \quad {}^2_{DQ}\right)\right\}\right) \qquad 5.1$$

Table 5.2: Results of the analysis of DQ build up curves for HD-SH and Di-TMPMP based networks at 100°C. The network fraction is the elastic part of the network that does not include unreacted monomers, additives as well as non-elastic segments such as loops (crosslinked to the same point) or tails (segment whose one end is not connected). For comparison, the gel fraction from swelling measurements are given. Note that the gel fraction includes the non-elastic segments such as loops that are covalently connected to the network which explains the slightly higher value.

Sample	f_1	$D_{res,1}$ [kHz]	f_2	$D_{res,2}$ [kHz]	Network fraction	Gel content
TATATO/HD-SH	-	7.81	-	-	0.93	0.96
TAIC/HD-SH	0.40	6.40	0.6	0.97	0.87	0.90
TATATO/*Di*-TMPMP		7.59			0.86	0.93
TAIC/*Di*-TMPMP	0.44	7.19	0.56	1.13	0.91	0.96

The results show a higher non-network contribution for TAIC/HD-SH network when compared to TATATO/HD-SH network which is agreement with conversion results from IR as well as gel content determined with swelling measurements (see Section 4.3 for swelling measurement conditions. Gel content amounts to 0.956±0.014 and 0.904±0.006 for TATATO/HD-SH and TAIC/HD-SH, respectively). The discrepancies in the absolute values can be accounted for by the dangling loops and tails which are part of gel content in swelling measurement but not of network fraction in NMR [189].

As briefly mentioned above, a single component fit of Equation (5.1) was sufficient to describe the DQ build up curve of TATATO/HD-SH, while a two-component fit was necessary to describe the TAIC/HD-SH network. For the latter, the two networks show a vastly different mobility resulting from the copolymeric and homopolymeric as well as any defect structures. The above observations can be qualitatively applied to allylic and acrylic Di-TMPMP based networks as well, however, repeated measurements as well as measurements at different temperatures on HBPA-SH networks did not yield a DQ build up. This can be understood as a result of the low conversion degree of the system not resulting in a gel and is under further investigation. Also, interesting to note

is that the weight fractions of the two networks agree qualitatively with the consumption of the two fractions obtained from FTIR experiments (see Figure 5.2).

5.1.4 Application Example

The efficient conversion of monomers into insoluble polymer networks was further employed for the preparation of negative-toned photoresists. The first experiments were carried out with TATATO using Di-TMPMP and HD-SH as thiol components. The resin formulations were cast on microscope slides to obtain thin films which subsequently were patterned by photolithographic techniques. After the UV exposure for 1.43 minutes with a Hg lamp through a quartz chromium mask, the non-crosslinked monomers were removed in a development step using acetone. The inscribed patterns were visualized by microscopic techniques and the optical micrographs of patterned TATATO/Di-TMPMP and TATATO/HD-SH networks are shown in Figure 5.4a and 5.4b, respectively. Polymer structures with a structure size of 25 µm were obtained in thiol-allyl networks.

In a second step, the applicability of the thiol-acrylate networks for the fabrication of photo-resists is evaluated for the system TAIC/Di-TMPMP. As provided in Figure 5.4c, patterns with a structure size of 25 µm were obtained after the development step clearly demonstrating the potential of binary thiol-acrylate systems in resist technology.

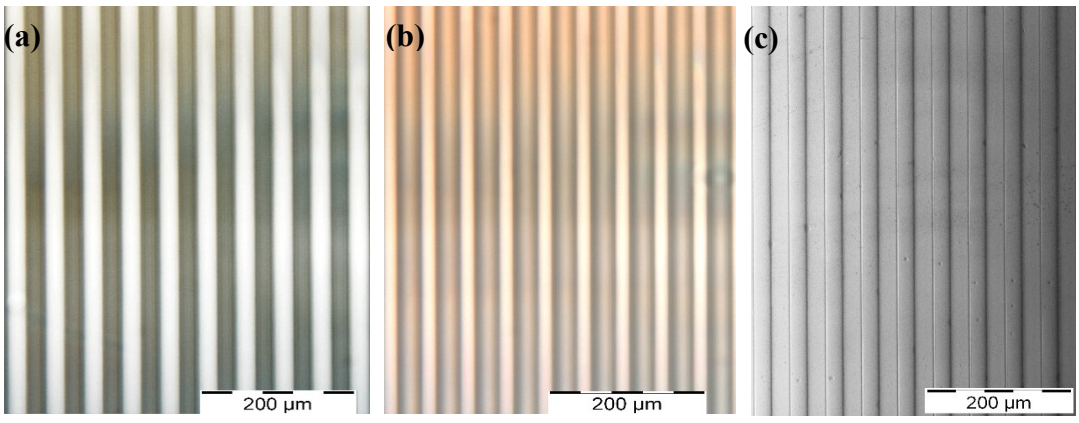

Figure 5.4: Optical micrographs of photo patterned (a) TATATO/HD-SH, (b) TATATO/di-TMPMP and (c) TAIC/di-TMPMP networks after the development in acetone.

5.2 Preparation of Photo-cured NR Elastomers with Low Migratable Thiol Components

In this part of the study, outstanding properties of photo-induced thiol-ene chemistry were exploited to cure natural rubber (NR) latex.

NR latex is a biodegradable and environmentally friendly material and it is applied in the production of various commercial products such as condoms, balloons, toys, catheters and medical gloves. NR latex is obtained from a tree called *Hevea brasiliensis* as a milky, white liquid [190]. Although it has been used for many years, its use as a glove material has been dramatically increased due to the concern about cross contamination of diseases since 1980s [14].

Medical gloves can be classified as examination and surgical gloves. Surgical gloves are characterized by their high tactile sensitivity and precise sizing and they are used in their sterilized form while examination gloves could be used in both non-sterile and sterile form. NR gloves provides good barrier properties against pathogens and typically exhibits excellent mechanical properties.

However, the use of NR based products can provoke allergenic reaction associated with proteins and chemicals used in the classic sulphur vulcanization [191–193]. Three types of allergy are reported which are caused by the use of NR latex gloves; Type I, type IV and irritant dermatitis. While Type I allergy is induced by proteins present in the raw material NR latex, the other two allergies originate from process chemicals such as accelerators used in the vulcanization process.

NR latex is conventionally cured by a sulphur vulcanization process for the preparation of surgical gloves. However, migration of unreacted chemicals (e.g. dithiocarbamate-type and 2-mercaptobenzothiazole-type accelerators) used in the sulphur curing causes latex type IV allergy. As latex allergy is a growing concern nowadays, alternative ways to prevent migration of the chemicals from latex to the skin has been searched. Elimination of these chemicals in the curing and employment of green chemistry for crosslinking reactions is one of the promising ways.

Photo-crosslinking of NR latex by employing thiol-ene reaction is a good alternative to sulphur vulcanization process and was already published in literature [194]. Radiation curing was accomplished through thiol-ene reaction involving the crosslinking of C=C

double bonds of the NR with thiol groups of the various crosslinkers as shown in Scheme 5.2.

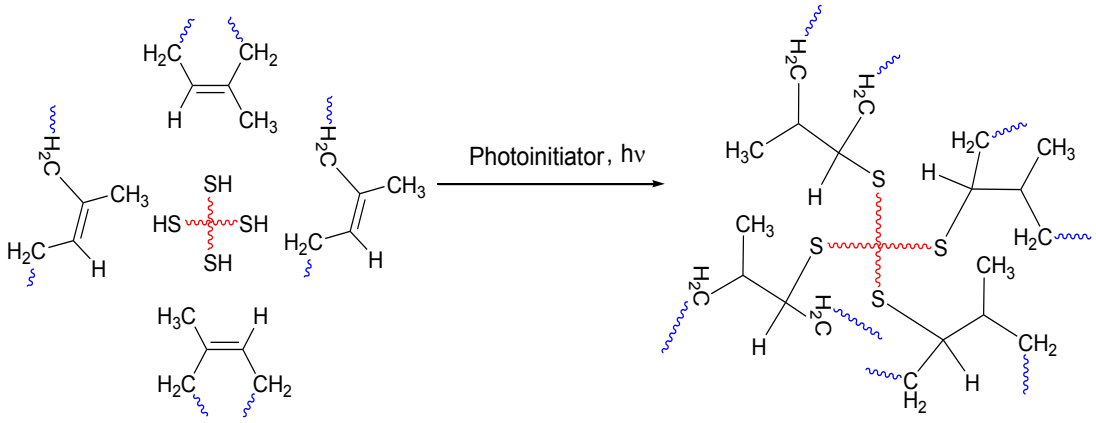

Scheme 5.2: Thiol-ene reaction between NR latex and thiol groups of a multifunctional thiol crosslinker

In the present work, crosslinking of NR latex with low migratable photochemicals was carried out by pursuing three different strategies. Firstly, thiol functional crosslinkers (either commercially available or synthetized) with a high molecular weight were used to cure NR latex. In the second strategy, newly synthesized siloxane based thiol oligomers were used as crosslinkers. As a final approach, zeolite and silica particles were modified with mercapto functional silanes and then used as low migratable crosslinker for the photo-curing of NR latex. Preparation of crosslinked NR latex was carried out as described in Section 3.6. 1 phr Irgacure TPO-L was used as initiator in all measurements in this Section.

Obtained samples were tested in view of their mechanical performance by tensile test measurements (see Section 4.6 for procedure)**.** Swelling measurements were done in toluene for 48 hours at room temperature to calculate the gel fractions. Gel fractions and mechanical properties were correlated with each other. Migration ability of selected thiols were investigated by Soxhlet extraction experiments. Subsequently, extractable contents were determined by elemental analysis.

5.2.1 Thiol-ene Chemistry with Multi-Functional Thiols

Photo-chemical crosslinking of NR latex with multifunctional thiol monomers was investigated and evaluated in view of number of crosslinking points, rigidity and flexibility of crosslinkers.

Three different curing procedures were applied and compared with each other. In the photo-induced post-curing, dried films were exposed to irradiation (3.9 J/cm^2) and the crosslinking took place in the solid film state. In contrast, a pre-curing procedure was applied by UV exposure (5.2 J/cm^2) of the liquid NR latex formulation. Films were then prepared from the pre-cured NR latex. In the third procedure, both pre-curing as well as post-curing (5.2 J/cm^2 and 2.6 J/cm^2, respectively) was carried out.

The structure of the used crosslinkers is shown in Scheme 5.3.

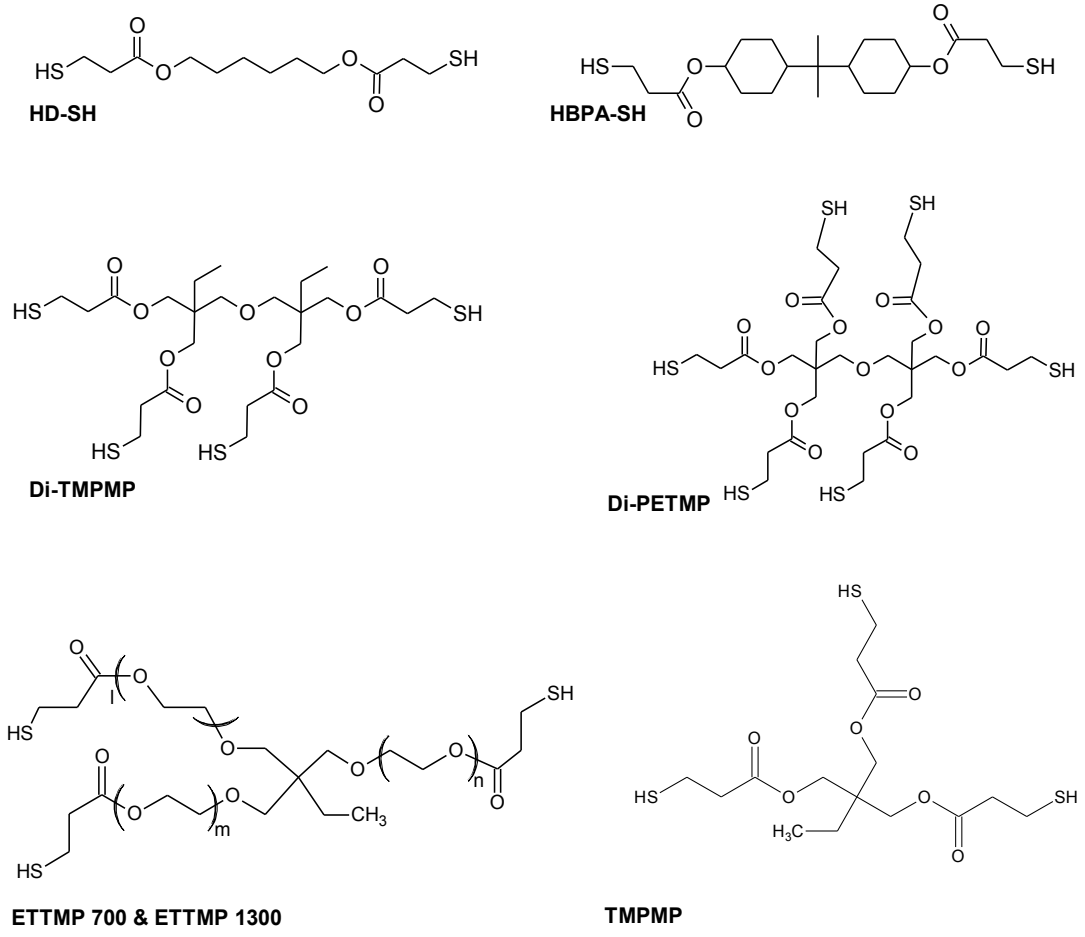

Scheme 5.3: Molecular structure of multifunctional thiols used for the photo-crosslinking of NR latex

In the first experiments, the low molecular weight and bifunctional thiols HD-SH and HBPA-SH were used for the curing of NR latex to study the influence of crosslinker structure on mechanical properties. Owed to the linear aliphatic character, HD-SH is a rather flexible crosslinker whilst the bulky cycloaliphatic groups of HBPA-SH contribute to a rigid character. The influence of crosslinker rigidity on tensile properties of NR samples are shown in Figure 5.5.

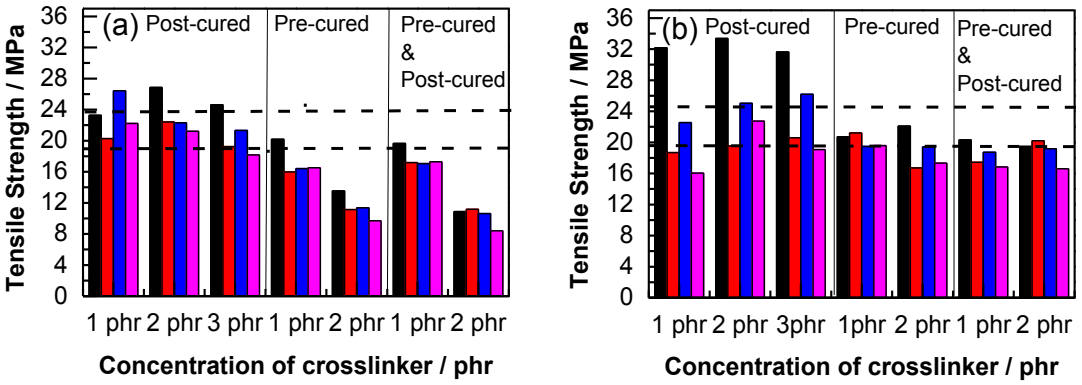

Figure 5.5: Tensile strength of NR latex films photo-crosslinked with varying concentrations of (a) HD-SH and (b) HBPA-SH as crosslinker in dependence on the treatment: (black) non-sterile and not aged, (red) non-sterile and aged at 70°C for 7 days, (blue) sterile and not aged and (magenta) sterile and aged at 70°C for 7 days. (exposure dose: -post-curing; 3.9 J/cm^2, -pre-curing; 5.2 J/cm^2, -post-curing&pre-curing; 2.6 and 5.2 J/cm^2, respectively)

Figure 5.5 shows that the tensile strength of NR samples cured with bifunctional thiol crosslinkers is the highest when only post-curing is applied. Particularly, crosslinking with HBPA-SH results in excellent tensile properties. Cycloaliphatic bifunctional HBPA-SH crosslinker leads to the formation of polymer networks with higher tensile strength due to its rigid structure compared the ones obtained with flexible HD-SH monomer. Some of the sterile NR latex films containing HBPA-SH as crosslinker exhibit a tensile strength higher than 20 MPa meeting the requirements to produce surgical gloves (>18 MPa). The tensile strength of samples crosslinked with either HBPA-SH or HD-SH decreases during an accelerated aging at 70°C for seven days. Ultimate elongation and modulus at 50% elongation values of the samples cured with HD-SH and HBPA-SH are shown in Figure 5.6 and 5.7, respectively.

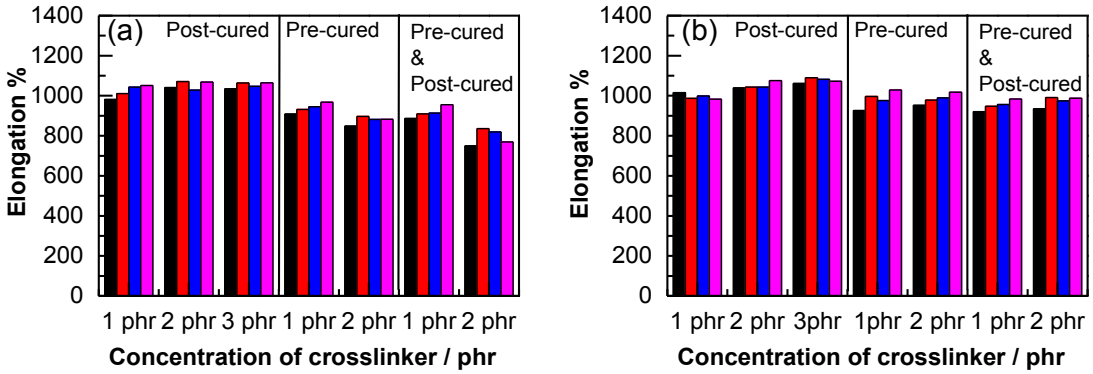

Figure 5.6: Elongation of NR latex films photo-crosslinked with varying concentrations of (a) HD-SH and (b) HBPA-SH as crosslinker in dependence on the treatment: (*black*) non-sterile and not aged, (*red*) non-sterile and aged at 70°C for 7 days, (*blue*) sterile and not aged and (*magenta*) sterile and aged at 70°C for 7 days. (exposure dose: -post-curing; 3.9 J/cm^2, -pre-curing; 5.2 J/cm^2, -post-curing&pre-curing; 2.6 and 5.2 J/cm^2, respectively)

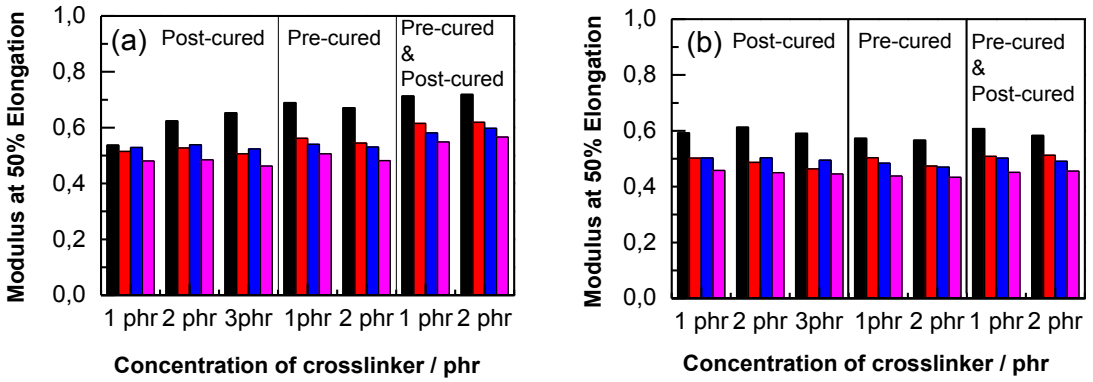

Figure 5.7: Modulus at 50% elongation of NR latex films photo-crosslinked with varying concentrations of (a) HD-SH and (b) HBPA-SH as crosslinker in dependence on the treatment: (*black*) non-sterile and not aged, (*red*) non-sterile and aged at 70°C for 7 days, (*blue*) sterile and not aged and (*magenta*) sterile and aged at 70°C for 7 days. (exposure dose: -post-curing; 3.9 J/cm^2, -pre-curing; 5.2 J/cm^2, -post-curing&pre-curing; 2.6 and 5.2 J/cm^2, respectively)

Elongation at break values are over 900% and moduli at 50% elongation are lower than 0.7 MPa which meet to required values for all samples. (See Table 2.2 for the mechanical requirements of surgical gloves).

Swelling degree and gel fraction of the NR latex cured with bifunctional thiols are illustrated in Figure 5.8. The swelling degree of all samples is around 5.3 and the gel

content values are ranging from 0.93 to 0.97. Samples post-cured either with HD-SH or with HBPA-SH exhibit the lowest gel fractions. Gel fraction values of all samples are correlating with the ultimate elongation values as a decrease in ultimate elongation is seen when the gel fraction is increasing due to the increase of crosslink density. Furthermore, moduli of post-cured samples crosslinked with HD-SH are lower than pre-cured and pre- & post- cured samples, which indicates the lowest crosslinking density of post-cured samples. On the contrary, modulus change due to the increasing crosslinked density is less pronounced in NR samples cured with HBPA-SH.

(a)

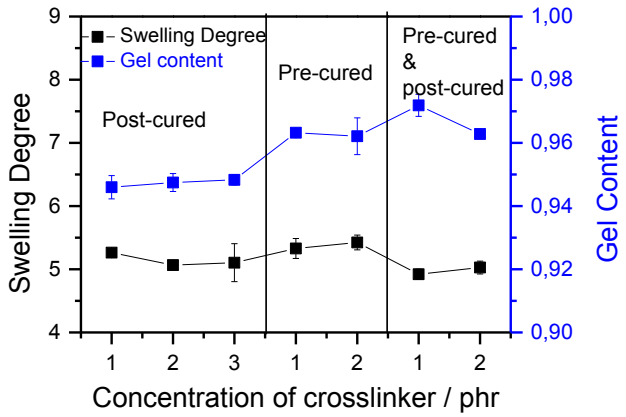

HD-SH

(b)

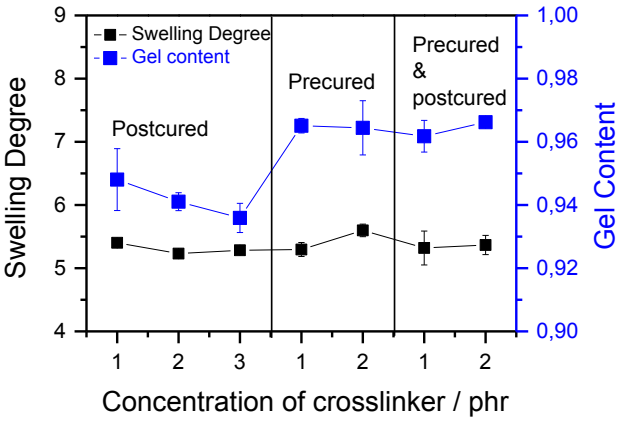

HBPA-SH

Figure 5.8: Swelling degree and gel content of NR latex cured with (a) HD-SH and (b) HBPA-SH as a function of the crosslinker concentration (exposure dose: -post-curing; 3.9 J/cm^2, -pre-curing; 5.2 J/cm^2, -post-curing&pre-curing; 2.6 and 5.2 J/cm^2, respectively)

Going from bi-functional weight crosslinker, further crosslinking studies of NR latex were carried out with multi-functional thiols. Di-TMPMP and Di-PETMP which bear 4 and 6 thiol functions respectively were applied as crosslinkers. Figure 5.9 shows the mechanical performance of NR samples crosslinked with either Di-TMPMP or Di-PETMP.

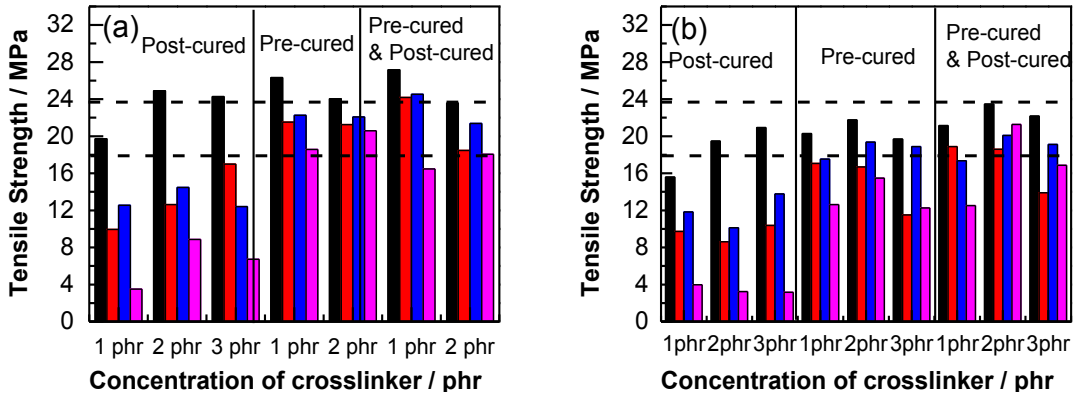

Figure 5.9: Tensile strength of NR latex photo-crosslinked with (a) Di-TMPMP and (b) Di-PETMP as a function of the crosslinker content and in dependence on the treatment: (*black*) non-sterile and not aged, (*red*) non-sterile and aged at 70°C for 7 days, (*blue*) sterile and not aged and (*magenta*) sterile and aged at 70°C for 7 days (exposure dose: -post-curing; 3.9 J/cm^2, -pre-curing; 5.2 J/cm^2, -post-curing&pre-curing; 2.6 and 5.2 J/cm^2, respectively)

Tensile test results (Figure 5.9) reveal that mechanical properties of photo-cured NR latex films are affected by both crosslinker type and concentration as well as curing methods. In general Di-TMPMP leads to higher tensile strengths compared to Di-PETMP. NR samples cured with Di-TMPMP as crosslinker meet the minimum tensile strength requirement of 24 MPa prior to sterilization (under certain curing conditions), whilst this is not the case for samples cured with Di-PETMP.

The tensile strength of NR samples decreases after aging and sterilization and this decrease is more pronounced in the case of samples which have only been post-cured. The elongation at break values (see Figure 5.10) are in the range of 800 % for each samples independent of the applied curing method, the crosslinker type (Di-TMPMP versus Di-PETMP) and the concentration of the crosslinker. On the contrary modulus

at 50% elongation (see Figure 5.11) is strongly affected by crosslinker type. Samples crosslinked with tetra-functional Di-TMPMP show higher moduli than the samples cured with Di-PETMP. Particularly, only post-curing of samples leads to lower modulus compared to their pre-cured and pre-&post-cured counterparts and this indicates a lower crosslinking degree of post-cured samples.

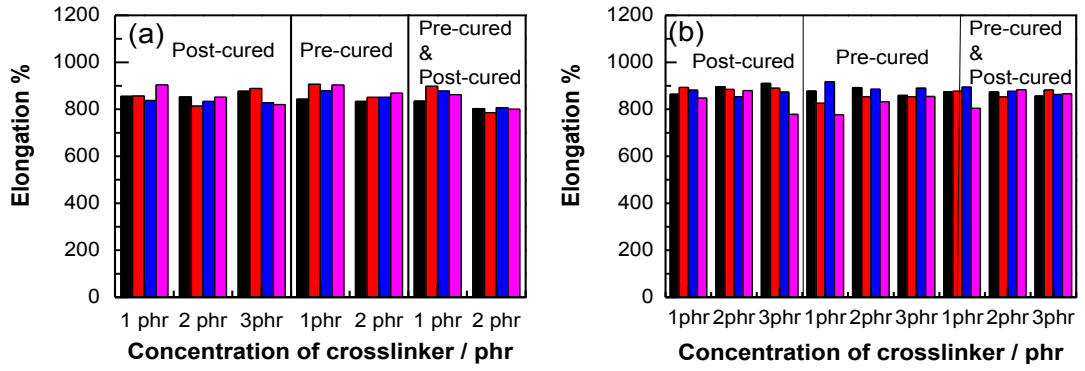

Figure 5.10: Elongation of NR latex photo-crosslinked with (a) Di-TMPMP and (b) Di-PETMP as a function of the crosslinker content and in dependence on the treatment: (*black*) non-sterile and not aged, (*red*) non-sterile and aged at 70°C for 7 days, (*blue*) sterile and not aged and (*magenta*) sterile and aged at 70°C for 7 days. (exposure dose: -post-curing; 3.9 J/cm^2, -pre-curing; 5.2 J/cm^2, -post-curing&pre-curing; 2.6 and 5.2 J/cm^2, respectively)

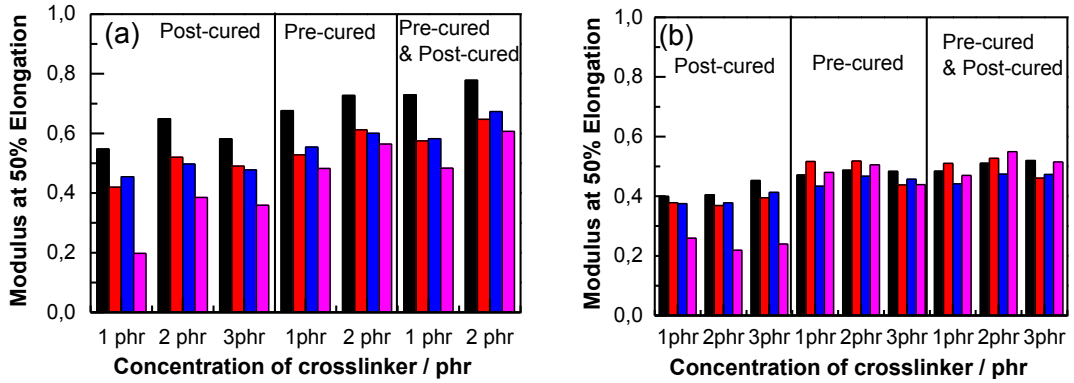

Figure 5.11: Modulus at 50% elongation of NR latex photo-crosslinked with (a) Di-TMPMP and (b) Di-PETMP as a function of the crosslinker content and in dependence on the treatment: (*black*) non-sterile and not aged, (*red*) non-sterile and aged at 70°C for 7 days, (*blue*) sterile and not aged and (*magenta*) sterile and aged at 70°C for 7 days. (exposure dose: -post-curing; 3.9 J/cm^2, -pre-curing; 5.2 J/cm^2, -post-curing&pre-curing; 2.6 and 5.2 J/cm^2, respectively)

Equilibrium swelling measurements (Figure 5.12) of NR samples cured with Di-TMPMP and Di-PETMP support the results of the tensile tests. In particular, the swelling degree of the post-cured samples are the highest indicating a lower crosslink density which is related to a lower modulus. In contrast, a reduced swelling degree is observed in NR latex samples which have been either pre-cured or pre- and post-cured. The lower swelling degree suggests a higher crosslink density corresponding to a higher modulus of the related NR latex films. These results point out the higher efficiency of multifunctional thiol crosslinker in both the pre-curing as well as in the pre- and post-curing of NR latex. Moreover, samples cured with Di-TMPMP show lower swelling ratio than the ones cured with Di-PETMP, which is in good agreement with the tensile properties of the latex films. High degree of swelling together with low moduli of post-cured NR samples, which are crosslinked with Di-PETMP, indicate a looser network structure compared to NR samples cured with Di-TMPMP.

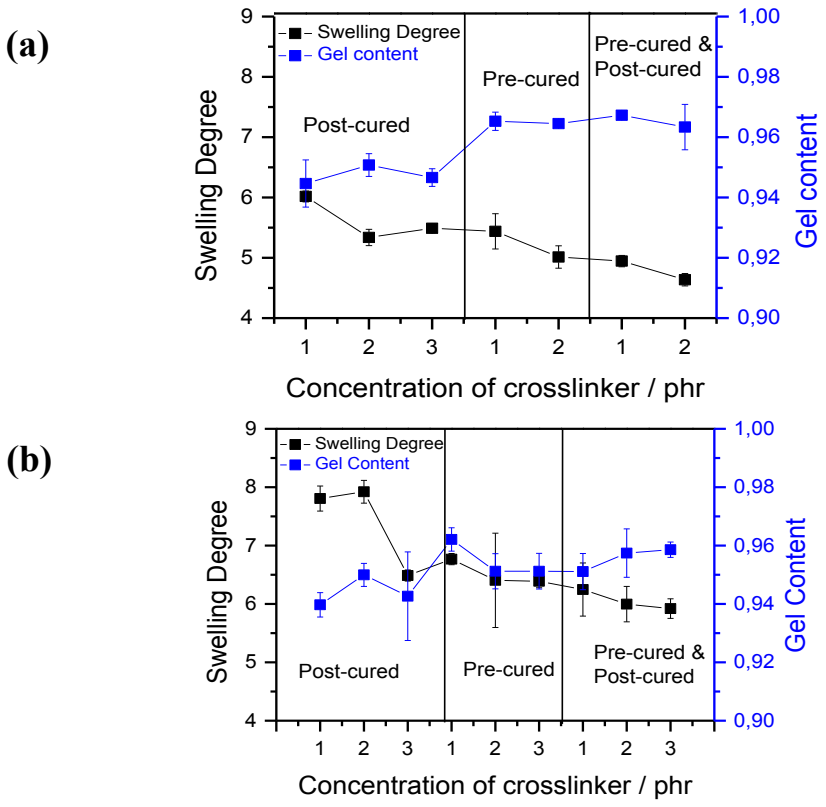

Figure 5.12: Swelling degree and gel content of NR latex films photo-cured with (a) Di-TMPMP and (b) Di-PETMP as a function of the crosslinker concentration. (exposure dose: -post-curing; 3.9 J/cm^2, -pre-curing; 5.2 J/cm^2, -post-curing&pre-curing; 2.6 and 5.2 J/cm^2, respectively)

In addition to low-molecular weight multifunctional thiols, high-molecular weight thiols based on mercaptopropionate ester structures were exploited for the photo-curing of NR latex. ETTMP 700 and ETTMP 1300 were tested and compared to their lower molecular weight counterpart TMPMP. The structure of ETTMP 700, 1300 and TMPMP crosslinker include mercaptopropionate groups (see Scheme 5.3); thus, for a comparable study their functionality per molecular weight was taken into account. Despite higher concentration of ETTMP 700 and 1300 (ensuring an equal concentration of mercapto moieties in the latex emulsion), the best tensile strength was obtained by using TMPMP as crosslinker. This difference in the tensile strength might be related to the lower mobility of the high-molecular weight initiators. Increased flexibility of the ETTMP 700 and 1300 crosslinker due to the longer oxyethylene spacer in their structure is reflected by high ultimate elongation and low modulus. However, the reduced modulus might be also a result of a lower crosslink density.

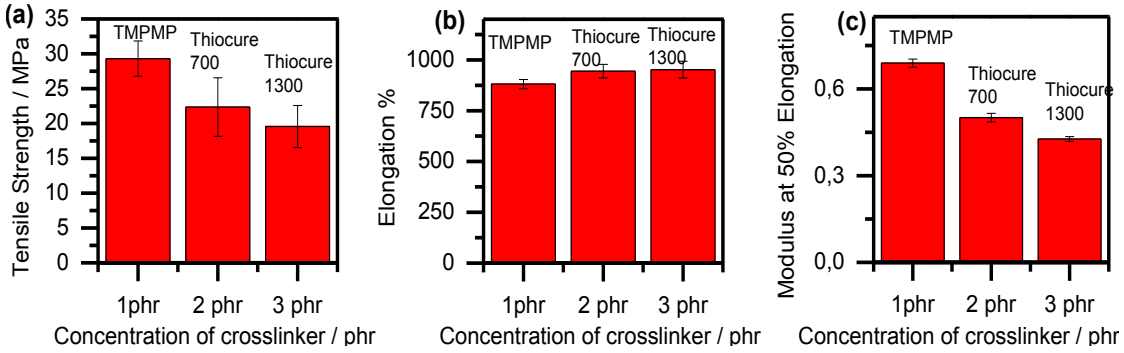

Figure 5.13: (a) Tensile strength, (b) elongation at break and (c) modulus at 50% elongation NR latex films post-cured with TMPMP, ETTMP 700 and ETTMP 1300 (Photoinitiator: 1 phr Irgacure TPOL and irradiation dose: 3.9 J/cm^2).

In conclusion, the tensile strength of crosslinked NR samples is affected by the used crosslinker type, crosslinker concentration and applied curing method. Thus, the tensile properties were optimized by determining the optimum crosslinker concentration and the best curing procedure, which are both strongly dependent on the crosslinker type. Mercaptopropionate ester based crosslinkers having bulky cycloaliphatic groups lead to higher tensile strength than the ones with linear alkyl chains (HBPA-SH versus HD-SH). Furthermore, increase in mercaptopropionate group functionality from 3 to

6 has an adverse effect on tensile strength of NR as tensile strength of post-cured NR samples show the following order; TMPMP > Di-TMPMP> Di-PETMP. Since moduli of aforementioned samples have the same increasing order, this increasing trend might be attributed to a tighter network formation (increased crosslinked density). Moreover, influence of oxyethylene spacer length in the crosslinker structure on the mechanical properties of cured NR samples was studied. The results point out that crosslinkers with longer oxyethylene spacer in their structure lead to formation of highly flexible samples, which is reflected by an enhanced ultimate elongation and a lower modulus.

5.2.2 Thiol-ene Chemistry with Siloxane Based Oligomeric Thiols

Markus Ast performed his bachelor within this project. Selected results of his thesis are discussed within this section.

Siloxane based oligomeric thiols were synthesized (see Section 3.3 for synthesis conditions) and characterized by GPC and FTIR spectroscopy. They were then applied as high-molecular weight crosslinker in the photo-curing of NR latex. The structure of silane monomers used in synthesis of the oligomeric siloxanes is shown in Scheme 5.4.

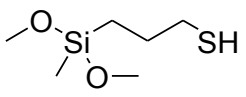

(3-Mercaptopropyl)methyldimethoxysilane

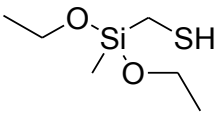

(Mercaptomethyl)methyldiethoxysilane

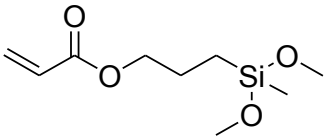

(3-Acryloxypropyl)methyldimethoxysilane

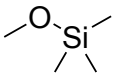

Trimethylmethoxysilane

Scheme 5.4: Structure of chemicals used in the synthesis of thiol functional siloxanes.

In the first part of this section, the properties such as molecular weight of the synthesized siloxanes are presented. This is followed by a discussion on the mechanical properties of photo-cured NR latex and on the extractability of selected oligomeric thiols from crosslinked NR latex films.

5.2.2.1 Determination of molecular weight

Molecular weight of the obtained siloxanes was analysed by gel permeation chromatography (GPC). Since product Siloxane-1 had a malodour, its monomeric form (mercaptomethyl)methyldiethoxysilane was not used to investigate the influence of any reaction parameters.

However, a comprehensive study on the effect of reaction parameters on the molecular weight of the related oligomers was performed with (3-mercaptopropyl)methyldimethoxysilane (3-MPMS) as a starting monomer.

Figure 5.14 shows the influence of the reaction time and the initial monomer concentration of 3-MPMS on the molecular weight of the products.

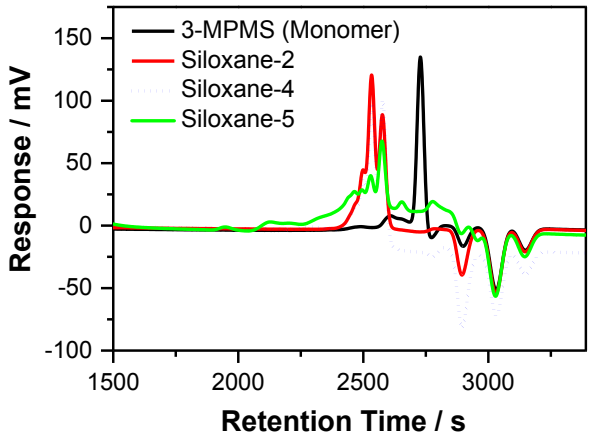

Figure 5.14: Molecular weight determination of siloxanes by GPC measurements (Synthesis conditions: *Siloxane-2*: 9 wt.% initial monomer concentration, 3 h reaction time; *Siloxane-4*: 9 wt.% initial monomer concentration, 9 h reaction time; *Siloxane-5*: 18 wt.% initial monomer concentration, 3 h reaction time)

As seen in Figure 5.14, the molecular weight of the product is slightly increasing when reaction time is extended from 3 h (siloxane-2) to 9 h (siloxane-4). Pentamer formation is observed at a reaction time of 9 h, whilst trimeric and tetrameric species are predominantly obtained under both reaction times. In contrast, the concentration of initial monomer has a stronger impact on the molecular weight of the oligomers. Figure 5.14 indicates higher polydispersity and higher molecular weight of siloxane-5 (PDI: 1.74, Mw~918 g/mol) compared to siloxane-2 (PDI: 1.03, Mw~520 g/mol). Addition of end

capping agents decreases the polydispersity and molecular weight of the reaction products as shown in Figure 5.15 for Siloxane-9.

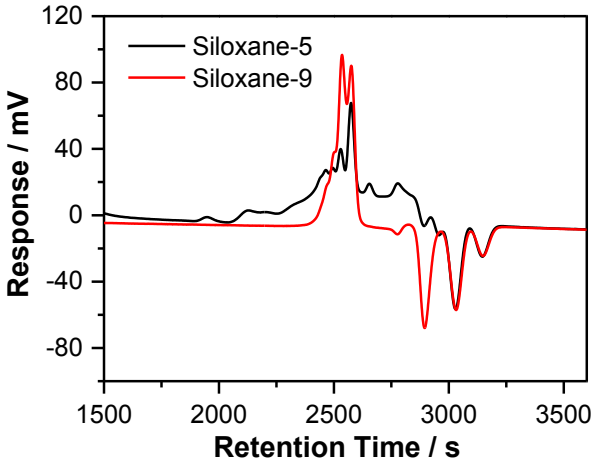

Figure 5.15: Influence of end-capping agent on molecular weight of siloxanes (Synthesis conditions: 18 wt.% initial monomer concentration, 3 h reaction time). Siloxane-9 and Siloxane-5 was synthesized with and without 3-methylmethoxysilane as end-capping agent, respectively.

Copolymerization of thiol functional silane monomers with acrylic silanes was also performed. In the synthesis, the reaction time was fixed to 3 h (referring to siloxane-6). These conditions result in the formation of an oligomeric product which has a higher molecular weight fraction (Mw of this fraction changes between1511 and 3121 g/mol) compared to siloxane-2 (see Figure 5.16).

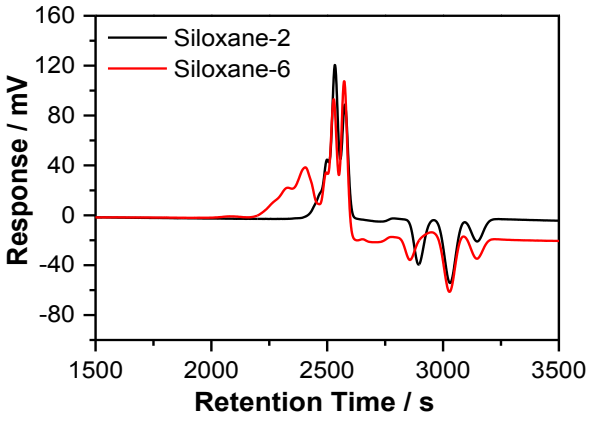

Figure 5.16: Influence of acrylic comonomer (3-acryloxypropyl)methyldimethoxysilane on molecular weight of synthesized siloxanes (Synthesis conditions: 9 wt.% initial monomer concentration, 3 h reaction time). Siloxane-6 is a copolymer which consists of functional thiol and acrylic groups whilst siloxane-2 is a homopolymer containing solely functional thiol groups.

From the results, it can be concluded that concentration and type of silane monomer (e.g. acrylic versus thiol functionalized silane), reaction time and addition of end capping agent have an influence on the molecular weight of the products. While the end-capping agent leads to oligomers with narrow polydispersity, increase in initial monomer concentration and copolymerization with the acrylic silane result in broader dispersity together with higher molecular weights.

5.2.2.2 FTIR Characterization

FTIR spectra of siloxane-2 and siloxane-6 are shown in Figure 5.17 (to avoid repetitive information, only two spectra from thiol and acrylate functional siloxanes were exemplified.)

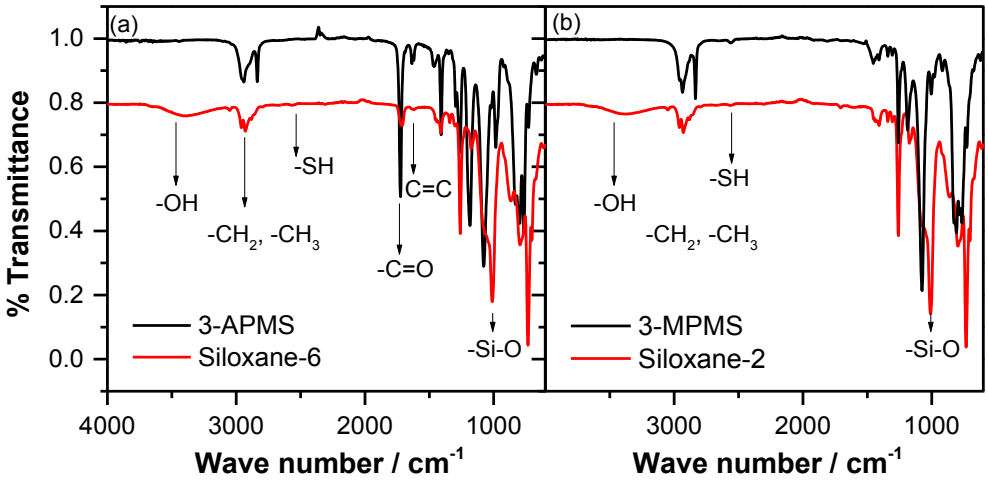

Figure 5.17: FTIR spectrum of (a) siloxane-6 and (b) siloxane-2 and their monomeric counterparts (Synthesis conditions: 9 wt.% initial monomer concentration, 3 h reaction time). Siloxane-6 is a copolymer which consists of functional thiol and acrylic groups whilst siloxane-2 is a homopolymer containing solely functional thiol groups.

In the IR spectra of the oligomers, a new band arises between 3700 and 3076 cm^{-1} which is related to the formation of hydroxyl groups due to the acid catalysed hydrolysis reaction. O-CH_3 rocking vibration at 1190 cm^{-1} decreased considerably due to the hydrolysis reaction of alkoxy groups. A weak stretching vibration band at 2570 cm^{-1} can be assigned to thiol groups. Formation of oligomeric species is indicated by the broadening of the Si-O absorption band around 1080 cm^{-1}. Similarly, copolymeric siloxane-6 also shows peak broadening of the characteristic Si-O absorption and the OH

vibration band. Additionally, siloxane-6 exhibits the stretching vibration of carbon double bonds at 1635 and 1620 cm^{-1} as well as carbonyl group band at 1720 cm^{-1}, which are related to the functional acrylate moieties.

5.2.2.3 Tensile Testing

Tensile tests were conducted with a Zwick Z005 according to ASTM D412-98a as described in Section 4.6. Coagulant dipping process was applied in sample preparation as described in Section 3.6. Then, all samples mentioned in this section were crosslinked with post-curing process (exposure dose 3.9 J/cm^2 is used for all samples). For the crosslinking of NR latex via photoinduced thiol-ene reaction, siloxane-1 and siloxane-2 were used as thiol crosslinker in the first experiments. Figure 5.18 shows the tensile properties of the crosslinked NR latex films.

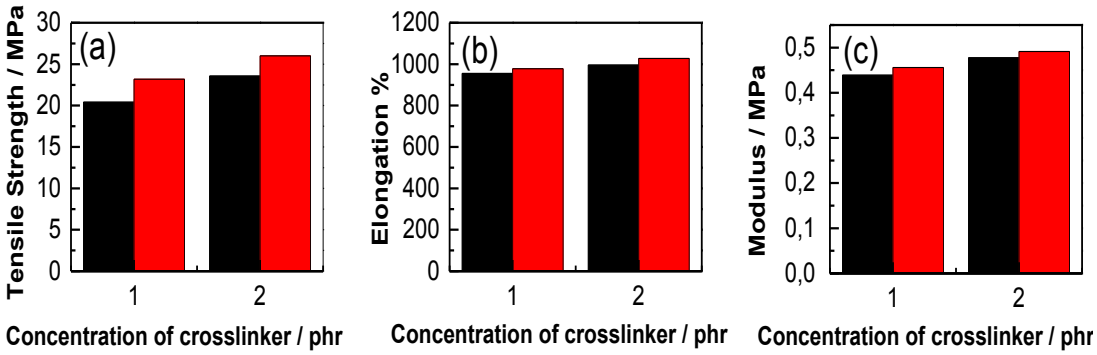

Figure 5.18: (a) Tensile strength, (b) elongation at break and (c) modulus at 50 % elongation of NR latex films cured with siloxane-1 (*red bars*) and siloxane-2 (*black bars*) (exposure dose: 3.9 J/cm^2)

Figure 5.18 shows that both thiol functional siloxane oligomers are highly efficient in the photo-curing of NR latex. Particularly, NR latex films crosslinked with 2 phr of either siloxane-1 or siloxane-2 meet the requirements to produce surgical gloves. The tensile strength amounts to 24 MPa whilst the modulus at 50 % elongation is below 1 MPa and the elongation at break is in the range of 750 %. However, siloxane-1 contained traces of the monomers, which could not be removed by the purification step, leading to a strong odour of the dried NR samples. Thus, no further experiments were conducted with this crosslinker.

As has already been discussed in the previous section, the reaction time has an influence on molecular weight and structure (linear/cyclic) of the synthesized crosslinkers. The influence of these parameters and the related molecular weight of the crosslinker on the mechanical properties of photo-cured NR latex films is depicted in Figure 5.19.

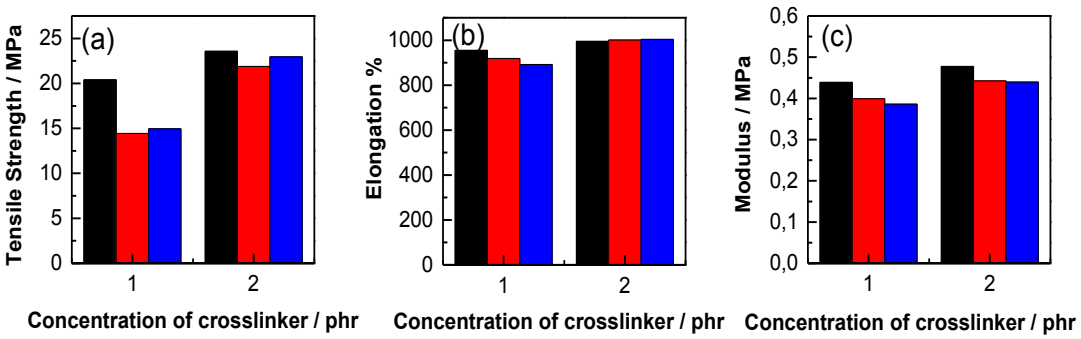

Figure 5.19: (a) Tensile strength, (b) elongation at break and (c) modulus at 50 % elongation of NR latex films cured with siloxane-2 (*black bars*), siloxane-3 (*red bars*) and siloxane-4 (*blue bars*) (exposure dose: 3.9 J/cm^2)

In these experiments curing was carried out with siloxane-2, siloxane-3 and siloxane-4, which have been synthesized with a reaction time of 3, 6 and 9 h, whilst the initial monomer concentration was kept constant. Thus, a slight increase in the molecular weight of the crosslinker from siloxane-2 to siloxane-4 was observed in the GPC measurements.

Among the three applied siloxanes, siloxane-2 shows the best performance as seen from tensile strength values. At a higher crosslinker concentration (2 phr), the tensile strength increases and all three siloxanes yield films with a comparable tensile strength (22 – 23 MPa). However, if the crosslinker concentration amounted to 1 phr, samples crosslinked with siloxane-2 showed the highest tensile strength and moduli at 50% elongation values. The improved mechanical properties might be attributed to higher crosslinking density as samples crosslinked with siloxane-2 show lower swelling ratios and higher gel fractions compared to samples crosslinked with either siloxane-3 or siloxane-4 (see Figure 5.20). The low crosslink density of samples cured with siloxane-3 or siloxane-4 might be attributed to presence of cyclic pentamer siloxane structures, which may have a lower reactivity in crosslinking reactions.

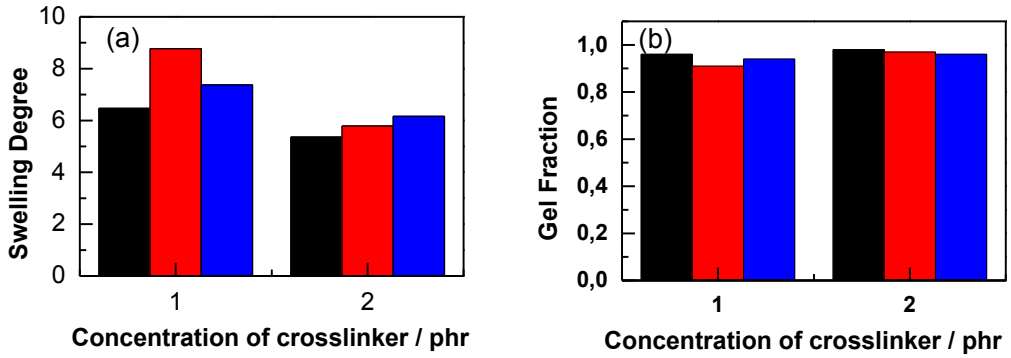

Figure 5.20: (a) Swelling degree, (b) Gel Fractions NRlatex films cured with siloxane-2 (*black bars*), siloxane-3 (*red bars*) and siloxane-4 (*blue bars*) (exposure dose: 3.9 J/cm^2)

In further studies, crosslinking of NR latex was carried out with siloxane-2 and siloxane-5 (see Figure 5.21). In the synthesis of both siloxanes the reaction time was 3 h, whilst the initial monomer was 9 and 18 wt.% for siloxane-2 and siloxane-5, respectively. As already discussed in GPC results, owed to the higher initial monomer concentration siloxane-5 exhibits a higher polydispersity and a higher molecular weight fraction in addition to the trimeric and the tetrameric species.

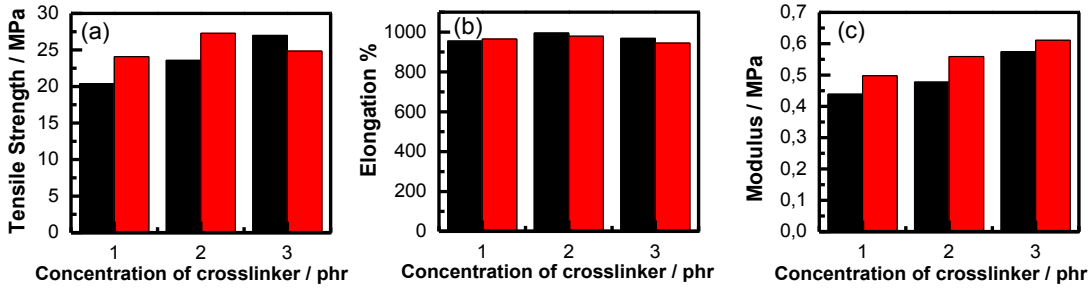

Figure 5.21: (a) Tensile strength, (b) elongation at break and (c) modulus at 50 % elongation of NR latex films cured with siloxane-2 (*black bars*) and siloxane-5 (*red bars*) (exposure dose: 3.9 J/cm^2)

Figure 5.21 reveals that photo-curing with siloxane-5 gives a slightly better tensile strength than siloxane-2. In addition, a higher modulus is obtained with siloxane-5 compared to siloxane-2. While modulus at 50% elongation increases with the rising crosslinker concentration the maximum tensile strength is achieved with a crosslinker concentration of 2 phr. In contrast, the ultimate elongation of the samples is neither affected by the type nor by the concentration of the crosslinker and is in the range of 900 %.

Increasing crosslinker concentration leads to a decrease in the swelling degree and a slight increase in gel content (see Figure 5.22). Swelling experiment results correlate with the mechanical measurements as moduli of samples also increase with the rising crosslinker concentration. Thus, these results reveal the formation of tighter networks with increasing crosslinker concentration.

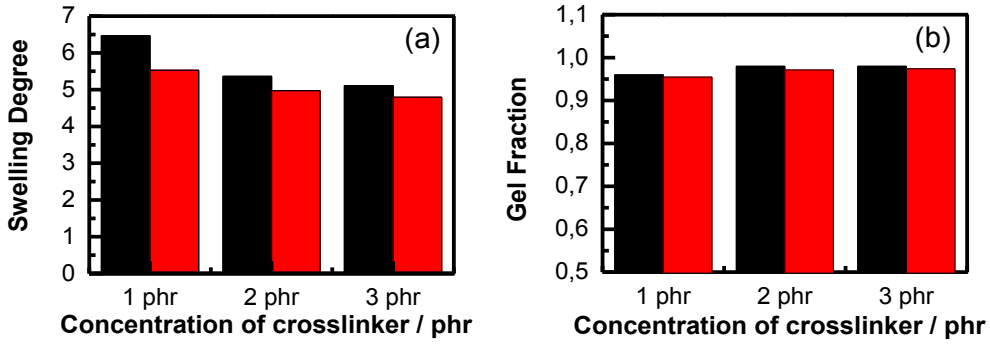

Figure 5.22: (a) Swelling degree, (b) Gel Fraction of NR latex films cured with siloxane-2 (*black bars*) and siloxane-5 (*red bars*) (exposure dose: 3.9 J/cm^2)

Along with homopolymeric crosslinker, copolymers containing functional acrylate and thiol units were used as crosslinker in the photo-curing of NR latex. In Figure 5.23 the tensile strength of NR latex films cured with copolymeric crosslinker are compared. It should be noted that the copolymeric crosslinker is able to undergo two different photo-induced reactions with the isoprene units of NR: (i) the functional thiol units undergo a photo-induced reaction with the carbon double bonds and (ii) the functional acrylate units undergo radical-mediated formation of direct C-C links with the carbon double bonds of the isoprene units. However, the copolymeric crosslinkers might also react with each other since acrylate groups are far more reactive in thiol-ene and radical induced addition reactions than alkenes. As both copolymers show excellent reactivity in the crosslinking of NR latex, these reactions might play a minor role. The tensile strength of the cured NR samples is over 25 MPa and at a concentration of 2 phr maximum tensile strength is observed (30 MPa) when using siloxane-6 as crosslinker. In contrast, the tensile strength of NR latex films cured with siloxane-7 is not significantly influenced by the crosslinker concentration and amounts to 27 MPa.

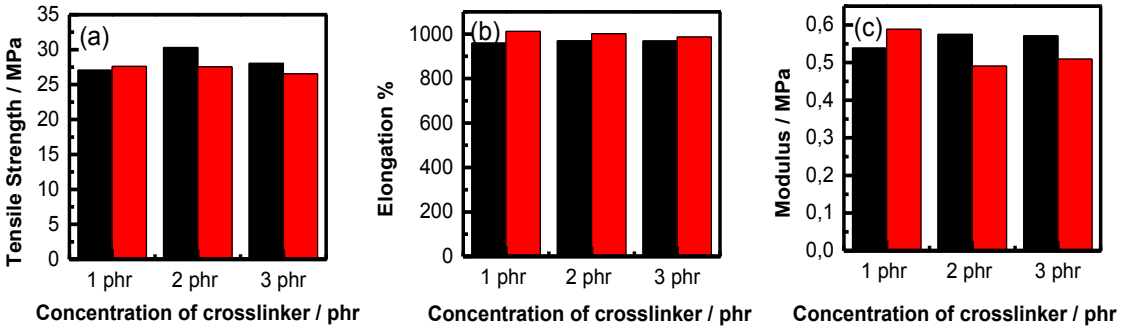

Figure 5.23: Tensile strength of NR latex photo-cured with siloxane-6 (*black bars*) and siloxane-7 (*red bars*) (exposure dose: 3.9 J/cm^2)

Equilibrium swelling measurements were carried out with latex films crosslinked with siloxane-6 and siloxane 7 to calculate the degree of swelling and gel fractions. The results of the swelling test are shown in Figure 5.24. Higher siloxane-6 and siloxane-7 concentration result in a lower degree of swelling, which can be attributed to a tighter network, as the degree of swelling decreases with increasing network density. Decrease in swelling degree with the rising crosslinker concentration is more pronounced for the samples crosslinked with siloxane-7.

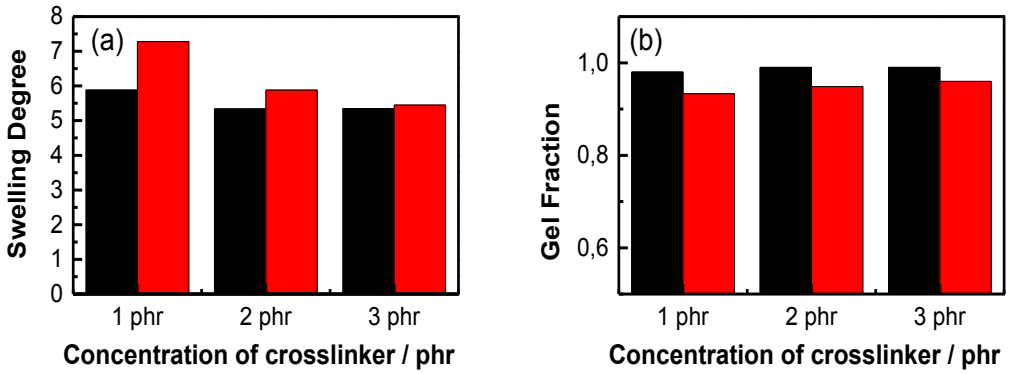

Figure 5.24: (a) Swelling degree, (b) Gel Fraction of NR latex photo-cured with siloxane-6 (*black bars*) and siloxane-7 (*red bars*) (exposure dose: 3.9 J/cm^2)

The properties of NR samples crosslinked with either the homopolymeric siloxane-5 ore the copolymeric siloxane-6 were investigated by subjecting the cured films to accelerated aging and sterilization. After each treatment, the mechanical properties of samples were determined and results of the tensile strength, ultimate elongation and moduli are shown in Figure 5.25, Figure 5.26 and Figure 5.27, respectively.

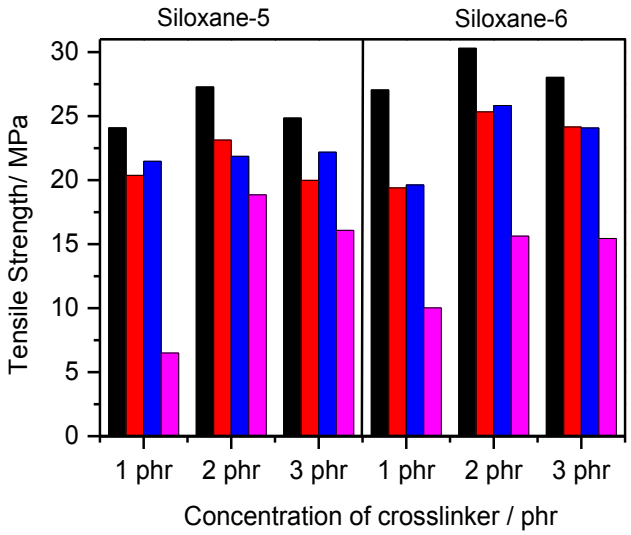

Figure 5.25: Tensile strength of NR latex films cured with either siloxane-5 or siloxane-6 (exposure dose: 3.9 J/cm^2) as a function of the crosslinker concentration and in dependence on the treatment: (*black*) non-sterile and not aged, (*red*) non-sterile and aged at 70°C for 7 days, (*blue*) sterile and not aged and (*magenta*) sterile and aged at 70°C for 7 days.

While maximum tensile strength is obtained with either siloxane-5 or siloxane-6 at a concentration of 2 phr, generally, the samples crosslinked with siloxane-6 show higher tensile strength than the samples crosslinked with siloxane-5. Both accelerated aging as well as sterilization lead to a slight decrease of the tensile strength indicating a degradation of samples (due to oxidative ageing and chain scission processes under high energy irradiation). However, the samples, which are exposed to a combined treatment of sterilization and aging deteriorate substantially and exhibit the lowest tensile strength values.

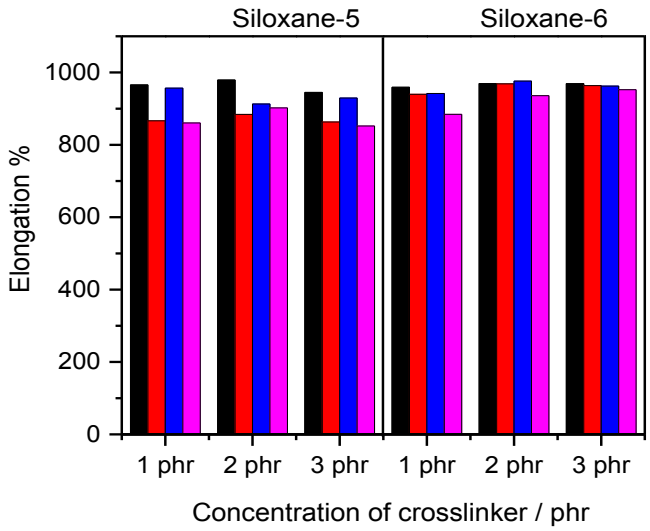

Figure 5.26: Elongation at break of NR latex films cured with either siloxane-5 or siloxane-6 (exposure dose: 3.9 J/cm^2) as a function of the crosslinker concentration and in dependence on the treatment: (*black*) non-sterile and not aged, (*red*) non-sterile and aged at 70°C for 7 days, (*blue*) sterile and not aged and (*magenta*) sterile and aged at 70°C for 7 days.

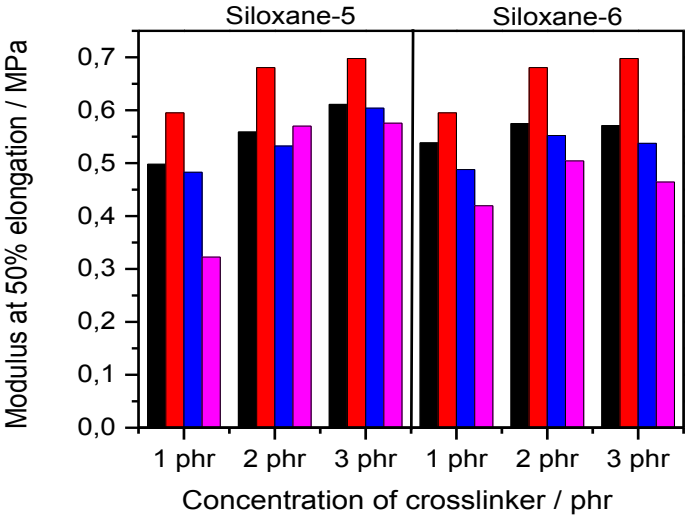

Figure 5.27: Modulus at 50 % elongation of NR latex films cured with either siloxane-5 or siloxane-6 (exposure dose: 3.9 J/cm^2) as a function of the crosslinker concentration and in dependence on the treatment: (*black*) non-sterile and not aged, (*red*) non-sterile and aged at 70°C for 7 days, (*blue*) sterile and not aged and (*magenta*) sterile and aged at 70°C for 7 days.

Ultimate elongation of samples crosslinked with either siloxane-5 or siloxane-6 are in a similar range (> 850 %) and don`t change significantly due to the sterilization and

aging treatments. On the contrary, moduli at 50 % elongation exhibit a significant dependency on crosslinker type, crosslinker concentration, ageing and sterilization treatments. In general moduli values of aforementioned samples increase with the rising crosslinker concentration (for both siloxane-5 and siloxane-6) indicating increasing crosslinker density. However, degradation due to the sterilization and aging is reflected by a decrease in moduli, which is typical for chain scission processes.

Summing up, siloxane based thiol functional crosslinkers, particularly siloxane-5 and siloxane-6, show excellent efficiency to crosslink NR latex. The obtained samples are characterized by high tensile strength (up to 30 MPa), high elongation (> 800 %) and reasonable moduli (< 1 MPa).

In further experiments, the extractable crosslinker content of NR latex films photocured with either low-molecular weight thiols or with the newly synthesized thiol functional oligomers was studied. The films were extracted by Soxhlet extraction and the residual crosslinker levels in the extract were quantified by elemental analysis. A reference extraction of non-crosslinked NR films was carried out to determine the sulphur content of proteins. The results are summarized in Table 5.3. It is evident, that the oligomeric crosslinkers comprise a lower extractability than TMPMP as a low-molecular weight thiol.

Table 5.3: Extractable sulphur content of crosslinked NR latex (samples were obtained by post-curing of NR latex. Irradiation dose:3.9 J/cm^2)

Sample	$w_{Extract}/g_{Latex}$ (%)	wt.%S/g_{Latex}
1 phr Lucirin TPO-L 2 phr Siloxane-6 (*oligomeric crosslinker*)	7.0	0.053
1 phr Lucirin TPO-L 2 phr Siloxane-5 (*oligomeric crosslinker*)	7.02	0.052
1 phr Lucirin TPO-L 2 phr TMPMP (*low-molecular weight crosslinker*)	10.0	0.2008

5.2.3 Thiol-ene chemistry with Functionalized Particles

Although the amount of extractable crosslinkers can be significantly reduced by employing oligomeric thiols, other routes must be pursued to minimize the extractable content below the detection limit of the analysis technique. Thus, in further studies the

functional thiol crosslinker was immobilized onto the surface of inorganic particles to reduce its extractability.

Thiol functional particles were prepared by using a convenient silanization technique (see Section 3.4.1) and they were employed for the photo-crosslinking of NR latex. Zeolite and silica particles were used as inorganic substrate since they provide a high surface area and a large amount of surface hydroxyl groups, which are exploited for the condensation reaction with the siloxane groups of (3-mercaptopropyl)trimethoxysilane (MPTMS). To increase the amount of surface hydroxyl groups and thus, the reactivity of the filler surface, the particles were pre-treated by exposure to acidic solution or corona discharge. In the following section, the characterization of unmodified and modified particles is described and subsequently, the mechanical behaviour of NR latex crosslinked with thiol functional particles are presented.

5.2.3.1 Characterization of Functionalized Zeolite Particles

The chemical surface composition of pristine zeolite particles was determined by XPS and impurities such as sodium, potassium and calcium metal ions were detected. The removal of such impurities is important prior to silanization in order to ensure a stable bonding between the particles and silane agents. Thus, particles were exposed to 5 wt.% $HCl_{(aq)}$ for 4 h to reduce the surface impurities. After washing with deionized water, the particles were immersed in $HNO_{3(aq)}$ solution to increase the number of OH groups on the surface (see Section 3.4.1). Table 5.4 shows the quantitative surface composition of zeolite particles prior to and after the two different acid treatments.

Table 5.4: Surface composition of zeolite particles prior to and after the two different acid treatments

element	Untreated zeolite at.%	HCl treated zeolite at.%	HCl & HNO_3 treated zeolite at.%	HNO_3 treated zeolite at.%
C1s	10.4	10.8	9.0	8.6
O1s	54.7	56.3	57.8	57.4
N1s	-	-	-	-
Si2p	23.3	26.9	27.1	27.6
S2p	-	-	-	-
Al2p	5.2	3.8	4.0	4.0
Mg1s	**3.4**	**1.6**	**1.6**	**1.8**
Ca2p	**1.3**	-	-	-
K2p	**1.3**	**0.6**	**0.5**	**0.6**
Na1s	**0.4**	-	-	-

The results evidence the reduced amount of alkali metals on the zeolite surface after the acid treatments. Calcium and sodium ions fully disappear whilst the reduction of magnesium and potassium ions amounts to 50 %. The effect of acid treatments on the surface oxidation and the formation of surface hydroxyl groups was investigated in a separate experiment which was adapted from reference [187]. The OH number of zeolite particles as a function of the treatment is summarized in Table 5.5.

Table 5.5: Number of OH groups on zeolite surface depending on the acid treatment

particle	treatment	OH number (mmol/g)
Zeolite	untreated	0.210
Zeolite	HCl treated	0.466
Zeolite	HNO_3 treated	0.516
Zeolite	HNO_3+HCl treated	0.522

Acid treatment of zeolite particles does not only reduce the alkali metal ion concentration but also increases the number of OH groups. Since OH number were the highest for particles treated with both HNO_3 and HCl aqueous solutions, these pre-treated particles were silanized with 3-MPTMS according to the procedure described in section 3.4.1. After silanization XPS and TGA measurements were carried out to detect and quantify the covalently attached thiol functional silanes.

Table 5.6: Comparison of the surface composition of pristine and MPTMS-modified zeolite particles

element	non pretreated & unmodified zeolite at.%	HCl & HNO_3 pre-treated zeolite at.%	HCl-HNO_3 pretreated-MPTMS modified zeolite at.%
C1s	**10.4**	**9.0**	**22.3**
O1s	**54.7**	**57.8**	**43.0**
N1s	-	-	-
Si2p	23.3	27.1	26.2
S2p	-	-	**5.7**
Al2p	5.2	4.0	2.1
Mg1s	3.4	1.6	0.7
Ca2p	1.3	-	-
K2p	1.3	0.5	-
Na1s	0.4	-	-

The presence of thiol groups on the modified zeolite particles was revealed by XPS measurements. The surface modification of zeolite with 3-MPTMS is evidenced by an arising sulphur peak, an increase in the carbon content and a decrease in oxygen atom concentration. Quantitative determination of the covalently attached 3-MPTMS was further obtained by using thermal gravimetric analysis. In a pre-conditioning step, the particles were dried at 150 °C for 30 min to remove water and volatile impurities.

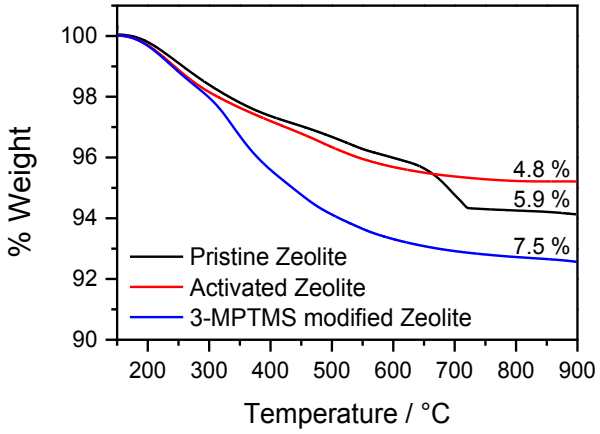

Figure 5.28: Normalized weight decrease of pristine, HNO_3 and $HCl_{(aq)}$ pre-treated and MPTMS-modified zeolite particles

Figure 5.28 shows that pristine zeolite particles exhibit a weight decrease of 5.9 % until 800 °C which is associated to the release of several forms of water in the zeolite mineral [195]. The loosely bound and adsorbed water molecules on the surface of the

particles are already removed in the pre-conditioning period prior to the TGA experiments. In contrast, water molecules which are interacting with potassium ions are lost around 170 °C and the detachment of hydroxyl groups from the crystal lattice takes place at temperatures above 400 °C.

TGA measurements indicate that the weight decrease of acid treated zeolite particles amounts to 4.8 %. The weight loss difference between pristine and acid treated zeolite particles is attributed to the removal of alkali metal impurities from the particles. With respect to the surface modified particles, the TGA results evidenced that the amount of organic groups is 2.7 wt.%.

5.2.3.2 Photo-crosslinking with Functionalized Zeolite Particles

The thiol modified zeolite particles were used as crosslinkers for synthetic *cis*-1,4 polyisoprene (40,000 g/mol). For evaluation of the crosslink efficiency, negative toned patterns were inscribed into thin polyisoprene films by photolithography and the structures were studied by optical microscopy after the development in an organic solvent. Optic micrographs of the negative toned structures after development step are shown in Figure 5.29. Negative toned resists are successfully obtained with a particle concentration ≥ 10 phr. The best patterned polyisoprene films were obtained with a crosslinker concentration of 40 phr.

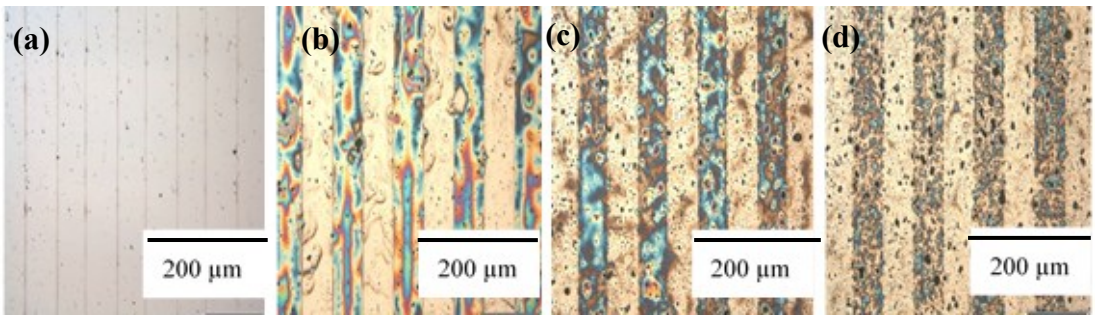

Figure 5.29: Optical micrographs of negative toned resins (photoinitiator: 1 phr Lucirin TPO-L, crosslinker: 3-MPTMS modified zeolite particles, exposure dose: 1.6 J/cm^2) containing (a) 5, (b) 10, (c) 20 and (d) 40 phr modified zeolite particles as thiol crosslinker.

In an additional experiment, the modified particles were used for the photo-crosslinking of NR-Latex. Interestingly, 3-MPTMS modified particles could not be dispersed in NR latex properly due to their hydrophobic character. The hydrophobic nature of modified particles may be attributed to presence of oligomeric silane layers.

Furthermore, NR latex emulsions containing more than 5 phr zeolite particles are not stable. Thus, 5 phr MPTMS modified particles were used in curing reaction for NR latex even if the previous studies revealed that a high particle content is beneficial for the crosslink density.

The mechanical properties of the photo-cured NR latex films are summarized in Table 5.7. The low amount of thiol functionalized particles does not lead to an efficient cross-linking of the rubber chains, which is reflected by the low tensile strength of the films.

Table 5.7: Mechanical properties of NR samples crosslinked with thiol functional zeolite particles (Initiator: 1 phr Irgacure TPO-L, exposure dose: 2.6 J/cm^2)

NR latex films post-cured with 5 phr MPTMS modified zeolite particles		
Tensile Strength (MPa)	**Elongation** (%)	**Modulus at 50% Elongation** (MPa)
13.8 ± 1.85	813 ± 34	0.41 ± 0.005

5.2.3.3 Characterization of Functionalized Silica Particles

Along with zeolite particles, fumed silica was used as inorganic substrate for the immobilisation of 3-MPTMS. The chemical surface composition of fumed silica particles was characterized by XPS measurements prior to and after a silanization with 3-MPTMS. In contrast to zeolite, the pristine silica surface does not show any alkali metal impurities. In terms of the modified silica particles, the presence of covalently attached thiol functional silanes is evidenced by the sulphur atom signal as shown in Table 5.8.

Table 5.8: XPS measurements of the surface composition of fumed silica prior to and after the silanization with 3-MPTMS.

element	Pristine fumed silica (at.%)	3-MPTMS modified fumed silica (at.%)
C1s	5.3	**7.7**
O1s	59.3	56.5
N1s	-	-
Si2p	35.4	34.7
S2p	-	**1.0**

The thiol functional silica particles were employed as crosslinkers in the photo-curing of NR latex. Since silica particles act as active filler, the influence of pristine silica particles on the tensile properties of NR latex films containing only the photoinitiator (no crosslinker was used) was studied. As shown in Figure 5.30, at a particle concentration of 5 phr, the attachment of thiol groups on the silica surface does not have a significant influence on tensile properties of irradiated NR latex. However, at a higher particle concentration, premature coagulation of the latex dispersion was observed.

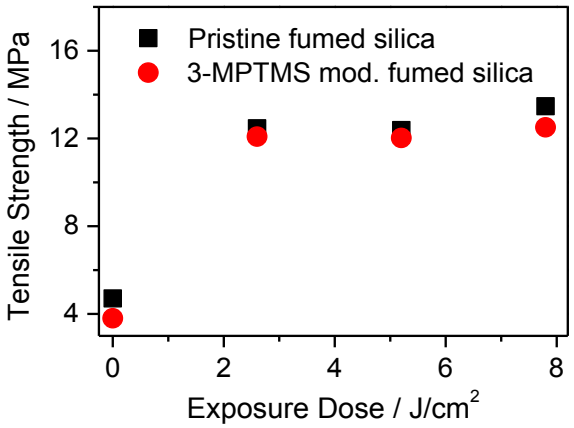

Figure 5.30: Tensile strength of NR latex cured with 5 phr of either pristine or thiol functional silica particles (Initiator: 1phr Irgacure TPO-L)

5.3 Preparation of Thiol-ene Systems with Low Migratable Photoinitators

Photoinitators form radicals upon absorption of light. These radicals can initiate polymerization of reactive resins and can be incorporated with the cured material. However, some of the cleavage products and non-reacted photoinitiator molecules are not covalently attached to polymer matrix and have the ability to migrate. These extractable residues may cause health hazards and thus, should be eliminated. Migration of photoinitiators from cured materials is a challenging issue particularly in medical gloves, dental applications, toys and food packaging [196]. Photoinitiators are one of the main components of photo-curable resins and they should fulfil the requirements of the related applications such as high curing speed, solubility in the resin and low extractability.

In this regard, reduction of their migration tendency and volatility is extremely important in food packaging, coating and medical applications. In this study, two different strategies were pursued to obtain low migratable photoinitiators: the first one involves the covalent immobilization of photoinitiators on particle surfaces and second one aims at the synthesis of low-molecular-weight photoinitiators with polymerizable groups (e.g., alkyne) that enable covalent bonding of the photoreactive species to the polymer network during the photopolymerization process.

5.3.1 Thiol-ene Chemistry with Photo-active Particles

Some of the results presented in this part of the study are publishe in 2 different papers:

(1) Synthesis and evaluation of new radical photoinitiators bearing trialkoxysilyl groups for surface immobilization, Polymer, 2017 (Ref. [169]).

(2) Photoactive Silica Nanoparticles: Influence of Surface Functionalization on Migration and Kinetics of Radical-induced Photopolymerization Reactions. European Polymer Journal, European Polymer Journal, 2017 (Ref. [197])

Photoactive particles were prepared by the covalent immobilization of 3-(trimethoxysilyl)propyl 3-[bis(2,4,6-trimethylbenzoyl)phosphinoyl]-2-methyl-propionate (TMESI^2-BAPO) and 1-{4-[2-(3-triethoxysilanylpropylcarbamoyloxy)ethoxy]-phenyl}-2-hydroxy-2-methyl-1-propane-1-one (TESI-IC2959) onto silica surfaces by exploiting convenient grafting reactions across the alkoxysilyl groups.

Photoactive particles with varying grafting density were prepared and the influence of the grafting method on the photocuring kinetics of thiol-ene resins was studied in detail. The degree of modification was conveniently adjusted by the reaction conditions using two different modification method. The degree of modification (combustible content) was determined by TGA measurements, whilst qualitative analysis of the attached initiators was performed by XPS and UV-Vis spectroscopy. In subsequent comparative FT-IR and photo-DSC studies, the influence of selected parameters such as the type of initiation (e.g. filler bound derivatives *versus* their reference counterparts Irgacure 819 and Irgacure 2959) as well as the amount and the chemical structure of the attached species on the thiol-ene reaction between a tri-functional "ene" and a di-functional thiol were characterized. In addition, cured photopolymers were extracted with organic solvents to determine the migration of the photoactive particles.

Details of modification methods was given in Section 3.4.2.

The structure of the chemicals used in this study is shown in Scheme 5.5.

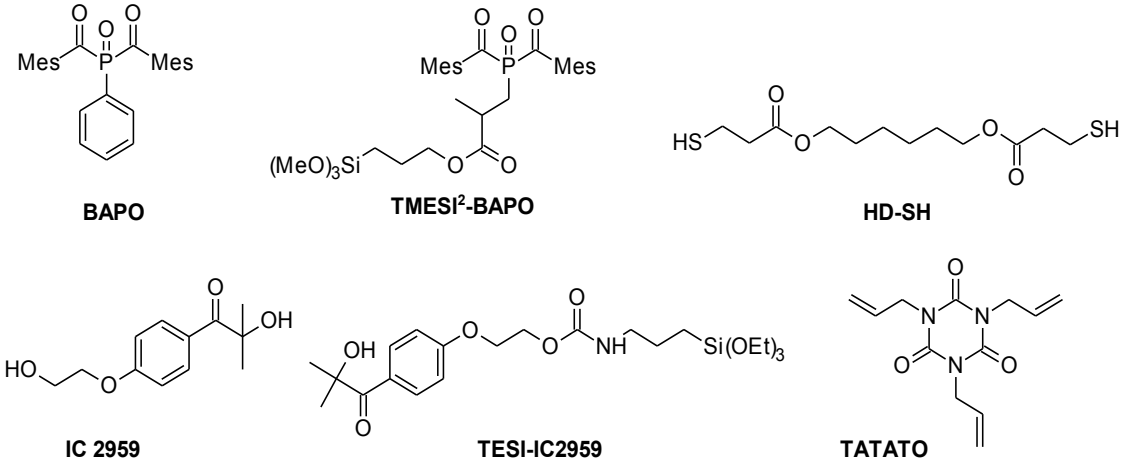

Scheme 5.5: Structure of monomers, reference initiators and alkoxysilyl functional initiators

5.3.1.1 TGA measurements

After the preparation of photoactive particles, the organic content of the modified particles was determined by TGA. Figure 5.31 illustrates the TGA weight loss of pristine and modified silica particles.

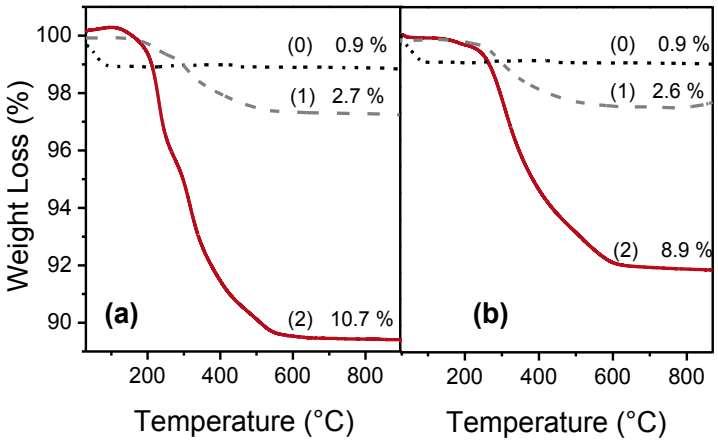

Figure 5.31: TGA curves of (a) TMESI^2-BAPO and (b) TESI-IC 2959 modified silica particles. (0) unmodified silica and photoactive silica particles obtained from (1) method-**1** and (2) method-**2.**

Untreated silica nanopowder exhibits a weight loss of 0.9 wt% which is associated with surface dehydration [198]. After surface modification, no significant weight loss is observed between 30 and 150 °C, which indicates that the majority of the pre-adsorbed water molecules has been removed and has been exchanged by the photoactive silanes. Under anhydrous conditions (method-1), particles modified with either TMESI^2-BAPO or TESI-IC2959 exhibit a comparable weight loss (2.5 wt.%). However, by changing the reaction conditions (method-2), a substantial increase in weight loss from 2.5 to 8.9 wt.% (TESI-IC2959) and 10.7 wt.% (TMESI^2-BAPO) was observed between 150 and 650 °C, which suggests a higher degree of functionalization and an increased thickness of the grafted photoactive layer. It is interesting to note that the two photoactive species show a different mechanism of thermal decomposition which is independent of modification method. By calculating the first derivative of the TGA curve, TMESI^2-BAPO modified particles exhibit two decomposition regions with maxima at 230 and 313 °C, which are independent of the modification method (see Figure 5.32). In contrast, only one decomposition region is observed for TESI-IC2959 bound particles, with a maximum weight decrease at 305 °C.

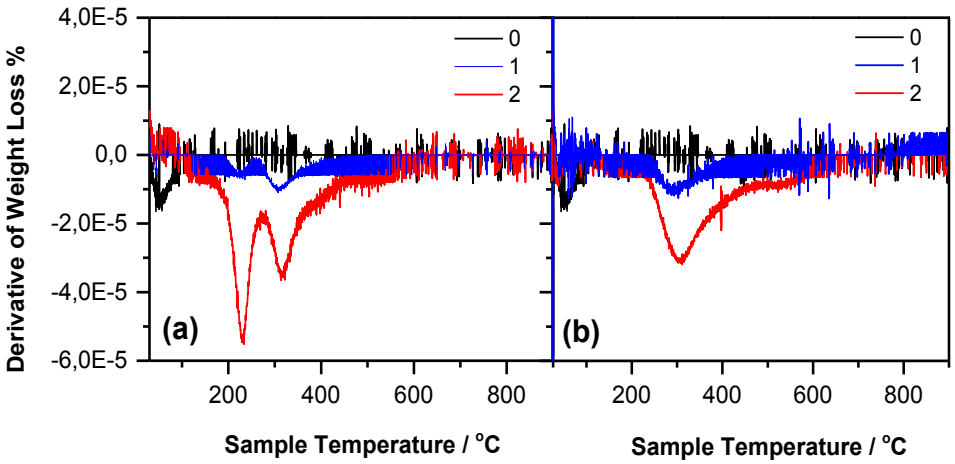

Figure 5.32: Derivative of TGA curves of (a) BAPO and (b) IC 2959 modified silica particles. (0) unmodified silica and photoactive silica particles obtained from (1) method-1 and (2) method-2. Measurements were done between 25 to 900 °C under oxygen atmosphere with a heating rate of 4 °C/min.

It should be considered that non-grafted oligo-condensates might also contribute to the enhanced degree of modification since no purification step was carried out in method-2. In a control experiment, these photoactive particles were washed and analysed by TGA.

Table 5.9: Weight decrease of modified particles prepared according to Method-2 before washing, after washing with acetone and weight decrease of obtained extract.

Sample	TGA Weight loss before washing (wt.%)	TGA Weight loss after washing (wt.%)	TGA Weight loss of the extract (wt.%)
TESI-IC2959 mod. Silica (Method-2)	8.9	7.1	12.4
TMESI^2-BAPO mod Silica (Method-2)	10.7	7.1	17.8

After washing of the photoactive particles (prepared according to method-2), the combustible content of particles decreases compared to unwashed photoactive particles as pointed out in Table 5.9. This can be attributed to the removal of some unattached oligomeric condensates, but also to the loss of the fraction of small particles during washing. Such loss was expected, since it was observed that the mass of the nanopowder sample decreased significantly after each washing step (14.5 % sample weight loss

after the first washing step for TESI-IC2959 modified silica). To prove that the supernatant from the washing did not contain significant amounts of non-attached polymer (i.e. soluble polycondensates of alkoxysilyl functional silanes) a TGA curve was recorded for the dried supernatant (see Table 5.9). A weight loss of organic content of 12.4 % and 17.8 % for TESI-IC2959 and TMESI^2-BAPO modified silica was observed, respectively, proving that this fraction still contained silica nanoparticles, albeit highly functionalized. From the TEM images in Fig. 5.24 it can be observed that the fraction of the smallest nanoparticle agglomerates is being lost during the process of centrifugal washing. Assuming that the particles removed during centrifugation had an organic content of at least 7.1 %, it can be calculated that over 90 % of the hydrolysed TESI-IC2959 was covalently attached to the nanoparticles and precipitated during centrifugation. This estimation is conservative, since it can be assumed that the fraction of the smallest nanoparticles, which do not precipitate upon centrifugation, has the highest specific surface area and thus, higher degree of functionalization (organic content) than the precipitate.

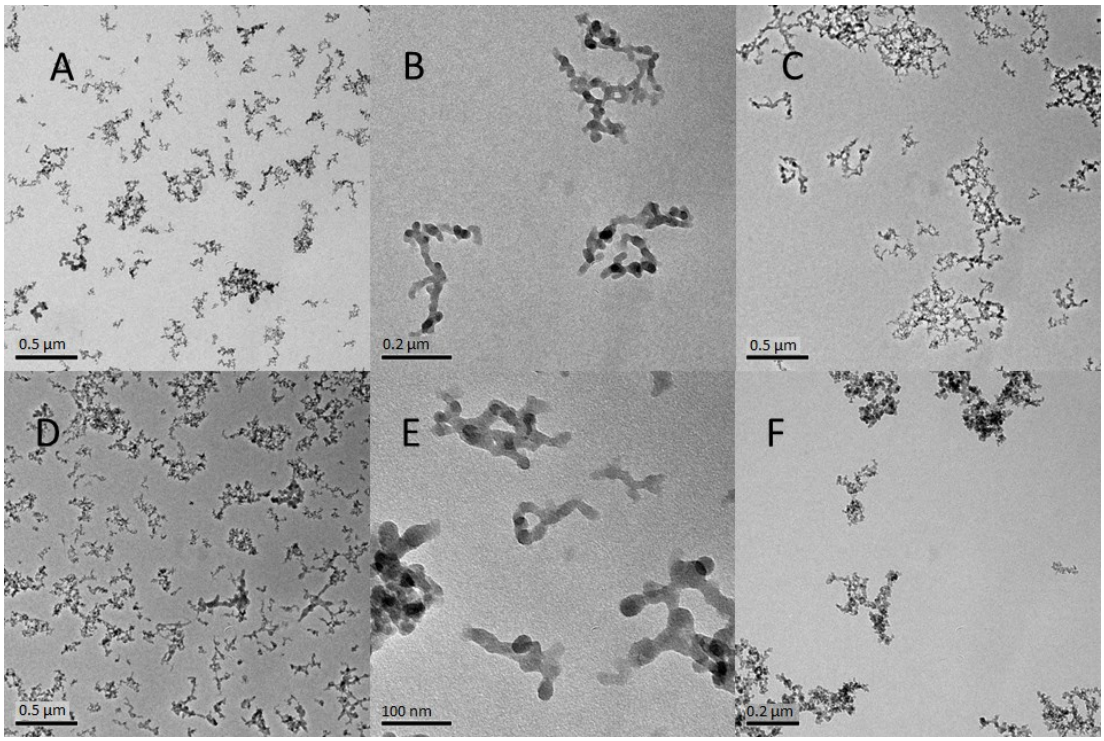

Figure 5.33: Typical TEM images of the pristine (A-C), and modified (D-F) silica nanopowder at different magnification. Images C and F show particles that have been purified by centrifugation. Please note the different scale bars.

5.3.1.2 XPS measurements

The chemical surface composition and the layer thickness of the photoactive particles were further determined by XPS spectroscopy (see Table 5.10). In the XPS spectrum of pristine silica particles the typical O1s (532.0 eV) and Si2p (103.5 eV) signals were observed. The peak at 103.5 eV (Si–O) is attributed to the surface of the inorganic silica particle. An additional weak C1s signal at 286.7 eV might be related to impurities. In contrast, XPS spectrum of photoactive silica particles show Si2p (103.5 eV and 102.0 eV) signals. Organic silicon (C–Si–O) signal at 102.0 eV indicates the presence of the photoactive silane layer The layer thickness of the photoactive layers is lower than 10 nm as XPS measurements have an information depth between 1 and 10 nm and the inorganic Si–O peak (103.5 eV) is detectable [199]. The immobilization of TMESI^2-BAPO is evidenced by the appearance of the characteristic phosphorous photoemission at 133.4 eV (P2p3 signal).

With respect to particles treated by method-2, the phosphor content was determined to be 1.0 at.%. Due to the low modification yield of silica particles functionalized by method-1, the phosphor signal was not detectable by XPS. However, the distinctive increase of the C1s signal gives an indication of the successful attachment of the photoactive species. In dependence on the synthesis route, the carbon content increased from 1.8 at.% (untreated) to 7.8 at.% (method-1) and 20.0 at.% (method-2). The presence of TESI-IC2959 on the surface of modified silica particles was also identified by the rising carbon content. Comparable to TMESI^2-BAPO modified particles, the carbon level amounted to 7.0 and 15.0 at.% after modification using method-1 and method-2, respectively. The N1s signal at 401.9 eV related to the C-linked nitrogen was not observed for particles modified using method-1, whilst it was higher (1.1 at.%) for the particles functionalized using method-2.

Table 5.10: Atomic concentration of pristine and modified silica surfaces determined by high resolution XPS spectroscopy

Silica particles	C (at.%)	Si (at.%)	O (at.%)	P (at.%)	N (at.%)
pristine	1.8	39.1	59.1	-	-
TMESI^2-BAPO method-**1**	7.8	41.1	51.1	-	-
TMESI^2-BAPO method-**2**	20	30.0	49.0	1.0	-
TESI-IC2959 method-**1**	7.0	46.7	46.3	-	-
TESI-IC2959 method-**2**	15.0	32.4	51.5	-	1.1

5.3.1.3 DLS measurements

The influence of the modification method on the particle size was determined by dynamic light scattering (DLS). In previous section, TEM studies revealed that the structure of the fumed silica is comprised of intergrown nano-sized grains with a diameter of 20 to 60 nm. They are fused into branched chains and form larger clusters with a length varying over several hundred nanometres. The dynamic light scattering experiments revealed that the average diameter of the clusters in untreated fumed silica is in the range of 180 nm (see Table 5.11). The size of the clusters does not change significantly by either coupling TMESI^2-BAPO or TESI-IC2959 via surface modification method-1. However, by performing the surface modification in the presence of a catalyst and water (method-2) a substantial increase of the cluster size in conjunction with a larger standard deviation of the cluster size is observed. This effect may be related to drying stresses that occur during the drying of the particles from polar surfaces which stabilize larger clusters [200]. The particles are brought closer together which also might induce crosslinking reactions across neighbouring particles, facilitated by the condensation reaction of the growing trialkoxy chains under the applied conditions.

Table 5.11: DLS results of pristine and modified silica particles

silica particles	z-average (nm)
pristine	178 ± 3
TMESI^2-BAPO mod.method-**1**	173 ± 3
TMESI^2-BAPO mod.method-**2**	449 ± 92
TESI-IC2959 mod.method-**1**	172 ± 5
TESI-IC2959 mod.method-**2**	328 ± 60

5.3.1.4 UV-VIS measurements

The absorption properties of the immobilized species were further characterized by UV-Vis experiments and compared to their free photoinitiator counterparts (see Fig. 5.34a, 5.34b and 5.34c).

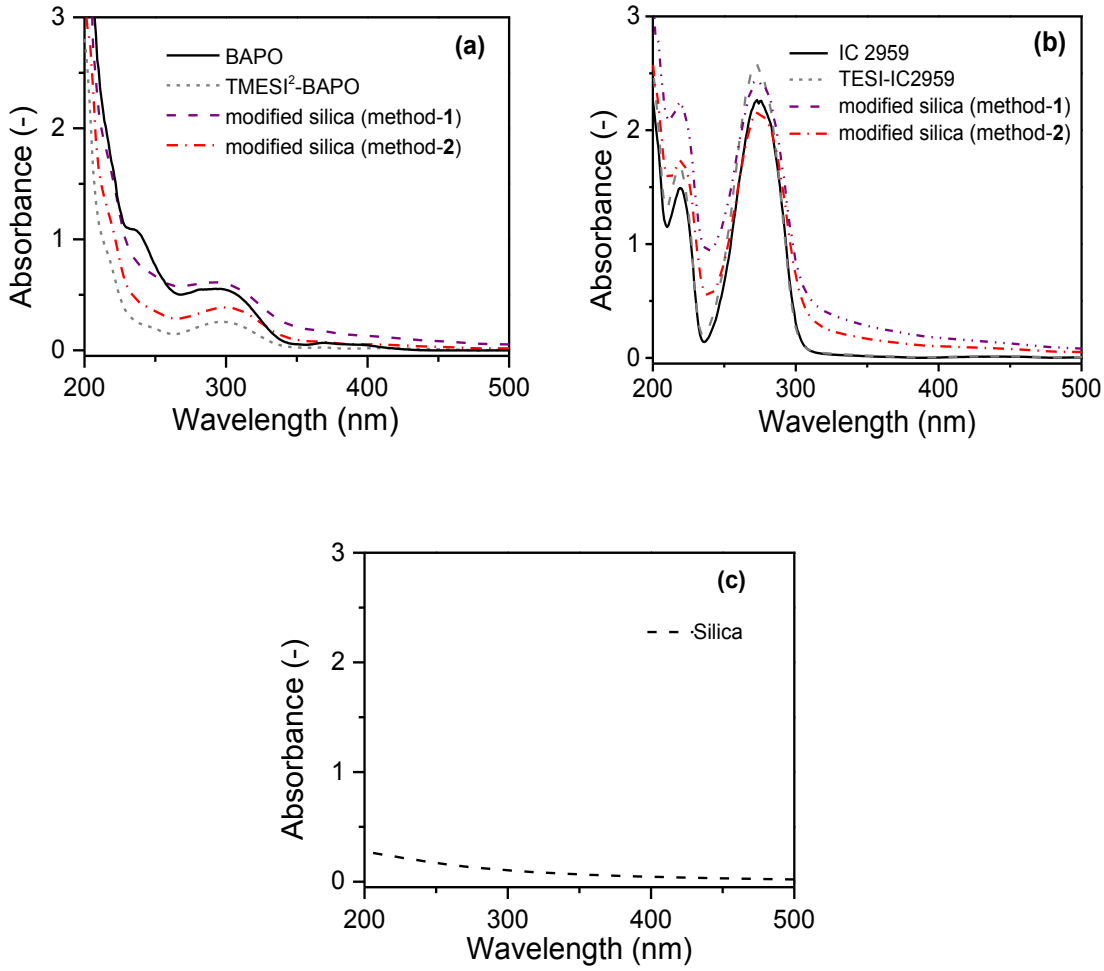

Figure 5.34: UV-Vis spectra of (a)TMESI^2- BAPO and (b) TESI-IC 2959 modified silica particles in comparison to free photoinitiators in acetonitrile: c_{BAPO}=0.278 mg/mL, c_{TEMSI^2BAPO}=0.25 mg/mL, $c_{TMESI^2BAPO\text{-modified particles (method-1)}}$=10 mg/mL, $c_{TMESI^2BAPO\text{ modified particles (method-2)}}$=5 mg/mL; c_{IC2959}=0.274 mg/mL, $c_{TESI\text{-}IC2959}$=0.684 mg/mL, $c_{TESI\text{-}IC2959\text{-modified particles (method-1)}}$=20 mg/mL, $c_{TESI\text{-}IC2959\text{ modified particles (method-2)}}$=5 mg/mL.

The spectra reveal that the modification of IC 2959, yielding TESI-IC2959 leads to a slight blue shift of λ_{max} from 275 to 272 nm. In contrast, the absorption spectrum of BAPO does not change upon functionalization with the trimethoxysilyl terminated linker. Independent of the synthetic procedure, the functionalized silica particles represent the characteristic absorption profile of the free trialkoxysilyl-functionalized initiators, which is clearly absent in the UV-Vis spectrum of untreated particles (see Fig. 5.34c). The absorption bands of the photoactive particles are somewhat broader and the baselines of particles show a positive linear variation, which are related to scattering effects from the inorganic particles.

5.3.1.5 Photo-DSC measurements

The reactivity of the modified silica particles in the radical-mediated thiol-ene reaction was evaluated by performing photo-DSC measurements with resin formulations comprising functional groups of TATATO and HD-SH monomers at equimolar concentrations. It should be noted that equal molar amounts of free and immobilized photoactive species (calculated from the modification yield obtained by thermogravimetric measurements) were used to allow a comparison of the curing performance, which implies that a proportionally higher mass fraction of particles was used for particles with a lower degree of modification. Composition of resin mixtures is shown in Table 5.12.

Table 5.12: Composition of thiol-ene resin formulations

sample	ratio SH:C=C (mol/mol)	photoinitiator	photoinitiator content (wt.%)
resin-R1	1:1	BAPO	0.2
resin-R2	1:1	IC 2959	0.2
resin-P1	1:1	TMESI^2-BAPO-modified silica (method-1)	8.8
resin-P2	1:1	TMESI^2-BAPO-modified silica (method-2)	2.2
resin-P3	1:1	TESI-IC2959-modified silica (method-1)	11.5
resin-P4	1:1	TESI-IC2959-modified silica (method-2)	3.3

In Table 5.13 the results of the photo-DSC measurements are summarized. It is shown that both immobilized Norrish Type I photoinitiators provide a good curing performance, which is not significantly affected by the degree of modification of the immobilized species. In particular, for TMESI^2-BAPO modified particles, the reaction time t_{max}, which is the time to reach the maximum polymerization enthalpy, is in a similar range as TATATO/HD-SH resin containing free BAPO as photoinitiator. As IC 2959 is characterized by a lower photoreactivity in free radical induced photopolymerization than BAPO, the corresponding photoactive particles also display a lower reactivity. The coupling of the photoinitiators on the inorganic particles influences both t_{max} as well as on the maximum heat flow (H_{max}) which correspond to the polymerization rate. By initiating the curing of the TATATO/HD-SH resin with the photoactive particles, the reaction heat decreases significantly compared to the free initiator.

Table 5.13: Photo-DSC results of a TATATO/HD-SH resin with free photoinitiators compared to a resin with photoactive silica particles.

Initiator	t_{max} (s)	H_{max} (mW/mg)
free BAPO	2.2	47.5
TMESI^2-BAPO mod. silica method-1	2.9	39.3
TMESI^2-BAPO mod silica method-2	3.1	37.4
free IC 2959	4.0	35.2
TESI-IC2959 mod. silica method-1	4.7	23.5
TESI-IC2959 mod. silica method-2	4.7	23.3

5.3.1.6 FTIR kinetic measurements

FT-IR experiments was conducted to determine the influence of the type of photoactive particles and the modification yield on final monomer conversion and the reaction kinetics of the thiol-ene resins. The consumption of the double bond of the tri-functional allyl monomer (monitored at 1645 cm^{-1}) and the conversion of the S-H stretching band (2570 cm^{-1}) of the bi-functional thiol were simultaneously followed upon prolonged UV-exposure time. Previous studied has shown that the addition of 8 – 20 wt% pristine silica with primary particle sizes in the range of 20 nm does not significantly affect the reaction progress of the thiol-ene photopolymerization [36]. Thus, in the present work, the FT-IR results are only compared to filler-free thiol-ene resins, containing only the free initiators. Table 5.12 shows the content of resin mixtures. Fig.

5.35a and b illustrate the FT-IR results of TMESI^2-BAPO modified particles in comparison to free BAPO. It is clearly shown that curing with photoactive silica particles leads to lower polymerization rates whilst the final C=C double bond (97 %) and thiol conversions (97 %) obtained after 80 s UV irradiation are comparable to the reference system with free BAPO. Regarding the conversion of the alkene monomer, the polymerization rate is even lower for particles obtained from method-2 (modification yield: 10.7 %) than for particles prepared by method-1 (modification yield: 2.7 %).

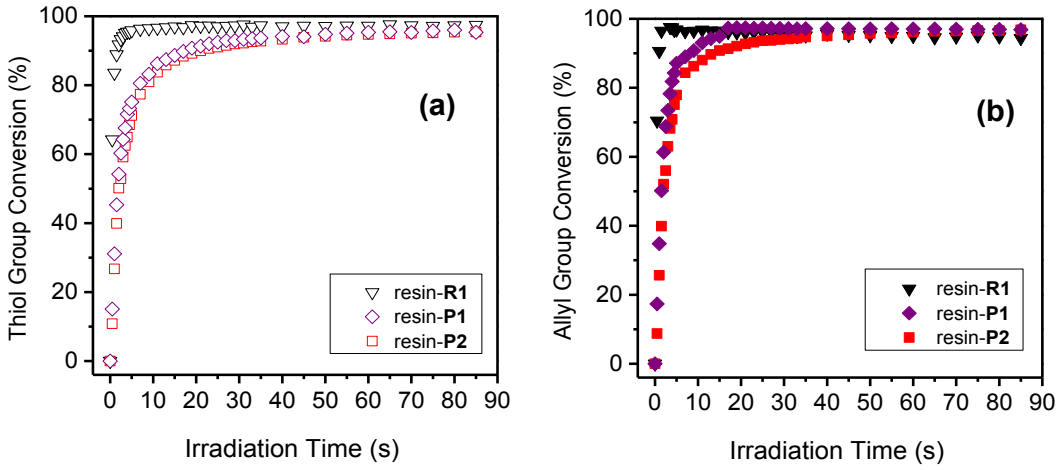

Figure 5.35: Influence of the addition of free BAPO (0.2 wt.%) and TMESI^2-BAPO modified silica particles (8.8 and 2.2 wt.% for method-1 and method-2) on the (a) thiol conversion and (b) C=C double bond of equimolar TATATO/HD-SH systems. UV irradiation was carried out with 25mW/cm^2 (λ = 250 - 470 nm) under inert conditions

Silica particles modified with TESI-IC2959 show a similar trend (see Fig. 5.36c and d). Independent on the initiating system (immobilized or free IC 2959) the final monomer conversions amounted to 96 % (SH group conversion) and 99 % (C=C group conversion). In contrast, the polymerization rate was significantly governed by both the degree of immobilization. Particularly, maximum C=C double bond conversion was observed after 4.0 s of UV exposure for the initiation with free IC 2959. By using the photoactive particles, maximum C=C double bond conversion was achieved after 12 s (method-1) and 28 s (method-2). The conversion of the thiol groups follows a comparable trend. This can be easily explained by the distribution and availability of photoinitiating radicals in the resin formulation. By keeping the concentration of photoinitiating species constant, more particles are required in the resin formulation if the

modification yield is lower. Thus, the initiating radicals are better distributed in the polymer matrix which facilitates the curing performance. In addition, DLS experiments clearly showed that the size of the clusters obtained from method-2 are significantly larger than the one accomplished with method-1, which further reduces the mobility and availability of the initiating species. Furthermore, it must be considered that in photoactive particles with a lower degree of modification, the photoinitiating radicals might be less prone to recombination reactions, since a localized concentration of radical species can be avoided. From the results, it can be concluded that employed grafting method has a crucial influence on the initiation efficiency of the modified silica in photopolymerization reactions as the kinetics is controlled by the distribution, size and the type of the photoactive species.

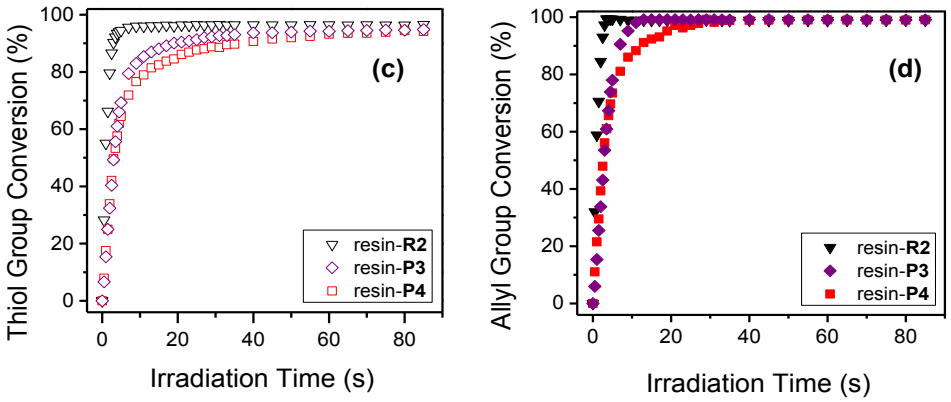

Figure 5.36: Effect of free IC 2959 (0.2 wt.%) and TESI-IC2959 modified silica particles (11.5 and 3.27 wt.% for method-1 and method-2) on the (c) thiol conversion and (d) C=C double bond of equimolar TATATO/HD-SH systems. UV irradiation was carried out with 25mW/cm^2 (λ = 250 - 470 nm) under inert conditions

5.3.1.7 Characterization of the Extractable Content

The use of photoactive particles is a promising strategy towards the reduction of the extractable initiator content in thiol-ene photopolymers, since we expect that after the photoinitiation, cleavage products as well as the non-reacted photoinitiators are attached onto the low-migrating silica filler. In addition, TMESI^2-BAPO modified particles can be covalently attached to the photopolymer matrix by a photoinduced hydrophosphinylation reaction between the immobilized phosphorus cleavage products and the allyl groups of TATATO [201]. The formation of insertion products between

particle surface and polymer matrix [particle-P(O)HR + $R_2C=CR_2$ -> particle-P(O)(CR_2CR_2H)R] might further prevent migration of the particles. The total extractable content as well as the extractable monomer and photoinitiator level obtained from elemental analysis are summarized in Table 5.14. With respect to the extractable monomer content, the results reveal that resin-R1 containing the free BAPO provides the lowest extractable thiol and alkene content, whilst both considerably increase in resin-P1 and resin-P2. In thin films, all three resin compositions exhibited a comparable final monomer conversion as shown by FT-IR experiments but the results suggest that the distribution and availability of photoinitiating radicals in the thicker samples becomes a dominating factor in the diffusion controlled thiol-ene photopolymerization. This is also confirmed by the lower extraction yields, which can be related to a higher monomer conversion in resin-P1, compared to resin-P2. This trend is more pronounced in the extractable thiol content and correlates well with the reaction rate of the resin compositions which was slower for the HD-SH conversion than the TATATO consumption.

Although resin-P2 has the highest extractable monomer contents, it is interesting to note that the amount of extractable photoinitiating species is below the detection limit of the elemental analysis. In contrast, the extractable content of the residual photoinitiator and phosphorous containing photocleavage products detected in resin-P1 is comparable to the reference resin-R1. The lower migration of the highly modified silica particles could be at first related to the larger size of the clusters obtained when using method-2. To study the influence of the cluster size on the extractable content, additional extraction experiments were carried out with a nanopowder, which was modified with $TMESI^2$-BAPO using method-2. The powder was additionally dispersed in acetone and sonicated for 2 min to break down the formed clusters. This process is repeated for 3 times. This post-treated powder comprised a z-average of 235.9 ± 13.0 nm, which is only slightly (~ 60 nm) larger than the clusters used in resin-P1. It is interesting to note, that the amount of extractable photoinitiating species was also below the detection limit of the elemental analysis, which indicates that the size of the clusters play a minor role. In terms of highly modified particles, the longer chain length of the attached photoactive silane oligomers are expected to increase the probability of the hydrophosphinylation reaction to occur between the organic shell and the

alkene monomers, thus leading to a covalent attachment of the particles to the polymer matrix.

Table 5.14: Extractable monomer and photoinitiator content in photocured thiol-ene resins

samples	total extract (wt.%)	TATATO ($mg/g_{Polymer}$)	HD-SH ($mg/g_{Polymer}$)	photoinitiator ($mg/g_{Polymer}$)
resin-R1	0.86	2.97	4.40	0.25
resin-P1	0.94	3.25	4.70	0.30
resin-P2	1.67	5.92	9.75	< 0.13[1]

[1]below the detection limit of the analysis method (< 0.05 wt.% phosphor)

5.3.2 Thiol-Ene Chemistry with Polymerizable Photoinitiators

One of the promising approaches to decrease the extractability of photoinitiators is the introduction of polymerizable functional groups within their structure as proposed in various papers [28,29].

In this study, a monoacylphosphine oxide type photoinitiator with alkyne functional groups, Prop-2-yn-1-yl phenyl(2,4,6-trimethylbenzoyl)phosphinate (modified TPOL), was synthesized and kindly provided by Meinhart Roth. The photoinitiator was used in the photo-crosslinking reaction of natural rubber (NR) latex using a low-molecular weight thiol (TMPMP) as crosslinker. The photopolymerizable alkyne groups introduced to the photoinitiator are expected to copolymerize with the carbon double bonds of the NR latex and thus, be covalently incorporated into the elastomer network. Extractability of the photoinitiator and its phosphorous containing cleavage products were studied by using a Soxhlet extraction method. In addition, UV crosslinked NR samples were evaluated in view of mechanical properties by applying tensile test measurements. The properties of the crosslinked NR latex samples were compared with the reference films, which were crosslinked with the commercially available derivative Irgacure TPO-L.

The structures of both parent initiator Irgacure TPO-L and modified TPO-L are shown in Scheme 5.6.

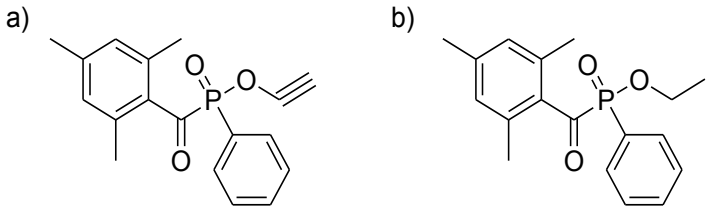

Scheme 5.6: Structure of monoacylphosphine oxide type photoinitiators with (a) polymerizable alkyne groups and its (b) parent initiators Irgacure TPO-L

The initiating ability of the modified TPO-L derivative was firstly investigated by preparing photo-patterned *cis*-1,4 polyisoprene films. After the development step with chloroform, microstructures with high resolution were obtained (see Figure 5.37).

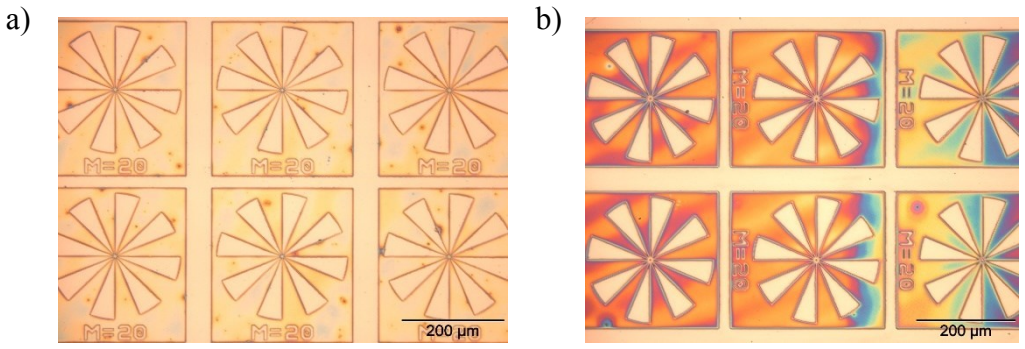

Figure 5.37: Optic microscopy images of photo-patterned *cis*-1,4 polyisoprene (M_w = 40,000 g/mol) films with (a) 1 phr Irgacure TPO-L (reference) and with (b) 1 phr modified TPO-L derivative (Crosslinker: 1 phr TMPMP; polyisoprene conc: 2% (w/w) in chloroform, exposure dose: 1.6 J/cm^2).

In subsequent tensile tests and extraction studies, the reactivity of modified TPO-L and its parent initiator was characterized as a function of both illumination dose as well as crosslinker concentration. Table 5.15 shows the selected curing conditions and composition of the NR latex formulations.

Table 5.15: Conditions for preparation of crosslinked NR samples.

	Initiator (1 phr)	TMPMP (phr)	Illumination Dose (J/cm^2)
Condition 1	Irgacure TPO-L	1	3.9
	Modified TPO-L		
Condition 2	Irgacure TPO-L	1	7.8
	Modified TPO-L		
Condition 3	Irgacure TPO-L	2	3.9
	Modified TPO-L		
Condition 4	Irgacure TPO-L	2	7.8
	Modified TPO-L		

(a)

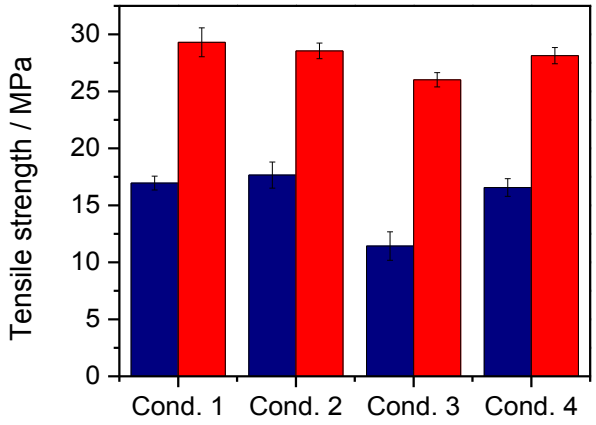

(b)

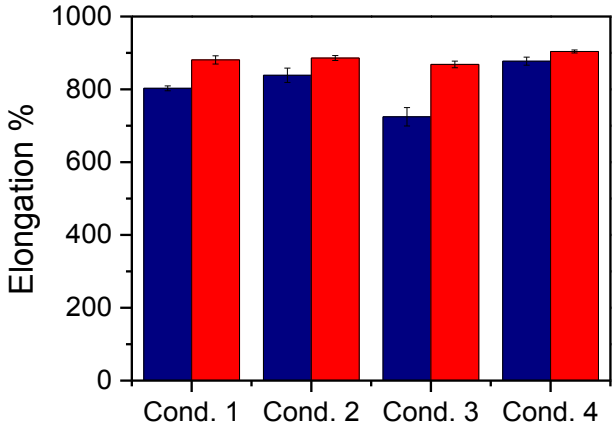

(c)

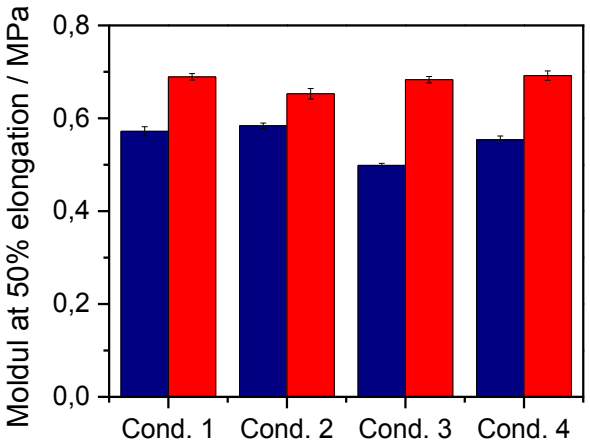

Figure 5.38: (a) Tensile Strength, (b) elongation at break and (c) modulus at 50% elongation of photo-cured NR latex films containing either Irgacure TPO-L (*red bars*) or its alkyne functional derivative (*blue bars*)

As can be seen in Figure 5.38, mechanical properties are strongly affected by the structure of initiators. NR samples with poor tensile strengths were obtained when the crosslinking reaction was initiated by the modified TPO-L while excellent mechanical properties obtained using parent initiator. The low tensile strength values might be attributed to lower crosslink density due to the reduced mobility of the modified TPO-L during the copolymerization reaction.

Moduli of these samples are also lower than the samples prepared with Irgacure TPO-L, which indicate a lower crosslinking density. Swelling experiments (see Figure 5.39) also confirm a lower degree of crosslinking density for the samples prepared with modified TPO-L due to their higher swelling ratios and lower gel fraction compared to the samples prepared with the parent initiators. However, employment of a higher illumination dose at a given crosslinker concentration of 1 phr (see Figure 5.39, cond. 1 versus cond. 2), leads to a decrease in the swelling degree and an increase in the gel fraction. This in turn results in a slight increase on tensile strength and moduli of samples prepared with modified TPO-L. Similarly, if the illumination dose is doubled at a constant crosslinker concentration (2 phr of TMPMP), tensile properties of samples prepared with modified TPO-L are improved (see Figure 5.38, cond. 3 and cond. 4). Thus, a higher crosslinking degree is achieved at a higher illumination dose for the systems which use modified TPO-L as photoinitiator. Particularly, samples prepared with 2 phr TMPMP and 1 phr initiator (both modified TPO-L and parent initiator)

require higher illumination dose to obtain better tensile properties (see Figure 5.38 cond. 3 and cond. 4).

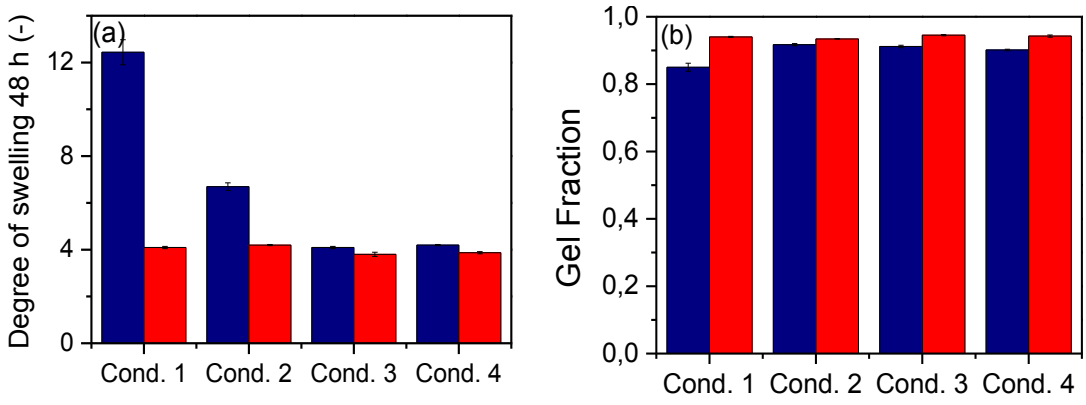

Figure 5.39: (a) Degree of swelling and (b) gel fraction of NR latex films photo-cured either with Irgacure TPO-L (*red bars*) or its alkyne functional derivative (*blue bars*).

Extractable photoinitiator content of crosslinked NR samples was further determined by Soxhlet extraction and the results are summarized in Table 5.16.

Table 5.16: Total extractable residues obtained by Soxhlet extraction (10 h with toluene at 135 °C) of crosslinked NR latex films

initiator (1phr)	crosslinker type and concentration	exposure dose (J/cm^2)	extracted amount (wt.%)
modified Irgacure TPO-L	TMPMP (2phr)	3.9	14.4
modified Irgacure TPO-L	TMPMP (2phr)	7.8	14.3
modified Irgacure TPO-L	TMPMP (1phr)	3.9	8.8
modified Irgacure TPO-L	TMPMP (1phr)	7.8	12.7
Irgacure TPO-L	TMPMP (2phr)	3.9	10.2
Irgacure TPO-L	TMPMP (2phr)	7.8	10.0
Irgacure TPO-L	TMPMP (1phr)	3.9	9.5
Irgacure TPO-L	TMPMP (1phr)	7.8	10.8

The lower gel fraction observed in samples, which have been crosslinked with modified TPO-L, generally also correlated with a higher amount of extractable residues as shown in Table 5.16. In particular, the samples prepared with 2 phr TMPMP and 1 phr modified TPOL show the highest amount of extracts. Extractable amount of photoinitiating and crosslinking species was determined by elemental analysis taking ad-

vantage of presence of phosphor and sulphur atoms in the structure of the photochemicals. For elemental analysis, samples were prepared by using an illumination dose of 7.8 J/cm^2.

Table 5.17: Elemental composition of the extracts obtained from crosslinked NR latex (exposure dose: 7.8 J/cm^2)

Initiator (1phr)	Crosslinker type and concentration	w-% C	w-% H	w-% N	w-% S	w-% P
modified Irgacure TPO-L	TMPMP (1phr)	85.285	11.748	0.047	0.437	0.038
Irgacure TPO-L	TMPMP (1phr)	82.385	11.243	0.133	0.808	0.134
modified Irgacure TPO-L	TMPMP (2phr)	82.84	11.455	0.108	1.487	0.042
Irgacure TPO-L	TMPMP (2phr)	79.86	10.633	0.193	2.008	0.064

Extract composition is influenced by the structure of initiator and crosslinker concentration. If the TMPMP concentration is increased from 1 phr to 2 phr, extracted sulphur amount also increases for samples prepared with both reference initiator and Irgacure TPO-L. Increased amount of sulphur could be at first related to the extractable crosslinker residues. However, extracted proteins from NR should be also taken into consideration since extracted nitrogen amount of the samples crosslinked with 2 phr TMPMP is also higher than the samples crosslinked with 1 phr TMPMP. Similarly, the extracted sulphur amount is higher for the samples prepared with the reference initiator compared to samples prepared with mod. TPO-L. The phosphor content of the extracts is considerably lower if mod. TPO-L is used as initiator. This reveals that most of the mod. TPO-L and the phosphorous containing cleavage products are covalently attached to the network structure.

Table 5.18: Extracted amount of sulphur and phosphor per one gram of photo-crosslinked NR latex films.

Initiator (1phr)	Crosslinker type and concentration	wt.%S/g_{Latex}	wt.%P/g_{Latex}
modified Irgacure TPO-L	TMPMP (1phr)	0.0555	0.0048
Irgacure TPO-L	TMPMP (1phr)	0.0873	0.0144
modified Irgacure TPO-L	TMPMP (2phr)	0.2126	0.0060
Irgacure TPO-L	TMPMP (2phr)	0.2008	0.0064

Table 5.18 shows the extracted amount of phosphor and sulphur atoms per 1 gram crosslinked NR. Extracted initiator amount is successfully decreased when modified TPOL is employed despite the high extraction yield.

5.4 Preparation of Photo-cured Composite Systems

The last part of the thesis is devoted to the preparation of photo-curable fibre reinforced composites. The performance of fibre-reinforced composites is strongly influenced by interactions at interphases due to the load transfer mechanism from matrix to fibre. To increase these physical and chemical interactions, glass fibre surfaces are typically modified with different silane coupling agents and other sizing materials.

The efficiency of surface treatments can be evaluated by micromechanical tests such as fragmentation, microbond, pull-out and push out tests. Single fibre pull-out test is a common method for evaluation of interactions at interphases. In this characterization method, a partly embedded single glass fibre is pulled out from a matrix droplet.

In this study, sized glass fibres were subjected to a 3-step purification method to obtain desized glass fibres. The desized glass fibres were then treated with methacryloxy functional silanes and silanes bearing photoactive group, which are able to co-react with an acrylate based resin. Both desizing and surface treatments were characterized by FTIR, XPS and zeta potential measurements. Surface modification and covalent bonding with the photopolymer was validated with single fibre pull-out tests.

The structure of the modification agents is shown in Scheme 5.7.

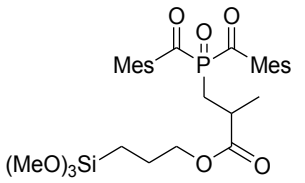

3-(trimethoxysilyl)propyl 3-[bis(2,4,6-trimethylbenzoyl) phosphinoyl]-2-methyl-propionate

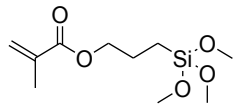

3-methacryloxypropyltrimethoxysilane

Scheme 5.7: Alkoxysilyl functional agents used in the modification of glass fibers

5.4.1 Characterization of Modified Glass Fibre Surfaces

5.4.1.1 FTIR measurements

FTIR analysis was performed on glass fibres as received and after washing with acetone (see section 3.5 for details of washing). Sizing material on commercially available glass fibres was also analysed as shown in Figure 5.40.

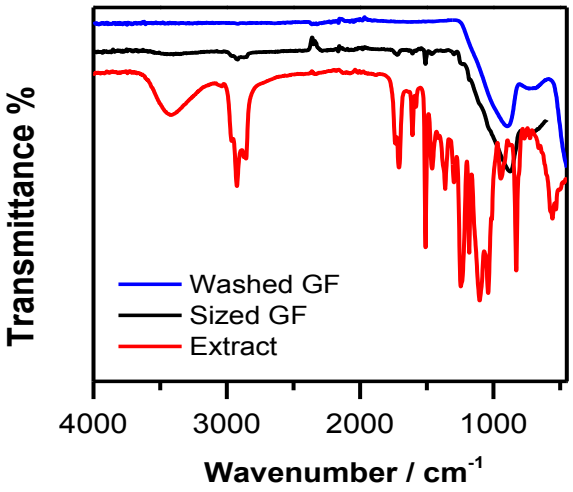

Figure 5.40: FT-IR spectra of commercially available sized glass fiber, extracted sizing material and glass fiber washed with acetone for 24 h.

The extract of commercially available sized glass fibre has a broad infrared absorption peak between 3660 and 3080 cm^{-1}, which is assigned to a stretching of N-H/O-H bonds. Stretching vibrations between 3000 and 2810 cm^{-1} are attributed to methyl, methylene and methine groups both in aromatic and aliphatic compounds. Two types of carbonyl bond stretching vibrations are observed around 1735 and 1710 cm^{-1}. The peaks at 1608 and 1509 cm^{-1} are attributed to aromatic C=C and C-C bonds, respectively. The signals at 1363 and 1461 cm^{-1} are assigned to CH bending vibrations, whilst the peaks at 1040 and 830 cm^{-1} bands are attributed to C-O-C bonds in ethers and oxiranes. The presence of oxirane groups is also indicated by the vibration bands at 1244 and 1181 cm^{-1}. The bands around 1100 cm^{-1} are assigned to C-O and Si-O stretching vibrations These results are in good agreement with literature and point out the presence of polyethylene oxide type surfactant and carbonyl and oxirane group bearing compounds in the sizing [202].

FTIR spectra of the glass fibres shown in Figure 5.40 (washed glass fibres and sized glass fibres as received) display a strong, broad band of Si-O-Si between 1260 and 810 cm^{-1}. The intensity of the Si-O-Si band is far stronger than the vibration bands of the organic sizing material due to the low weight percentage of sizing used for the modification of the glass surface. Due to the low weight percentage of sizing, some peaks are seen as shoulders in the sized glass fibres' spectra. After Soxhlet extraction of the glass fibers with acetone (corresponds to washed glass fibres), most of the organic compounds are removed and not detectable any more in the FTIR.

After extraction with acetone, the glass fibres were exposed to acidic and then basic piranha treatments to get rid of any residual strongly bonded sizing and to generate OH groups for further modifications.

Figure 5.41 shows that after acidic piranha treatments of the glass fibres, the characteristic OH band arises between 3660 and 3080 cm^{-1}. However, the hydroxyl band disappears again after basic piranha treatment.

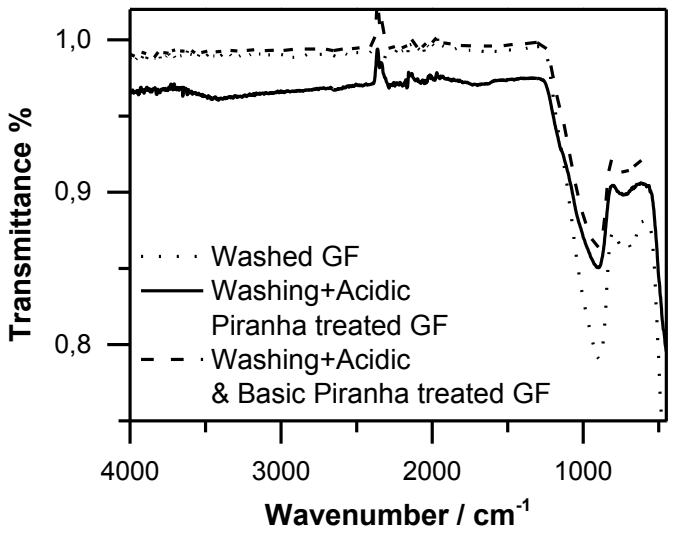

Figure 5.41: FT-IR spectra of washed, acidic and basic piranha treated glass fibers

5.4.1.2 XPS Measurements

XPS measurements were performed to determine the C, Si, O, Ca, Al, P, N, S content change on the surface of glass fibres during the desizing steps and subsequent modification. First step: Soxhlet extraction with acetone, second step: acidic piranha treatment, third step: basic piranha treatment and forth step: surface modification of glass

fibres by silanization with TMESI[2]-BAPO and 3-methacryloxypropyltrimethoxy silane.

The change in the chemical surface composition of the sized glass fibre during the applied desizing steps is summarized in Table 5.19.

On the surface of the sized glass fibre, silicon oxide (Si–O) at 103.5 eV, and organic silicon (C–Si–O) at 101.8 eV, as well as chemically bonded and physically adsorbed carbon (76.2 at.%) were detected [199,203,204]. Figure 5.42a and Figure 5.42b show the deconvoluted high resolution XPS Si 2p spectra of a sized glass fibre and a desized glass fibre after the 3-step cleaning process, respectively. Neither calcium (Ca) nor aluminium (Al) was detected on the sized glass fibre surface, which suggests that the thickness of sizing agent is above 10 nm (probing depth of XPS), as Ca and Al are components of the glass fibre [205]. After acetone extraction (first cleaning step) the carbon content (72.1 at.%) decreased slightly and the oxygen content (20.4 at.%) increased, suggesting that the amount of organic impurities were reduced by the acetone extraction. However, XPS results reveal that covalently bound sizing still covers most of the surface since carbon content is still high (~ 72 at.%), which indicates that only physically attached sizing is removed within the first cleaning step.

Acidic piranha treatment of glass fibres after Soxhlet extraction leads to a distinctive decrease (decrease is ~20 at.%.) of C content on the surface, revealing the high efficiency of peroxymonosulfuric acid to remove organic residuals and impurities. An elemental analysis from the XPS survey spectrum indicates the presence of small amounts of sulphur on the glass fibre surface after acidic piranha treatment. The sulphur might have diffused into the glass during the chemical etching with acidic piranha [206]. The sulfuric acid signal disappears after basic piranha treatment due to the neutralization of the fibre surface. Additionally, the silicon and oxygen content on the surface increased after acidic piranha treatment. This also proves the removal of the sizing agent to a certain extent.

After the basic piranha treatment of sized glass fibres (final cleaning step) the carbon content (36.8 at%) decreases significantly whilst the oxygen content increases (37.7 at.%.) Furthermore, in the Si 2p spectrum only one silicon oxide signal at 103.5 eV is observed, which is the expected value for silicon oxide without sizing agent [199,203]

(Figure 5.42b). Thus, this result confirms that the sizing agent has been removed from the glass fibre surface, mostly by the basic piranha treatment which reduces the amount of organic impurities [205]. The detected carbon content is attributed to physisorbed atmospheric hydrocarbon and CO_2, as the basic piranha treatment increases the surface energy of glass fibres [207]. Additionally, calcium and aluminium were detected on the surface after the acidic and basic piranha treatment.

Table 5.19: Surface chemical composition of glass fiber surfaces as derived from XPS data: sized glass fibers as received and glass fibers during each cleaning steps

Fibre	Relative Concentration [at.%]							
	C	O	Si	Ca	Al	S	N	P
Sized	76.2	16.5	7.3	–	–	–	-	-
Cleaning Step 1	72.1	20.4	7.5	–	–	–	-	-
Cleaning Step 2	52.4	30.4	12.1	3.0	1.0	1.1	-	-
Cleaning Step 3	36.8	37.7	17.0	4.2	4.3	–	-	-
Burned off	37.2	38.3	19.6	3.3	1.6	-	-	-

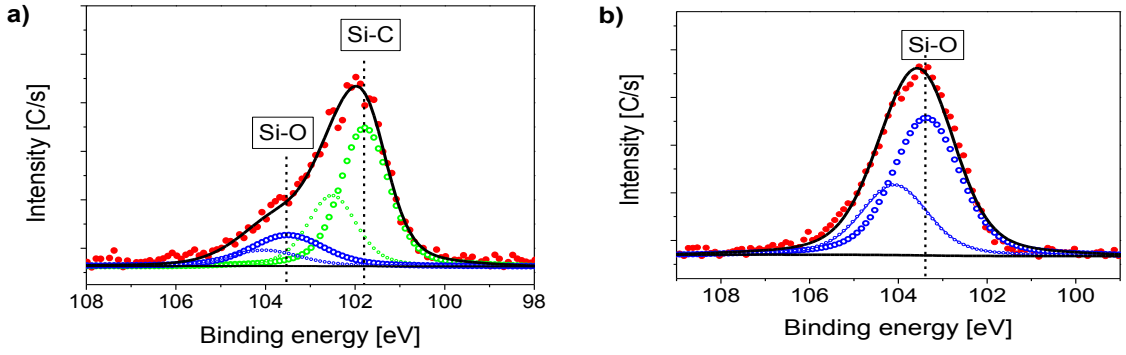

Figure 5.42: High resolution Si 2p XPS spectra of (a) sized and (b) desized glass fibres

To sum up, received sized glass fibres contain ~76 % carbon atoms on their surface. During cleaning steps, the carbon content is decreasing gradually (from step 1 to step 3) while oxygen and silicon content on the surface are increasing.

To verify the efficiency of the applied cleaning method in this study, a well-known method in desizing of glass fibres was applied, which involves burning off the organic

content. In this method, sized glass fibres as received were subjected to a burning at 565 °C for 2 h. Atomic content of burned glass fibre surface was compared with the glass fibres which were desized with the 3-step cleaning method. XPS analysis of burned glass fibres also indicates a similar carbon atom content as the one reached with the 3-step cleaning process (see Table 5.19).

After desizing, the glass fibre surface was modified with either a methacryloxy functional silane or the photoactive silane TMESI^2-BAPO.

XPS was further used to analyse the chemical composition of the modified glass fibre surface. Deconvoluted XPS high resolution C 1s and Si 2p spectra of TMESI^2-BAPO and methacrylate modified glass fibres are shown in Figure 5.43.

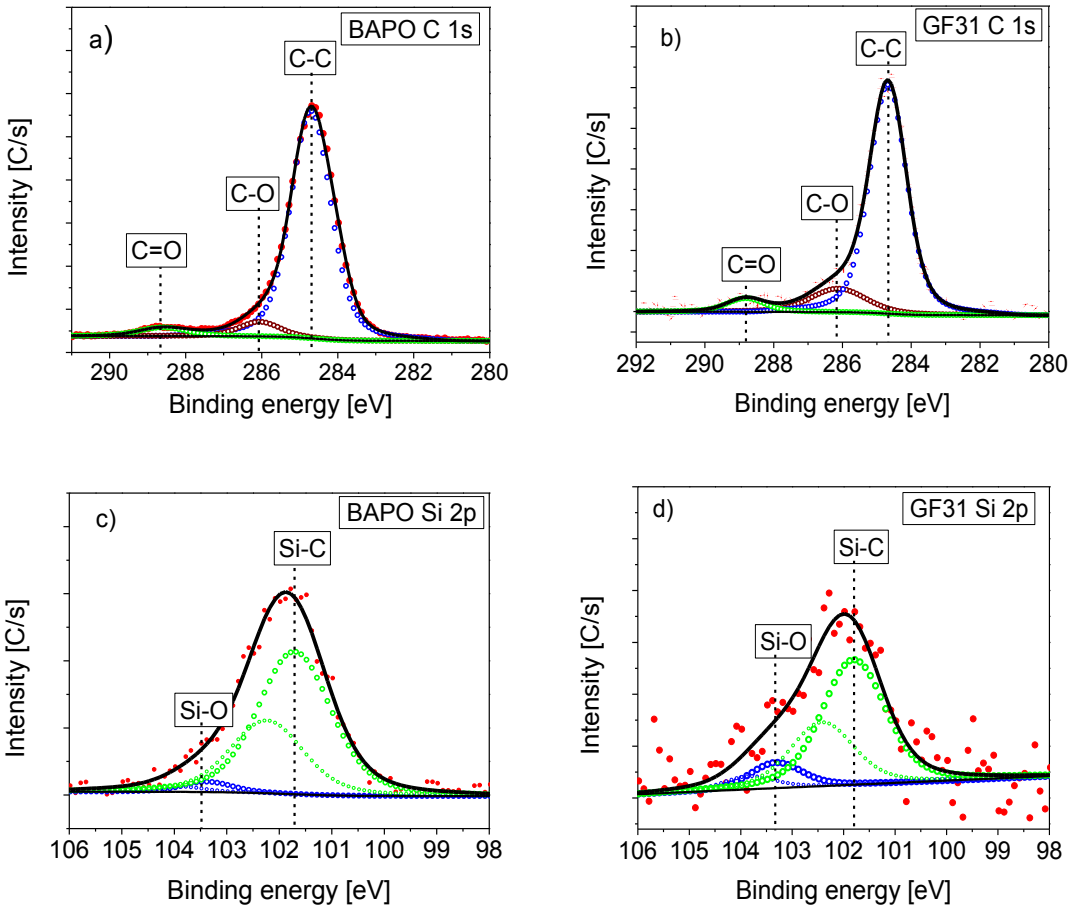

Figure 5.43: Deconvolution of high resolution XPS spectra (a) and b) C 1s spectra for BAPO and methacrylate layer on glass fiber surface, respectively. c) and d) Si 2p spectra for BAPO and methacrylate layer on glass fiber surface, respectively

Both the C 1s spectra of TMESI^2-BAPO and methacrylate modified glass fibres show one main peak at 284.7 eV, which is due to presence of the hydrocarbon (C–C) chain group [208–210]. Other fitted peaks include the C–O peaks at 286.2 eV, and C=O at 288.7 eV [209–211]. The Si 2p high resolution XPS spectra of TMESI^2-BAPO and methacrylate modified surfaces indicate two characteristic groups: Si–O at 103.5 eV, and C–Si–O at 101.7 eV [199,203,204]. These groups are attributed to the glass fibre surface and organic silane layer (C–Si–O) respectively. On the basis of the C–Si–O spectra, the functionalization of the desized glass fibre with TMESI^2-BAPO and methacrylate was proved clearly as already described in previous study [35]. Since XPS measurements provide information up to 10 nm depth, the detection of the Si-O peak reveals that the attached organic layer thickness is below 10 nm [205]. Additionally, a deconvoluted P 2p spectrum of TMESI^2-BAPO was measured. The high resolution of P 2p of TMESI^2-BAPO modified glass fibre exhibits two types of P atom: P–C at 132.3 eV, and P–O at 133.5 eV (see Figure 5.44).

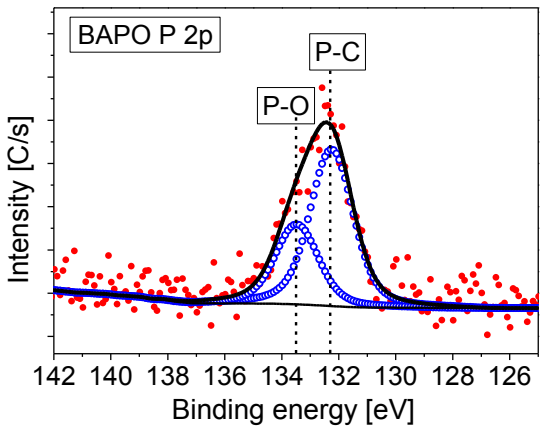

Figure 5.44: Deconvoluted high resolution P 2p XPS spectra of TMESI^2-BAPO on glass fiber surfaces

The assignments of high resolution C 1s, Si 2p and P 2p XPS spectra are summarized in Table 5.20.

Table 5.20: Assigned chemical components in deconvoluted high resolution C 1s, Si 2p and P 2p spectra of of TMESI^2-BAPO modified glass fibres

Chemical shift	C 1s [eV]	Si 2p [eV]	P 2p [eV]
C–C	284.7		
C–O	286.2		
C=O	288.7		
C–Si–O		101.7-101.8	
Si–O		~103.5	
P–O			132.3-133.7

The chemical composition of the basic piranha treated glass fibre, and of organic layers of TMESI^2-BAPO and methacrylate on glass fibre is given in Table 5.21.

Table 5.21: Chemical composition of basic piranha treated, and TMESI^2-BAPO and methacrylate modified glass fiber surfaces as derived from XPS data

Fibre	Relative Concentration [At.-%]					
	C	O	Si	Ca	Al	P
Desized	36.8	37.7	17.0	4.2	4.3	–
Methacrylate modified	55.7	28.1	9.9	4.2	2.0	–
TMESI^2-BAPO modified	72.1	19.8	4.1	2.0	–	2.0

5.4.1.3 Zeta Potential Measurements

Surface properties of sized glass fibres as received, desized glass fibers and silanized glass fibres (both methacrylate as well as TMESI^2-BAPO) were characterized by zeta potential measurements. Zeta potentials were measured using the streaming potential method in order to determine the acid–base character of the glass fibre surfaces.

Figure 5.45 shows the pH dependence of the zeta potential for the glass fibres prior to and after the cleaning and modification procedures whilst Table 5.22 shows the isoelectric point of related fibres (IEP, pH where $\zeta = 0$ mV). Photoactive glass fibres (TMESI^2-BAPO modified) were also exposed to UV irradiation and washed a few times with acetone, and then subjected to zeta potential measurements.

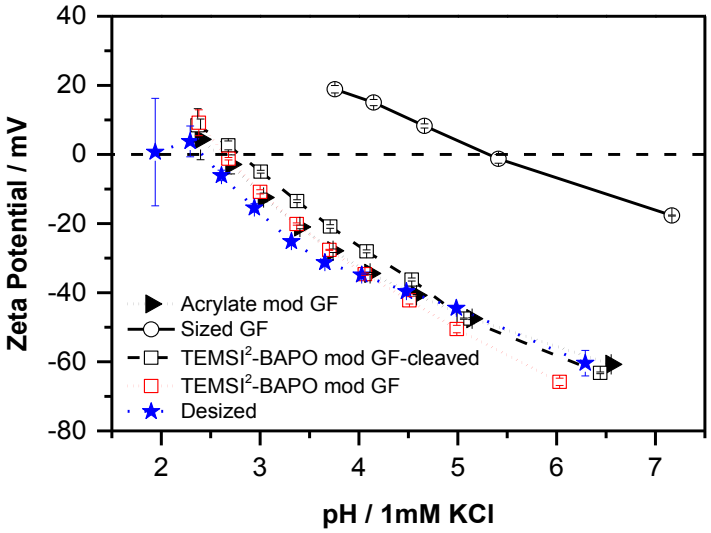

Figure 5.45: pH versus zeta potential values of glass fibers (GF) after various treatments

Table 5.22: Isoelectric point of glass fibers (GF) after various treatments

Name	IEP
Sized GF	5.31
Desized GF	2.41
Methacrylate modified GF	2.58
TMESI²-BAPO modified GF	2.65
UV exposed TMESI²-BAPO modified GF	2.79

Prior to the cleaning step, the IEP of the sized fibres (commercially available one) amounts to 5.3, which indicates the presence of neutral groups from the applied sizing. After a 3-step desizing procedure, the IEP amounts to 2.41 indicating acidic surface functions. The subsequent silanization of the desized glass fibres results in a slight shift of the IEP to higher values, which indicates the replacement of acidic surface OH groups by immobilization of the organosilanes. An additional UV exposure of TMESI²-BAPO does not lead to the formation of phosphonic acids as the IEP of the illuminated fibres occurs at a higher pH value than the non-illuminated ones.

The negative zeta potential values are typical for glass surfaces, as the acidic surface groups are fully dissociated in the basic pH range and form negative surface charges [212]. Whilst the surface charges of the inorganic fibre mainly rely on the protonation and deprotonation of the silanol groups, also other elements on the fibre surface (e.g. Al-OH, Ca-OH) contribute to them [212].

5.4.1.4 Single Fiber Pull-out Tests

The surface chemistry of glass fibres has a substantial effect on their interaction with polymeric matrixes at the interface. To investigate the interface properties between an acrylate based photopolymer and a glass fibre as a function of the applied modification procedure, single fibre pull-out tests were carried out.

A typical pull-out test consists of three main steps [213,214]. In the first step, interfacial forces resist to the applied pull-out forces and only elastic deformations are allowed. Here, both fibres and matrix may show elastic deformations. The second step starts when the maximum shear stress at the fibre embedding point is higher than the bond strength. As a result, debonding (crack formation) starts and grows along the interface until full debonding occurs. After crack initiation, the slope of the force displacement curve changes[215]. Crack growth may proceed either slow or accelerated and the pull-out force may also increase or decrease during displacements depending on the bond strength and frictional strength. After complete debonding of the interface, frictional sliding is observed in the third step.

Surface modification of fibres has an important effect on the load response of the fibre-matrix composites. Sized fibres as received, desized and modified fibres show different behaviour in the related force-displacement curve, reflecting a different failure mechanism as shown in Figure 5.46.

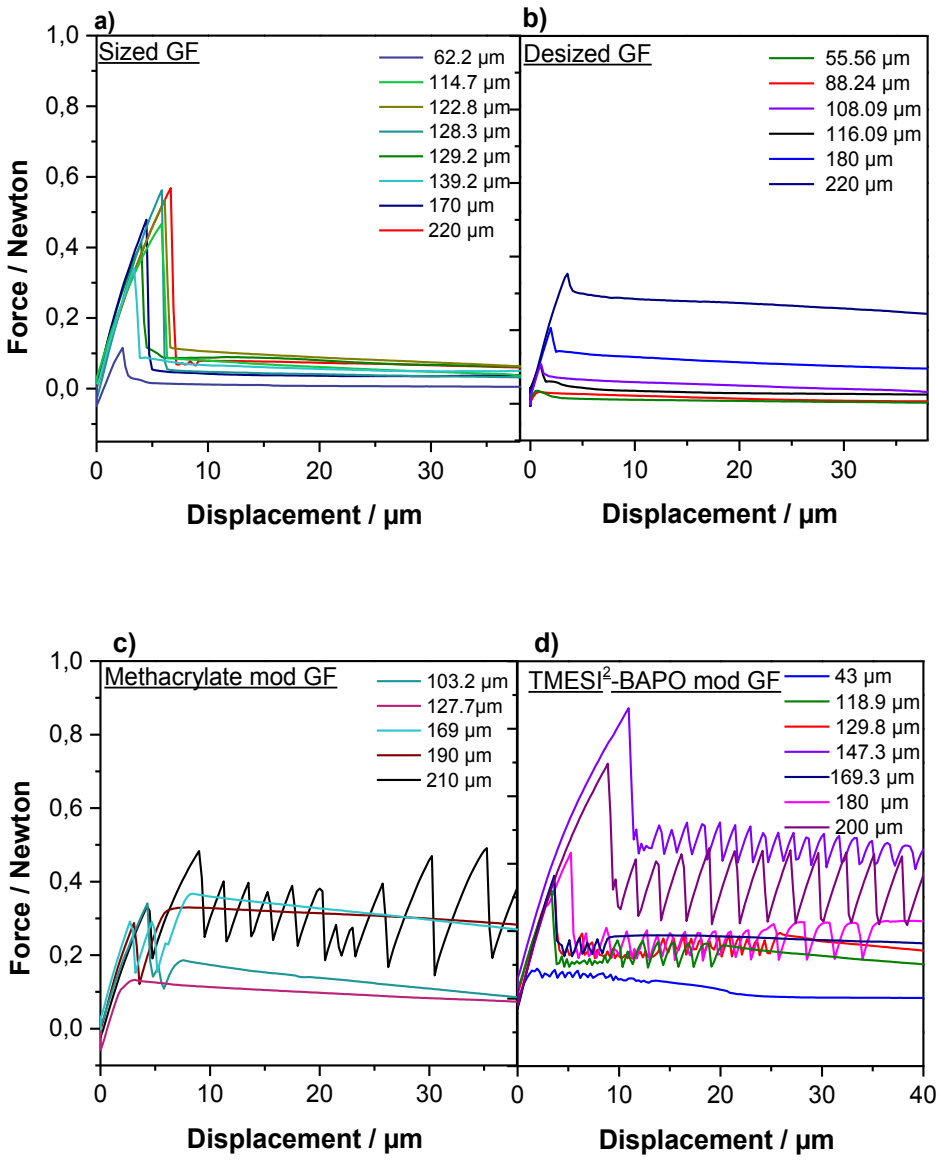

Figure 5.46: Force-displacement curves of (a) sized, (b) desized, (c) methacrylate modified and (d) TMESI^2-BAPO modified glass fibres depending on their embedding length

As can be seen in Figure 5.46, the functionality of the surface has an important influence on the pull-out behaviour. In all glass fibre-acrylate matrix combinations, the force is slightly non-linear in the force displacement curve.

In the sized glass fibre-acrylate matrix combination, abrupt failure of the force is observed while in the desized fibre-acrylate matrix combination a gradual failure occurs. Abrupt failure indicates a high adhesion along with low friction [216]. On the other hand,

gradual failure indicates low adhesion together with strong friction [216]. In both systems, constant friction is observed after the debonding process. Methacrylate modified glass fibre-acrylate matrix combination shows a slip hardening behaviour. In the case of TMESI^2-BAPO modified glass fibres, slip-stick effect is seen.

Figure 5.47 shows the maximum pull-out force of (a) sized, (b) desized, (c) methacrylate modified and (d) TMESI^2-BAPO modified glass fibres versus embedded area. The slope corresponds to the average apparent interfacial shear strength [217].

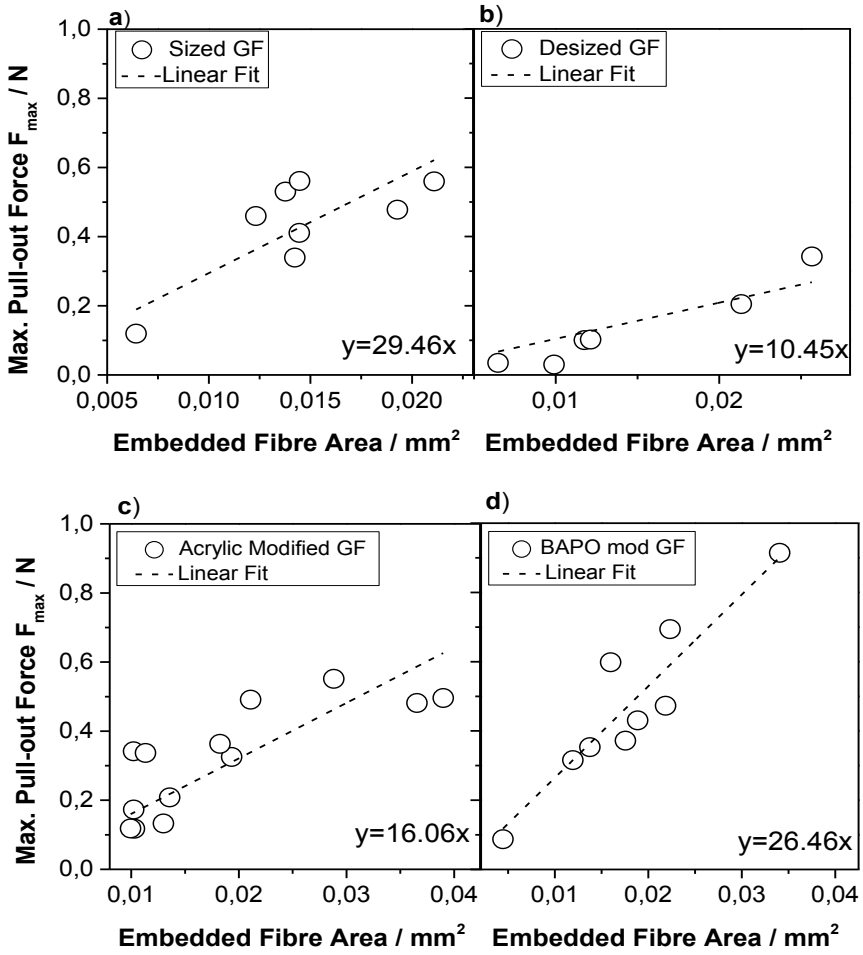

Figure 5.47: Maximum pull-out force of (a) sized, (b) desized, (c) methacrylate modified and (d) TMESI^2-BAPO modified glass fibers versus embedded fibre area.

Average apparent interfacial shear strength of the desized glass fibre-acrylate matrix is the lowest (lowest slope) corresponding to the lowest apparent adhesion strength. It increases for methacrylate modified glass fibres and it is highest for the sized and

TMESI^2-BAPO modified glass fibres. Thus, adhesion strength is larger for the sized and TMESI^2-BAPO modified glass fibres.

Further characteristics of interface between glass fibres and acrylate matrix were investigated by plotting the apparent interfacial shear strength (τ_{IFSS}) and frictional force per unit area versus embedding length of fibres (see Figure 5.48). τ_{IFSS} was calculated as following:

$$\tau_{\mathrm{IFSS}} = \frac{F_{max}}{A_e} \qquad A_e = d_f . \Pi . L_e \tag{5.2}$$

Where F_{max} is the maximum force, A_e is the embedded surface area and L_e is the embedded fibre length.

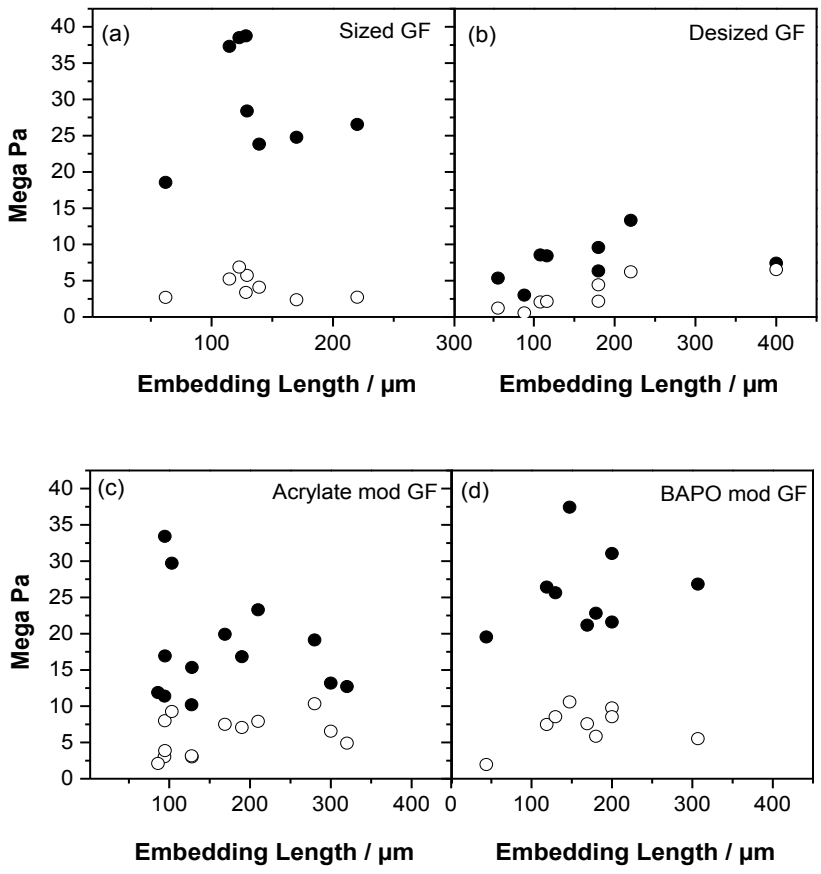

Figure 5.48: Apparent interfacial shear strength (filled symbols) and frictional force per unit area (empty symbols) versus embedding length of fibers; (a) sized, (b) desized, (c) methacrylate modified and (d) TMESI^2-BAPO modified glass fibers

τ_{IFSS} values of all composites show a broad scattering as well as independence of embedding length (see Figure 5.48). Independence of τ_{IFSS} to embedding length indicates ductile-type failure of the fibre-matrix interface. Figure 5.48 also confirms that the desized glass fiber-acrylate composite has the lowest shear strength while shear strength of the methacrylate modified glass fibre-acrylate matrix interface is stronger. Sized glass fibre - and TMESI^2-BAPO modified glass fibre-acrylate composites have the strongest interface (highest shear strength) between these four glass fibres. Moreover, Figure 5.48 points out that frictional force per unit area of the interface is lower than τ_{IFSS} values for all mentioned composite systems.

Summing up, the results clearly showed that interfacial properties of fibre reinforced composites can be conveniently tailored by the chemical composition and the surface reactivity of the fibres.

6 CONCLUSION

In the present thesis, strategies towards the preparation of low-migratable thiol-ene photopolymers have been pursued. Network evolution, mechanical properties and migration behaviour of the photopolymer networks have been studied in detail, thus enabling the establishment of structure-property relationships.

In the first part of this study, thiol-allyl and binary thiol-acrylate networks were prepared by radical-mediated thiol-ene chemistry. In thin films, the photoinduced step-growth mechanism is strongly governed by the reactivity of both the -ene as well by the thiol component. In terms of thiol-acrylate systems, the reaction kinetics is mainly influenced by the simultaneous chain growth of the acrylate monomers whilst the homopolymerization of the -ene component plays a minor part in thiol-allyl networks. From FT-IR experiments it can be concluded that the yield of homopolymerization of both the acrylate as well as the allyl monomer is increased if thiols with either low thiol functionality or with low reactivity in the thiol-ene photopolymerization are applied. The yield of homopolymerization correlates with the heterogeneity of the networks as revealed by a broad glass transition temperature range and the network dynamics obtained from NMR relaxometry experiments.

Along with thiol-allyl and binary thiol-acrylate systems, thiol-ene networks were prepared by using low migratable thiol components and natural rubber (NR) latex as the -ene component. Crosslinking of NR latex via thiol-ene reaction is an alternative method to the conventionally used sulphur curing. As the thiol-ene photoreaction does not rely on the use of hazardous accelerators and provides a fast and energy efficient technology, it has become a promising method for the efficient production of low-allergenic latex articles. In the photo-curing of NR latex, not only the curing method (pre-curing in latex state or post-curing in solid film state) but also the structure of the thiol crosslinker (e.g. molecular weight and number of thiol functionality) play an important role in the mechanical properties of the final products. The results of the tensile tests revealed that crosslinking with low molecular weight thiols yields higher tensile

strengths compared to higher molecular weight counterparts with the same number of functionality in their structure (see TMPMP versus Thiocure 700 and Thiocure 1300). It was further observed that thiols with a rigid cycloaliphatic structure (HBPA-SH) are superior to linear aliphatic ones (HD-SH) with respect to the tensile strength.

To increase both molecular weight and functionality of thiol crosslinker, siloxane based oligomeric thiols were synthesized. In particular, acid catalysed hydrolytic polycondensation of mercapto-functional silanes with two hydrolysable alkoxy groups was used for the synthesis of the thiol functional siloxane oligomers. These conditions favour the formation of trimeric, tetrameric and pentameric species. Longer reaction times and high concentration of monomeric silanes as well as the addition of acrylate functional silanes to reaction mixture leads to formation of higher molecular weight fraction in addition to cyclic species. NR latex films photo-cured with the newly synthesized silane oligomers exhibit excellent tensile properties. Particularly, copolymeric siloxanes with thiol and acrylic functionality leads to efficient crosslinking of NR latex with low amount of extractable species.

Another strategy towards high molecular weight crosslinker is the covalent attachment of low molecular thiol functional silanes on the surface of inorganic fillers (e.g. silica). Surface-bound crosslinkers are expected to have less ability to migrate out from polymeric networks. Thus, zeolite and silica particles bearing thiol functionality on their surface were prepared via anhydrous liquid phase deposition of silanes. However, these thiol functionalized particles were inefficient in the photo-crosslinking of NR since the related films exhibited low tensile strength. This was mainly related to the low reactivity of the immobilized thiols.

Besides the thiol crosslinker, this study also focused on the preparation of low-migratable photoinitiators. For this aim, surface-bound initiators were prepared by immobilizing trialkoxysilyl-functionalized Norrish Type I photoinitiators onto the surface of nano-sized silica. The degree of modification was controlled by the synthesis procedures. Two different alkoxysilyl functional initiators were attached to the particle surface by two different silanization methods. TGA experiments revealed that under anhydrous conditions the degree of functionalization of the photoactive particles was in the range of 2.5 wt% (method-1). It substantially increased to ~10 % if a two-step modification route was carried out in the presence of a catalyst and in water containing

solvents (method-2). DLS experiments further revealed that the size of the silica clusters significantly increases with the modification method-2, which is attributed to an inter-particle condensation (probably during the evaporation of the water containing, polar solvent during the preparation). Independent of the modification yield, the functionalized particles exhibited the characteristic UV absorption as well as thermal decomposition profile of the related free photoinitiators, which was confirmed by UV-Vis spectroscopy. The functionalized particles were then employed as photoinitiator in free radical-mediated thiol-ene photopolymerization using TATATO as the "ene" component and HD-SH as the functional thiol. Photo-DSC and FT-IR measurements revealed that the photoactivity of the particles is not only influenced by the type of initiating species but also by the employed grafting method, since it controls the size, distribution and degree of functionalization of the photoactive particles. At a given concentration of photoinitiating species, smaller silica clusters with lower modification yield (method-1) lead to a higher polymerization rate as the photoactive groups are distributed more homogenously in the thiol-ene matrix. In contrast, a high degree of modification of the silica clusters (method-2) is crucial for a low extractability, which was confirmed by Soxhlet extraction experiments. The results evidenced that the extractable content of photoinitiator is below the detection limit in samples photocured with the modified particles (prepared via method-2). From the results it can be concluded that by conveniently tailoring the organic shell of photoactive particles by the conditions of the modification process, crucial properties of the photopolymers such as reactions kinetics and migration behaviour can be controlled. For industrial applications with low-migration levels, it has to be considered that a higher content of the highly modified particles has to be used to ensure both quantitative conversion of the monomers as well as low extractability of the photoinitiator.

Another approach towards low extractable photoinitiators was based on the introduction of polymerizable functional groups within their structure. A cleavage type photoinitiator with allyl functional groups was employed in the radiation curing of NR latex. Although it is effective enough to initiate the thiol-ene reaction as confirmed in preparation of the negative-toned photoresists, tensile properties of the cured NR samples are lower than the samples prepared with the reference initiator which does not have any allyl groups. This can be explained by the limited diffusion of the initiating

radicals due to the copolymerization of it with the network or the thiol functional crosslinker. The inefficient initiation of the thiol-ene reaction in NR latex is also confirmed by equilibrium swelling measurements. Samples cured with the side chain modified photoinitiator showed a higher swelling degree and a lower gel fraction which are attributed to a lower crosslink density. However, elemental analysis of the extracts evidenced the reduced amount of extractable initiator compared to its commercially available counterpart.

Going beyond the design of low-migratable photopolymers, the last part of this thesis, aims at the modification of glass fibre surfaces to control the interface properties of fibre reinforced photopolymer composites. Selected silanes including a trialkoxysilyl bearing photoinitiator and a silyl functionalized acrylate were immobilized onto glass fibres to tune the interface characteristics in glass fibre reinforced composites. For the sample preparation, commercially available sized glass fibers were subjected to a three-step purification method to obtain desized glass fibers. The change of the surface properties after each purification step was monitored by XPS spectroscopy. The desized GFs were then functionalized by either attaching the functional silanes via a condensation reaction across the hydroxyl groups of the glass surface. Thus, the surface properties of glass fibres can be conveniently changed by exploiting silanization reactions. The attachment of the functional groups was confirmed by XPS and zeta potential measurements. From single fibre pull-out tests it was found that the surface properties of the fibres have a strong influence on the properties of the fibre-matrix interface. In particular, shear strength increased if functionalized groups were attached on the fibres, which were then able to react with the matrix during the photoinduced curing reaction. Further research on functionalized photopolymer composites has to be performed to study and evaluate the influence of fibre-matrix interactions on thermo-mechanical properties of macroscopic components.

To sum up, structure of both the photoinitiators and the monomers was correlated with network evolution, mechanical properties and migration behaviour of the polymer networks. Furthermore, materials that exhibit both low extractability and excellent mechanical properties were successfully produced.

7 REFERENCES

[1] C. Esposito Corcione, M. Frigione, *Thermochimica Acta* **2012**, *534*, 21.

[2] J. P. Fouassier, D. Burr, Crivello, J. V., *Journal of Macromolecular Science, Part A* **1994**, *31*, 677.

[3] J. M. Shaw, J. D. Gelorme, N. C. LaBianca, W. E. Conley, S. J. Holmes, *IBM J. Res. Dev.* **1997**, *41*, 81.

[4] J. Stampfl, S. Baudis, C. Heller, R. Liska, A. Neumeister, R. Kling, A. Ostendorf, M. Spitzbart, *Journal of Micromechanics and Microengineering* **2008**, *18*, 125014.

[5] T. Griesser, A. Wolfberger, U. Daschiel, V. Schmidt, A. Fian, A. Jerrar, C. Teichert, W. Kern, *Polym. Chem.* **2013**, *4*, 1708.

[6] A. A. Pawar, G. Saada, I. Cooperstein, L. Larush, J. A. Jackman, S. R. Tabaei, N.-J. Cho, S. Magdassi, *Science Advances* **2016**, *2*.

[7] K. M. Jeong, J. M. Won, Y. K. Lee, K. Koseki, *Journal of Korea Technical Association of The Pulp and Paper Industry* **2014**, *46*, 46.

[8] F. H. Mostegel, M. Roth, M. Gassner, A. Oesterreicher, R. Piock, M. Edler, T. Griesser, *Progress in Organic Coatings* **2016**, *94*, 116.

[9] L. G. Lovell, K. A. Berchtold, J. E. Elliott, H. Lu, C. N. Bowman, *Polymers for Advanced Technologies* **2001**, *12*, 335.

[10] L. G. Lovell, H. Lu, J. E. Elliott, J. W. Stansbury, C. N. Bowman, *Dental Materials*, *17*, 504.

[11] L. G. Lovell, S. M. Newman, M. M. Donaldson, C. N. Bowman, *Dental Materials*, *19*, 458.

[12] J. W. Stansbury, *Journal of Esthetic and Restorative Dentistry* **2000**, *12*, 300.

[13] F. A. Rueggeberg, *Dental Materials*, *27*, 39.

[14] S. Schlögl, A. Temel, R. Schaller, A. Holzner, W. Kern, *Rubber Chemistry and Technology* **2010**, *83*, 133.

[15] J. V. Crivello, E. Reichmanis, *Chemistry of Materials* **2014**, *26*, 533.

[16] Z.-W. Wang, *Packaging Technology and Science* **2008**, *21*, 115.

[17] J. L. Aparicio, M. Elizalde, *Packaging Technology and Science* **2015**, *28*, 181.

[18] K. Dietliker, R. Hüsler, Birbaum, J., L., S. Ilg, S. Villeneuve, K. Studer, T. Jung, J. Benkhoff, H. Kura, A. Matsumoto, H. Oka, *Progress in Organic Coatings* **2007**, *58*, 146.

[19] Van Den Houwe, Kathy, C. Evrard, J. van Loco, F. Lynen, E. van Hoeck, *Food Additives & Contaminants: Part A* **2016**, *33*, 913.

[20] V. M. Vaubert, P. C. Moon, B. J. Love, *Journal of biomedical materials research* **1999**, *48*, 5.

[21] P. A. Leggat, U. Kedjarune, *International dental journal* **2003**, *53*, 126.

[22] A. Bakopoulou, T. Papadopoulos, P. Garefis, *International journal of molecular sciences* **2009**, *10*, 3861.

[23] S. M. Mousavinasab, *Dental research journal* **2011**, *8*, S21-9.

[24] S. Amr, M. E. Bollinger, *Environmental Health Perspectives* **2004**, *112*, 378.

[25] V. Kujala, H. Alenius, T. Palosuo, J. Karvonen, P. Pfäffli, K. Reijula, *Clinical & Experimental Allergy* **2002**, *32*, 1077.

[26] R. T. Jones, D. L. Scheppmann, D. K. Heilman, J. W. Yunginger, *Annals of allergy* **1994**, *73*, 321.

[27] Van Den Houwe, K., A. van Heyst, C. Evrard, J. van Loco, F. Bolle, F. Lynen, E. van Hoeck, *Packaging Technology and Science* **2016**, *29*, 121.

[28] W. D. Davies, F. D. Jones, J. Garrett, I. Hutchinson, G. Walton, *Surface Coatings International Part B: Coatings Transactions* **2001**, *84*, 213.

[29] P. Xiao, H. Zhang, M. Dai, J. Nie, *Progress in Organic Coatings* **2009**, *64*, 510.

[30] T. Corrales, F. Catalina, C. Peinado, N. S. Allen, *Journal of Photochemistry and Photobiology A: Chemistry* **2003**, *159*, 103.

[31] Crivello, J. V., K. Dietliker, G. Bradley, *Photoinitiators for free radical cationic & anionic photopolymerisation*, J. Wiley in association with SITA Technology, Chichester, West Sussex, England, New York **1998**.

[32] R. C. Advincula, *Journal of Dispersion Science and Technology* **2003**, *24*, 343.

[33] M. Kamigaito, T. Ando, M. Sawamoto, *Chemical Reviews* **2001**, *101*, 3689.

[34] R. Barbey, L. Lavanant, D. Paripovic, N. Schüwer, C. Sugnaux, S. Tugulu, H.-A. Klok, *Chemical Reviews* **2009**, *109*, 5437.

[35] M. Sangermano, M. Periolatto, M. Castellino, J. Wang, K. Dietliker, J. L. Grützmacher, H. Grützmacher, *ACS Applied Materials & Interfaces* **2016**, *8*, 19764.

[36] M. Sahin, S. Schlögl, S. Kaiser, W. Kern, J. Wang, H. Grützmacher, *Journal of Polymer Science Part A: Polymer Chemistry* **2017**, *55*, 894.

[37] A. Huber, A. Kuschel, T. Ott, G. Santiso-Quinones, D. Stein, J. Bräuer, R. Kissner, F. Krumeich, H. Schönberg, J. Levalois-Grützmacher, H. Grützmacher, *Angewandte Chemie International Edition* **2012**, *51*, 4648.

[38] H. Arai, *Inorganic particle dispersions, cured films thereof, and their manufacture (JP5471522)*.

[39] H. Arai, *Preparation of inorganic particle dispersions forming hard coatings with excellent scratch resistance (JP2011157435)*.

[40] H. Y. Choi, C. H. Cho, *Method of manufacturing flexible display device using UV-decomposable silane compound to easily detach flexible display board from carrier board (KR 2014136560)*.

[41] GUANGZHOU BOSSIN POLYMERIZATION MATERIALS CO. LTD., *Containing siloxane groups of the long-wave absorption of light initiator and its prepa-ration method (CN103333276 B)* **2015**.

[42] J.-P. Fouassier, J. F. RABEK (Eds.), *Radiation Curing in Polymer Science and Technology: Fundamentals and methods*, Springer Netherlands **1993**.

[43] W. A. Green, *Industrial Photoinitiators: A Technical Guide*, CRC Press.

[44] H. H. Jaffe, A. L. Miller, *Journal of Chemical Education* **1966**, *43*, 469.

[45] B. Wardle, *Principles and Applications of Photochemistry*, John Wiley & Sons, Ltd **2009**.

[46] V. Helms, *Principles of Computational Cell Biology: Fluorescence Resonance Energy Transfer*, Wiley-VCH **2008**.

[47] S. K. Upadhyay, *Chemical Kinetics and Reaction Dynamics*, Springer, New York.

[48] K. Rohatgi, *Fundamentals of Photochemistry*, New Age International.

[49] N. S. Allen, M. C. Marin, M. Edge, D. W. Davies, J. Garrett, F. Jones, S. Navaratnam, B. J. Parsons, *Journal of Photochemistry and Photobiology A: Chemistry* **1999**, *126*, 135.

[50] J. P. Fouassier, J. Lalevée, *Polymers* **2014**, *6*, 2588.

[51] C. Decker, K. Zahouily, D. Decker, T. Nguyen, T. Viet, *Polymer* **2001**, *42*, 7551.

[52] R. Jahn, T. Jung, *Progress in Organic Coatings* **2001**, *43*, 50.

[53] D. G. Leppard, M. Kohler, L. Misev, *Daylight curing compositions containing bisacylphosphine oxide photoinitiators (US 5534559 A)* **1996**.

[54] J. Suhadolnik, M. G. Wood, R. Ravichandran, W. L. Renz, A. R. Roberts, N. N. Cliff, E. V. Sitzmann, D. Bramer, *Photo-cured and stabilized coatings (CA 2523569 A1)* **2004**.

[55] K. Dietliker, T. Jung, J. Benkhoff, H. Kura, A. Matsumoto, H. Oka, D. Hristova, G. Gescheidt, G. Rist, *Macromolecular Symposia* **2004**, *217*, 77.

[56] J. Xu, G. Ma, K. Wang, J. Gu, S. Jiang, J. Nie, *Journal of Applied Polymer Science* **2012**, *123*, 725.

[57] Y. YÜKSEL DURMAZ, *Macromolecular engineering by end group modifications (PhD Thesis)* **2009**.

[58] M. de Brito, *Investigation of interpenetrating polymer networks and recent UV curable chemistries (PhD Thesis)* **2016**.

[59] J. G. Drobny, *Radiation Technology for Polymers*, CRC Press, 2 Edition **2010**.

[60] C. E. Hoyle, J. F. Kinstle, *Radiation curing of polymeric materials: Photocurable Coatings*, ACS Publications **1990**.

[61] RadTech e (Ed.), *Latest Investigations in Formulation and Processing of Pigmented UV-coatings* **2004**.

[62] H. Wang, J. Wei, X. Jiang, J. Yin, *Polymer* **2006**, *47*, 4967.

[63] S. C. Clark, C. E. Hoyle, S. Jönsson, F. Morel, C. Decker, *Polymer* **1999**, *40*, 5063.

[64] S. Pastorelli, A. Sanches-Silva, J. M. Cruz, C. Simoneau, P. P. Losada, *European Food Research and Technology* **2008**, *227*, 1585.

[65] T. Rothenbacher, M. Baumann, D. Fügel, *Food Additives & Contaminants* **2007**, *24*, 438.

[66] R. Koivikko, S. Pastorelli, Rodríguez-Bernaldo de Quirós, A., R. Paseiro-Cerrato, P. Paseiro-Losada, C. Simoneau, *Food Additives & Contaminants: Part A* **2010**, *27*, 1478.

[67] N. Caiger (Ed.), *Industrial application of UV-curing jet inks* **2001**.

[68] M. A. Lago, Rodríguez-Bernaldo de Quirós, Ana, R. Sendón, J. Bustos, M. T. Nieto, P. Paseiro, *Food Additives & Contaminants: Part A* **2015**, *32*, 779.

[69] L. Angiolini, D. Caretti, E. Salatelli, *Macromol. Chem. Phys.* **2000**, *201*, 2646.

[70] H. Esselbrugge, *European Coatings Journal* **2007**.

[71] R. S. Davidson, *Journal of Photochemistry and Photobiology A: Chemistry* **1993**, *69*, 263.

[72] J. Qiu, J. Wei, *Journal of Polymer Research* **2014**, *21*, 559.

[73] R. Klos, H. Gruber, G. Greber, *Journal of Macromolecular Science: Part A - Chemistry* **1991**, *28*, 925.

[74] R. Phillips, *Journal of Photochemistry* **1984**, *25*, 79.

[75] N. Moszner, U. Salz, *Macromolecular Materials and Engineering* **2007**, *292*, 245.

[76] J. W. Stansbury, *Dental Materials*, *28*, 13.

[77] C. Decker, *Progress in Polymer Science* **1996**, *21*, 593.

[78] A. Oesterreicher, C. Gorsche, S. Ayalur-Karunakaran, A. Moser, M. Edler, G. Pinter, S. Schlögl, R. Liska, T. Griesser, *Macromolecular Rapid Communications* **2016**, *37*, 1701.

[79] C. Gorsche, K. Seidler, P. Knaack, P. Dorfinger, T. Koch, J. Stampfl, N. Moszner, R. Liska, *Polym. Chem.* **2016**, *7*, 2009.

[80] F. R. Wight, I. M. Nunez, *Journal of radiation curing* **1989**, *16*, 3.

[81] C. Decker, A. D. Jenkins, *Macromolecules* **1985**, *18*, 1241.

[82] M. Höfer, N. Moszner, R. Liska, *Journal of Polymer Science Part A: Polymer Chemistry* **2008**, *46*, 6916.

[83] K. Studer, C. Decker, E. Beck, R. Schwalm, *Progress in Organic Coatings* **2003**, *48*, 92.

[84] M. Awokola, W. Lenhard, H. Löffler, C. Flosbach, P. Frese, *Progress in Organic Coatings* **2002**, *44*, 211.

[85] M. P. Stevens (Ed.), *Polymer chemistry: An Introduction*, Oxford university press, Oxford, New York, **1999**.

[86] T. Posner, *Berichte der deutschen chemischen Gesellschaft* **1905**, *38*, 646.

[87] P. Lundberg, A. Bruin, J. W. Klijnstra, A. M. Nyström, M. Johansson, M. Malkoch, A. Hult, *ACS Applied Materials & Interfaces* **2010**, *2*, 903.

[88] M. Black, J. W. Rawlins, *European Polymer Journal* **2009**, *45*, 1433.

[89] Z. Chen, B. J. Chisholm, R. Patani, J. F. Wu, S. Fernando, K. Jogodzinski, D. C. Webster, *Journal of Coatings Technology and Research* **2010**, *7*, 603.

[90] M. Sangermano, Colucci, G., M. Fragale, G. Rizza, *Reactive and Functional Polymers* **2009**, *69*, 719.

[91] T. M. Roper, T. Kwee, T. Y. Lee, C. A. Guymon, C. E. Hoyle, *Polymer* **2004**, *45*, 2921.

[92] C. M. Platnich, A. Banerjee, V. Ozhukil Kollath, K. Karan, S. Trudel, *Can. J. Chem.* **2017**.

[93] J. Mehlich, B. J. Ravoo, *Org. Biomol. Chem.* **2011**, *9*, 4108.

[94] A. J. Guenthner, D. M. Hess, J. J. Cash, *Polymer* **2008**, *49*, 5533.

[95] D.-H. Lim, H.-S. Do, H.-J. Kim, J.-S. Bang, G.-H. Yoon, *Journal of Adhesion Science and Technology* **2007**, *21*, 589.

[96] Q. Wang, G. X. Chen, J. L. Tai, Q. F. Chen, *Applied Mechanics and Materials* **2014**, *469*, 162.

[97] C. E. Hoyle, T. Y. Lee, T. Roper, *Journal of Polymer Science Part A: Polymer Chemistry* **2004**, *42*, 5301.

[98] C. R. Morgan, F. Magnotta, A. D. Ketley, *Journal of Polymer Science: Polymer Chemistry Edition* **1977**, *15*, 627.

[99] M. Sahin, S. Ayalur-Karunakaran, J. Manhart, M. Wolfahrt, W. Kern, S. Schlögl, *Advanced Engineering Materials* **2017**, *19*, 1600620-n/a.

[100] K. Wutticharoenwong, M. D. Soucek, *Journal of Applied Polymer Science* **2009**, *113*, 2173.

[101] E. Yilgör, I. Yilgör, *Progress in Polymer Science* **2014**, *39*, 1165.

[102] J. E. Mark, in *Silicones and Silicone-Modified Materials*, p. 1.

[103] Y. Abe, T. Gunji, *Progress in Polymer Science* **2004**, *29*, 149.

[104] K. W. O'Brien, *Synthesis of Functionalized Poly(dimethylsiloxane)s and the Preparation of Magnetite Nanoparticle Complexes and Dispersions*, Blacksburg, Virginia **2003**.

[105] G. P. Cai, W. P. Weber, *Macromolecules* **2000**, *33*, 6310.

[106] P. Böhm, *Functional Silicones and Silicone-Containing Block Copolymers (PhD Thesis): Silicones and Silicone-Containing Polymer Structures-Synthesis and Applications* **n.d.**

[107] P. Boehm, M. Mondeshki, H. Frey, *Macromolecular Rapid Communications* **2012**, *33*, 1861.

[108] C. J. Brinker, *Journal of Non-Crystalline Solids* **1988**, *100*, 31.

[109] H. Ishida, G. Kumar (Eds.), *Molecular Characterization of Composite Interfaces*, Plenum, New York **1985**.

[110] F. D. Osterholtz, E. R. Pohl, *Journal of Adhesion Science and Technology* **1992**, *6*, 127.

[111] A. S. Lee, Y. Y. Jo, H. Jeon, S.-S. Choi, K.-Y. Baek, S. S. Hwang, *Polymer* **2015**, *68*, 140.

[112] D. B. Cordes, P. D. Lickiss, F. Rataboul, *Chemical Reviews* **2010**, *110*, 2081.

[113] K. L. Chan, P. Sonar, A. Sellinger, *J. Mater. Chem.* **2009**, *19*, 9103.

[114] J. Chojnowski, W. Fortuniak, P. Rościszewski, W. Werel, J. Łukasiak, W. Kamysz, R. Hałasa, *Journal of Inorganic and Organometallic Polymers and Materials* **2006**, *16*, 219.

[115] P. Majumdar, J. He, E. Lee, A. Kallam, N. Gubbins, S. J. Stafslien, J. Daniels, B. J. Chisholm, *Journal of Coatings Technology and Research* **2010**, *7*, 455.

[116] H. Azizi, J. Morshedian, M. Barikani, *Journal of Vinyl and Additive Technology* **2009**, *15*, 184.

[117] E. P. Plueddemann, *Silane Coupling Agents*, Plenum, New York **1982**.

[118] A. T. DiBenedetto, *Materials Science and Engineering: A* **2001**, *302*, 74.

[119] K. L. Mittal (Ed.), *Silanes and Other Coupling Agents, VSP,*, VSP, The Netherlands.

[120] M. Honkanen, M. Hoikkanen, M. Vippola, Vuorinen, Jyrki, T. Lepistö, P. Jussila, H. Ali-Löytty, M. Lampimäki, M. Valden, *Applied Surface Science* **2011**, *257*, 9335.

[121] P. Jussila, H. Ali-Löytty, K. Lahtonen, M. Hirsimäki, M. Valden, *Surface and Interface Analysis* **2010**, *42*, 157.

[122] V. Dugas, Y. Chevalier, *Journal of Colloid and Interface Science* **2003**, *264*, 354.

[123] S. Guhathakurta, A. Subramanian, *Journal of The Electrochemical Society* **2007**, *154*, P136-P146.

[124] Y. Han, D. Mayer, A. Offenhäusser, S. Ingebrandt, *Thin Solid Films* **2006**, *510*, 175.

[125] S. Kaya, P. Rajan, H. Dasari, D. C. Ingram, W. Jadwisienczak, F. Rahman, *ACS Applied Materials & Interfaces* **2015**, *7*, 25024.

[126] B. Kaynak, C. Alpan, M. Kratzer, C. Ganser, C. Teichert, W. Kern, *Applied Surface Science* **2017**, *416*, 824.

[127] Z. TVARÚŽKOVÁ, V. Bosáček, *Chem. zvesti* **1975**, *29*, 325.

[128] A. P. Legrand, H. Hommel, A. Tuel, A. Vidal, H. Balard, E. Papirer, P. Levitz, M. Czernichowski, R. Erre, H. van Damme, J. P. Gallas, J. F. Hemidy, J. C. Lavalley, O. Barres, A. Burneau, Y. Grillet, *Advances in Colloid and Interface Science* **1990**, *33*, 91.

[129] N. R. Glass, R. Tjeung, P. Chan, L. Y. Yeo, J. R. Friend, *Biomicrofluidics* **2011**, *5*.

[130] F. Zhang, K. Sautter, A. M. Larsen, D. A. Findley, R. C. Davis, H. Samha, M. R. Linford, *Langmuir* **2010**, *26*, 14648.

[131] F. Zhang, *Chemical Vapor Deposition of Silanes and Patterning on Silicon* **2011**.

[132] C. Cherkouk, L. Rebohle, W. Skorupa, T. Strache, H. Reuther, M. Helm, *Journal of Colloid and Interface Science* **2009**, *337*, 375.

[133] M. W. Daniels, J. Sefcik, L. F. Francis, A. V. McCormick, *Journal of Colloid and Interface Science* **1999**, *219*, 351.

[134] J. P. Matinlinna, L. V. Lassila, P. K. Vallittu, *Dental Materials* **2007**, *23*, 1173.

[135] GuimarÃ£es, Angela de Mello Ferreira, Ciminelli, VirgÃ\-nia Sampaio Teixeira, W. L. Vasconcelos, *Materials Research*, *10*, 37.

[136] K. C. Vrancken, K. Possemiers, Van Der Voort, P, E. F. Vansant, *Colloids and Surfaces A: Physicochemical and Engineering Aspects* **1995**, *98*, 235.

[137] Prado, Luis A. S. A., M. Sriyai, M. Ghislandi, A. Barros-Timmons, K. Schulte, *Journal of the Brazilian Chemical Society*, *21*, 2238.

[138] S. A. Kulkarni, S. B. Ogale, K. P. Vijayamohanan, *Journal of Colloid and Interface Science* **2008**, *318*, 372.

[139] W. Wang, Vaughn, Mark. W., *Scanning* **2008**, *30*, 65.

[140] N. Aissaoui, L. Bergaoui, J. Landoulsi, J.-F. Lambert, S. Boujday, *Langmuir* **2012**, *28*, 656.

[141] P. van Vlasselaer, S. W. Hasan, *Process for making silanized colloidal silica (US 6015843 A)* **2000**.

[142] H.-H. Kim, S.-Y. Kim, D.-H. Kim, C.-Y. Oh, N.-J. Jo, *Journal of Materials Science and Chemical Engineering* **2014**, *2*, 38.

[143] F. Saeed, A. Ansarifar, R. J. Ellis, Y. Haile-Meskel, M. S. Irfan, *Journal of Applied Polymer Science* **2012**, *123*, 1518.

[144] S. Nandi, H. H. Winter, *Macromolecules* **2005**, *38*, 4447.

[145] M. Gottlieb, in *Biological and Synthetic Polymer Networks* (Ed.: O. Kramer), Springer Netherlands. Dordrecht **1988**, p. 403.

[146] T. K. Kwei, *Journal of Polymer Science Part A: General Papers* **1963**, *1*, 2977.

[147] Y.-H. Zang, R. Muller, D. Froelich, *Polymer* **1989**, *30*, 2060.

[148] S. M. Stark, S. P. Rowland, *Journal of Applied Polymer Science* **1966**, *10*, 1777.

[149] T1 - Residual Dipolar Couplings in Small-Molecule NMR A2 - Lindon, John C, G. E. Tranter, D. W. Koppenaal (Eds.), *Encyclopedia of Spectroscopy and Spectrometry (Third Edition)*, Academic Press, Oxford **2017**.

[150] J.-H. Chen, S. Singer, in *The Handbook of Metabonomics and Metabolomics*, Elsevier Science B.V. Amsterdam **2007**, p. 113.

[151] K. Saalwächter, *Progress in Nuclear Magnetic Resonance Spectroscopy* **2007**, *51*, 1.

[152] R. Graf, D. E. Demco, S. Hafner, H. W. Spiess, *Solid State Nuclear Magnetic Resonance* **1998**, *12*, 139.

[153] W. Chassé, J. L. Valentín, G. D. Genesky, C. Cohen, K. Saalwächter, *The Journal of Chemical Physics* **2011**, *134*, 44907.

[154] M. Schneider, L. Gasper, D. E. Demco, B. Blümich, *The Journal of Chemical Physics* **1999**, *111*, 402.

[155] J. Höpfner, G. Guthausen, K. Saalwächter, M. Wilhelm, *Macromolecules* **2014**, *47*, 4251.

[156] K. Saalwächter, *Rubber Chemistry and Technology* **2012**, *85*, 350.

[157] M. V. Ramiah, *Journal of Applied Polymer Science* **1970**, *14*, 1323.

[158] De Jesus, Juan C., I. González, A. Quevedo, T. Puerta, *Proceedings of the Third San Luis Symposium on Surfaces, Interfaces and Catalysis* **2005**, *228*, 283.

[159] P. R. Hornsby, J. Wang, R. Rothon, G. Jackson, G. Wilkinson, K. Cossick, *Polymer Degradation and Stability* **1996**, *51*, 235.

[160] S. Ullah, M. A. Bustam, M. Nadeem, M. Y. Naz, W. L. Tan, A. M. Shariff, *The Scientific World Journal* **2014**, *2014*, 6.

[161] P. M. Schaber, J. Colson, S. Higgins, D. Thielen, B. Anspach, J. Brauer, *Thermochimica Acta* **2004**, *424*, 131.

[162] X.-G. Li, Y. Lv, B.-G. Ma, W.-Q. Wang, S.-W. Jian, *Arabian Journal of Chemistry* **2017**, *10*, S2534.

[163] G. A. Sotiriou, D. Singh, F. Zhang, M.-C. G. Chalbot, E. Spielman-Sun, L. Hoering, I. G. Kavouras, G. V. Lowry, W. Wohlleben, P. Demokritou, *Journal of Hazardous Materials* **2016**, *305*, 87.

[164] R. L. Lehman, J. S. Gentry, N. G. Glumac, *Thermochimica Acta* **1998**, *316*, 1.

[165] Coats, A. W., Redfern, J. P., *Analyst* **1963**, *88*, 906.

[166] J. Lin, B. Mishra, J. J. Moore, W. D. Sproul, *Surface and Coatings Technology* **2008**, *202*, 3272.

[167] P. J. Haines, *Thermal Methods of Analysis: Principles, Applications and Problems*, Springer.

[168] R. B. Seymour, C. E. Carraher, in *Structure—Property Relationships in Polymers* (Eds.: R. B. Seymour, C. E. Carraher), Springer US. Boston, MA **1984**, p. 57.

[169] P. Roszkowski, M. Sahin, S. Ayalur-Karunakaran, C. Gammer, S. Schlögl, W. Kern, K. K. Krawczyk, *Polymer* **2017**.

[170] P. Gabbott (Ed.), *Principles and Applications of Thermal Analysis*, Wiley-Blackwell **2008**.

[171] S. J. Clarson, K. Dodgson, J. A. Semlyen, *Polymer* **1985**, *26*, 930.

[172] L.-P. Blanchard, J. Hesse, S. L. Malhotra, *Can. J. Chem.* **1974**, *52*, 3170.

[173] A. Oesterreicher, J. Wiener, M. Roth, A. Moser, R. Gmeiner, M. Edler, G. Pinter, T. Griesser, *Polym. Chem.* **2016**, *7*, 5169.

[174] K. Balani, V. Verma, A. Agarwal, R. Narayan, in *Biosurfaces*, John Wiley & Sons, Inc **2015**, p. 329.

[175] J. Pelleg, *Mechanical Properties of Materials [recurso electrónico]*, Springer Science & Business Media **2012**.

[176] R. L. Sakaguchi, J. M. Powers, *Craig's restorative dental materials*, Elsevier/Mosby, St. Louis, Mo **2012**.

[177] P. J. Evans, C. T. Slade, Robert, J. R. Varcoe, K. E. Young, *J. Mater. Chem.* **1999**, *9*, 3015.

[178] *Single-use sterile rubber surgical gloves – Specification. (ISO 10282)* **2014**.

[179] *Standard Test Methods for Vulcanized Rubber and Thermoplastic Rubbers and Thermoplastic Elastomers-Tension*, ASTM International, West Conshohocken, PA **1998**.

[180] J. Baum, A. Pines, *Journal of the American Chemical Society* **1986**, *108*, 7447.

[181] K. Saalwächter, P. Ziegler, O. Spyckerelle, B. Haidar, A. Vidal, J.-U. Sommer, *The Journal of Chemical Physics* **2003**, *119*, 3468.

[182] M. A. Voda, D. E. Demco, J. Perlo, R. A. Orza, B. Blümich, *Journal of Magnetic Resonance* **2005**, *172*, 98.

[183] J. L. Valentín, P. Posadas, A. Fernández-Torres, M. A. Malmierca, L. González, W. Chassé, K. Saalwächter, *Macromolecules* **2010**, *43*, 4210.

[184] M. A. Malmierca, A. González-Jiménez, I. Mora-Barrantes, P. Posadas, A. Rodríguez, L. Ibarra, A. Nogales, K. Saalwächter, J. L. Valentín, *Macromolecules* **2014**, *47*, 5655.

[185] D. Haba, M. Barbezat, S. Ayalur-Karunakaran, S. Schlögl, A. J. Brunner, G. Pinter, *Journal of Polymer Science Part B: Polymer Physics* **2016**, *54*, 1738.

[186] A. E. Taylor, C. W. Miller, H. Roth., Mikrochemie **1944**, 292.

[187] S. Yuasa, M. Okabayashi, H. Ohno, K. Suzuki, K. Kusumoto, *Amorphous, spherical inorganic compound and process for preparation thereof (US 4567030 A)* **1986**.

[188] N. B. Cramer, C. N. Bowman, *Journal of Polymer Science Part A: Polymer Chemistry* **2001**, *39*, 3311.

[189] W. Chassé, M. Lang, J.-U. Sommer, K. Saalwächter, *Macromolecules* **2012**, *45*, 899.

[190] J.E. Puskas, K. Chiang, B. Barkakaty, in *Chemistry, Manufacture and Applications of Natural Rubber* (Eds.: S. Kohjiya, Y. Ikeda), Woodhead Publishing **2014**, p. 30.

[191] K. Turjanmaa, H. Alenius, S. Mäkinen-Kiljunen, T. Reunala, T. Palosuo, *Allergy* **1996**, *51*, 593.

[192] E. Yip, P. Cacioli, *Journal of Allergy and Clinical Immunology* **2002**, *110*, S3 - S14.

[193] S. Mäkinen-Kiljunen, K. Turjanmaa, T. Palosuo, T. Reunala, *Journal of Allergy and Clinical Immunology* **1992**, *90*, 230.

[194] S. Schlögl, A. Temel, R. Schaller, A. Holzner, W. Kern, *J. Appl. Polym. Sci.* **2012**, *124*, 3478.

[195] A. M. Akimkhan, in *Ion Exchange Technologies* (Ed.: A. Kilislioğlu), InTech. Rijeka **2012**.

[196] J. Loccufier, R. Claes, J. van Luppen, *Polymerizable photoinitiators and radiation curable compositions (US 8530510 B2)*, Google Patents **2013**.

[197] M. Sahin, K. K. Krawczyk, P. Roszkowski, J. Wang, B. Kaynak, W. Kern, S. Schlögl, H. Grützmacher, *European Polymer Journal*, https://www.sciencedirect.com/science/article/pii/S0014305717316117.

[198] J. M. Kim, S. M. Chang, S. M. Kong, K.-S. Kim, J. Kim, W.-S. Kim, *Ceramics International* **2009**, *35*, 1015.

[199] L.-A. O'Hare, B. Parbhoo, S. R. Leadley, *Surface and Interface Analysis* **2004**, *36*, 1427.

[200] L. L. Perez, M. J. Ortiz-Iniesta, Z. Zhang, I. Agirrezabal-Telleria, M. Santes, H. J. Heeres, I. Melian-Cabrera, *J. Mater. Chem. A* **2013**, *1*, 4747.

[201] Shin-ichi Kawaguchi, Akihiro Nomoto, Motohiro Sonoda, Akiya Ogawa, *Tetrahedron Letters* **2009**, *50*, 624.

[202] H. N. Petersen, Y. Kusano, P. Brøndsted, K. Almdal, *Risoe International Symposium on Materials Science. Proceedings* **2013**, *34*, 333.

[203] M. Veres, M. Koós, S. Tóth, M. Füle, I. Pócsik, A. Tóth, M. Mohai, I. Bertóti, *Diamond and Related Materials* **2005**, *14*, 1051.

[204] C. Önneby, C. G. Pantano, *Journal of Vacuum Science & Technology A: Vacuum, Surfaces, and Films* **1997**, *15*, 1597.

[205] S. Feih, J. Wei, P. Kingshott, B. F. Sørensen, *Composites Part A: Applied Science and Manufacturing* **2005**, *36*, 245.

[206] H. K. Jang, Y. D. Chung, S. W. Whangbo, Y. S. Lee, I. W. Lyo, C. N. Whang, S. J. Lee, G. Kim, *Journal of Vacuum Science & Technology A: Vacuum, Surfaces, and Films* **2000**, *18*, 401.

[207] G.-W. Lee, N.-J. Lee, J. Jang, K.-J. Lee, J.-D. Nam, *Composites Science and Technology* **2002**, *62*, 9.

[208] I. Roppolo, A. Chiappone, K. Bejtka, E. Celasco, A. Chiodoni, F. Giorgis, M. Sangermano, S. Porro, *Carbon* **2014**, *77*, 226.

[209] C. Sow, B. Riedl, P. Blanchet, *Progress in Organic Coatings* **2010**, *67*, 188.

[210] S. Stankovich, D. A. Dikin, R. D. Piner, K. A. Kohlhaas, A. Kleinhammes, Y. Jia, Y. Wu, S. T. Nguyen, R. S. Ruoff, *Carbon* **2007**, *45*, 1558.

[211] A. E. Ozcam, K. E. Roskov, R. J. Spontak, J. Genzer, *J. Mater. Chem.* **2012**, *22*, 5855.

[212] A. Bismarck, A. R. Boccaccini, E. Egia-Ajuriagojeaskoa, D. Hülsenberg, T. Leutbecher, *Journal of materials science* **2004**, *39*, 401.

[213] J. D. Rathod, *Journal of Civil & Environmental Engineering* **2014**, *4*, 1.

[214] S. Zhandarov, E. Mäder, *Composites Science and Technology* **2005**, *65*, 149.

[215] A. Hampe, G. Kalinka, S. Meretz, E. Schulz, *Composites* **1995**, *26*, 40.

[216] C. Marotzke, G. Kalinka **2006**.

[217] Ho, Kingsley K. C., S. Lamoriniere, G. Kalinka, E. Schulz, A. Bismarck, *Journal of Colloid and Interface Science* **2007**, *313*, 476.

8 LIST OF TABLES

9 LIST OF SCHEMES

10 LIST OF FIGURES